

Star Formation Properties of a Large Sample of Irregular Galaxies

Deidre A. Hunter

Lowell Observatory, 1400 West Mars Hill Road, Flagstaff, Arizona 86001 USA

dah@lowell.edu

and

Bruce G. Elmegreen

IBM T. J. Watson Research Center, PO Box 218, Yorktown Heights, New York 10598 USA

bge@watson.ibm.com

ABSTRACT

We present the results of H α imaging of a large sample of irregular galaxies. Our sample includes 94 galaxies with morphological classifications of Im, 26 Blue Compact Dwarfs (BCDs), and 20 Sm systems. The sample spans a large range in galactic parameters including integrated absolute magnitude (M_V of -9 to -19), average surface brightness (20 to 27 mag/arcsec²), current star formation activity (0 to 1.3 M_\odot yr⁻¹ kpc⁻²), and relative gas content (0.02 to 5 M_\odot/L_B).

The H α images were used to measure the integrated star formation rates, determine the extents of star formation in the disks, and compare azimuthally-averaged radial profiles of current star formation to older starlight. The integrated star formation rates of Im galaxies normalized to the physical size of the galaxy span a range of a factor of 10^4 with 10% Im galaxies and one Sm system having no measureable star formation at the present time. The BCDs fall, on average, at the high star formation rate end of the range. We find no correlation between star formation activity and proximity to other catalogued galaxies. Two galaxies located in voids are similar in properties to the Sm group in our sample.

The H II regions in these galaxies are most often found within the Holmberg radius R_H , although in a few systems H II regions are traced as far as $1.7R_H$. Similarly, most of the star formation is found within 3 disk scale-lengths R_D , but in some galaxies H II regions are traced as far as $6R_D$.

A comparison of H α surface photometry with V-band surface photometry shows that the two approximately follow each other with radius in Sm galaxies, but in most BCDs there is an excess of H α emission in the centers that drops

with radius. In approximately half of the Im galaxies $H\alpha$ and V correspond well, and in the rest there are small to large differences in the relative rate of fall-off with radius.

The cases with strong gradients in the $L_{H\alpha}/L_V$ ratios and with high central star formation rate densities, which include most of the BCDs, require a significant fraction of their gas to migrate to the center in the last Gyr. We discuss possible torques that could have caused this without leaving an obvious signature, including dark matter bars and past interactions or mergers with small galaxies or HI clouds. There is now a substantial amount of evidence for these processes among many surveys of BCDs. We note that such gas migration will also increase the local pressure and possibly enhance the formation of massive dense clusters, but conclude that the star formation process itself does not appear to differ much among BCD, Im and Sm types. In particular, there is evidence in the distribution function for $H\alpha$ surface brightness that the turbulent Mach numbers are all about the same in these systems. This follows from the $H\alpha$ distribution functions corrected for exponential disk gradients, which are log-normal with a nearly constant dispersion. Thus the influence of shock triggered star formation is apparently no greater in BCDs than in Im and Sm types.

Subject headings: galaxies: irregular—galaxies: star formation

1. Introduction

Irregular galaxies are interesting systems for many reasons. Not only are they smaller, less evolved, and have lower amounts of dust and shear in their interstellar mediums (ISM) than most spirals, but they are also the most common type of galaxy in the universe. In some models dwarf irregulars (dIm) are the galaxies that formed first and became the building blocks of larger galaxies. Because these tiny galaxies have evolved relatively slowly over time, they chemically resemble the outer parts of present-day spirals. In fact, ultra-low surface brightness dImS may represent the slowest evolving galaxies in the universe (van den Hoek et al. 2000).

For purposes of star formation studies, the lack of spiral density waves in Im galaxies means that all of the non-spiral star formation processes can be examined more clearly. In fact Hunter, Gallagher, & Rautenkranz (1982) and Hunter & Gallagher (1986) have shown that some Im galaxies have star formation rates normalized to their size that are comparable even to those of spiral galaxies. Thus, spiral density waves are not necessary to a vigorous production of stars (see also Elmegreen & Elmegreen 1986). Furthermore, Hunter

and Gallagher showed that irregular galaxies span a large range in integrated star formation rates. What then regulates star formation in tiny galaxies and determines how fast an Im galaxy evolves?

To address this question, we have conducted a multi-wavelength survey of a large sample of reasonably normal, relatively nearby, non-interacting galaxies without spiral arms. The data consist of UBV and H α images for the entire sample, and JHK images, H I maps, CO observations, and H II region spectrophotometry for a sub-sample. The H α , UBV, and JHK image sets act as probes of star formation on three different times scales: H α images trace the most recent star formation (≤ 10 Myrs) through the ionization of natal clouds by the short-lived massive stars; UBV, while a more complicated clue, is dominated by the stars formed over the past Gyr for on-going star formation (Gallagher et al. 1984); and JHK integrates over the lifetime of the galaxy where even in Im galaxies global JHK colors are characteristic of old stellar populations (Hunter & Gallagher 1985b). We have already used these data to conduct a case study of the Im galaxy NGC 2366 (Hunter, Elmegreen, & van Woerden 2001) as well as studies of the H II region luminosity function and distributions (Youngblood & Hunter 1999, Roye & Hunter 2000), gas abundances (Hunter & Hoffman 1999), and pressures of H II regions relative to the background galactic disk (Elmegreen & Hunter 2000).

Here we present the H α data—integrated star formation rates, azimuthally-averaged H α surface brightnesses, and extents of star formation—of the full sample for the first time, and we discuss the current star formation activity in these galaxies. Because this is the first presentation of the full survey sample, in the next section we will discuss the sample and some of its properties although results from broad-band imaging will be reported in detail in a separate paper. In Section 3 we present the H α observations, and in Section 4 we discuss star formation rates, the radial extents of star formation, and H α surface photometry. A discussion of selected aspects is given in Section 5.

2. The Sample

The sample galaxies are listed in Table 1 where we have grouped the galaxies into three categories: Im, Blue Compact Dwarf (BCD), and Sm. Our sample includes 140 galaxies: 94 Im systems, 26 BCDs, and 20 Sms. Our broad-band images will be presented in a separate paper, but in order to characterize the sample we include here several plots of integrated properties taken from that data set: a UBV color-color diagram in Figure 1, a histogram of reddening-corrected M_{V_0} values in Figure 2, a histogram of μ_{25} (average surface brightness within a B-band isophote of 25 magnitudes of one arcsec²) in Figure 3, and a histogram of

M_{HI}/L_B in Figure 4.

The morphological classifications were taken from de Vaucouleurs et al. (1991=RC3). Most are simply classed as Im or Sm with minor modifications. However, the morphological classifications of the BCDs are complex and varied, reflecting the difficulty in determining just where these systems fit in. One galaxy, NGC 3413, is classed as an “S0sp” but we include it in the Im galaxy sample where our imaging suggests that it belongs. In addition to morphological classification, most of the galaxies in this study were chosen to be relatively nearby; most are closer than 30 Mpc.

The original sample of galaxies was chosen to be those classed as Im in the HI catalog of Fisher & Tully (1975), and so the sample is biased to systems containing gas. A few Sm systems were added from this catalog for comparison. To this collection we later added galaxies that promised to probe the extremes in various properties of the dwarf galaxies since the extremes may hold important clues to a complete picture of the evolution of these galaxies. One such property is surface brightness. We added low surface brightness systems cataloged from the surveys of Schombert & Bothun (1988) and Schombert et al. (1992), particularly those with HI maps obtained by de Blok et al. (1996). These galaxies are more distant than our core sample, the most distant being 86 Mpc. There were 15 Im galaxies added in this way that form 16% of our total Im sample, and 3 Sm systems that form 15% of the Sm sample. In Figure 3 all but 2 of these Im systems turn out to have typical μ_{25} surface brightnesses and fall at the peak in the number distribution of the entire sample, but they are not responsible for defining the peak. The other two systems form the two extreme bins at the faint end. Of the Sm systems, one has a typical μ_{25} and the other two form the extreme bins at the faint end of the distribution. Thus, the augmentation of the original sample with these systems only produced two Im (2% of the total sample) and two Sm (10%) galaxies that really do form an extreme.

Another potential property of interest is the relative gas content. We added 5 systems (5% of our total Im sample) designated as having high M_{HI}/L_B ratios from the study by van Zee, Haynes, & Giovanelli (1995). Of these one turned out to have an average M_{HI}/L_B , as seen in Figure 4, 3 have modestly high M_{HI}/L_B ($\log M_{HI}/L_B > 0.25$) but are not extreme, and one is in the highest bin, although there are 6 other galaxies in that bin too. Thus, this augmentation of the original sample produced one extreme Im galaxy, 1% of the entire Im sample.

In addition to Im and a small sample of Sm galaxies, we include a sample of BCD systems, kept as a separate group, in order to see how their star-forming properties compare to those of Im galaxies. BCDs are generally characterized by intense emission-lines from H II regions. Some, although not all, BCDs have luminosities, sizes, and other properties

that make them likely to be related to Im systems (Kunth 1987). Furthermore, detailed examination of one BCD with the *Hubble Space Telescope (HST)*, VII Zw 403, has shown that it resembles an Im galaxy but with an unusual star-formation past (Lynds et al. 1998). Yet other integrated properties of BCDs are statistically different from those of Im galaxies (Chamaraux 1977, Papaderos et al. 1996).

Most BCDs were chosen from the list of Thuan & Martin (1981). The BCD or H II galaxy class appears to be a mixed bag of objects. Indeed some BCD galaxies are actually star-forming pieces of other galaxies (for example, NGC 2363 in NGC 2366). In order to select BCDs that are most likely comparable systems to the Im galaxies we have imposed an additional selection criteria not applied to the rest of the sample. We used W_{20} , the width at 20% intensity of the integrated HI profile, since it is related to the dynamical mass, to select systems that are comparable in mass to Im systems. We chose systems with $W_{20} \leq 175$ km s⁻¹ since this value corresponds to the upper envelope for the Im systems in our sample.

Our sample, thus, is not complete in any sense, but it spans a large range in galactic parameters including integrated luminosity (M_V of -9 to -19), average surface brightness (20 to 27 mag/arcsec²), current star formation activity (0 to 1.3 M_⊙ yr⁻¹ kpc⁻²), and relative gas content (0.02 to 5 M_⊙ /L_B). A large sample is necessary in order to probe the full range in galactic parameters and to allow a meaningful probe of galaxies that are proving to be very complex and diverse.

The original sample of Im and Sm galaxies was taken from the HI survey of Fisher & Tully (1975) that was based on the catalog of dwarfs compiled by van den Bergh (1959, 1966) from a search of the National Geographic Society and Palomar Sky Survey plates. Fisher & Tully (1981) then went on to produce a more complete survey of galaxies, dwarfs and non-dwarfs of all Hubble types. They argue that their 1981 study is reasonably complete to radial velocities less than 1000 km s⁻¹, sizes greater than 1.5', declinations higher than -35° , and Galactic latitudes more than 30° from the plane. Their 1981 sample included 99 Im systems and 36 Sm systems that satisfy these criteria. 37 galaxies from our Im sample (39% of our sample) represent 37% of the Fisher and Tully sample, and 7 galaxies from our Sm sample (35% of our sample) represent 19% of their sample.

There are 14 Im galaxies (15% of our sample) and two Sm galaxies (10% of our sample) that are not part of the Fisher and Tully 1981 HI survey or the augmentation samples discussed above. In the figures we see that most of the added Im galaxies have typical integrated properties. The exceptions are as follows: 3 fall near the blue end and 2 near the red end of UBV colors; 8 are at the high end of M_V ($M_V < -17$), two are at the low end ($M_V > -12.6$), and one is the lowest ($M_V = -9.4$); 7 are high in surface brightness ($\mu_{25} < 22$ mag arcsec⁻²) and none are low ($\mu_{25} > 24$ mag arcsec⁻²); 3 are low in M_{HI}/L_B

($\log M_{HI}/L_B < -0.5$) and none are high ($\log M_{HI}/L_B > 0.5$); and 6 have high star formation rates ($\log \dot{M} \geq -1$), two have low rates ($\log \dot{M} \leq -3$), and two have no current measurable star formation. The two Sm galaxies are typical in all properties. Thus, while our sample of galaxies is not complete, it is representative.

The distances to the galaxies in our sample are given in Table 1. We used distances determined from stellar population studies, often from variable stars or the tip of the Red Giant Branch, if they were available. Other distances were determined from the radial velocity relative to the Galactic standard of rest V_{GSR} (RC3) and a “Hubble constant” of $65 \text{ km s}^{-1} \text{ Mpc}^{-1}$. References are given in Table 1.

Any system known to be interacting was excluded because we are interested only in internal processes. However, inclusion in this sample is not a guarantee that a galaxy has not been affected by other galaxies at some time in the past. Surprises sometimes await us when we learn more about individual galaxies (for example, NGC 4449: Hunter et al. 1998b). NED was used to search for galaxies within 1 Mpc and 150 km s^{-1} of our sample galaxies. The distance to the nearest galaxy and their radial velocity difference are given in Table 1.

For comparison to spiral galaxies we have used the sample compiled by Kennicutt (1983). This sample spans the range of morphologies from Sab to Sd with 74 systems. Kennicutt has measured $H\alpha$ fluxes for these galaxies. Other properties were obtained from RC3 and Fisher & Tully (1981).

Foreground reddening was determined from Burstein & Heiles (1978) and values are given in Table 1. An internal reddening correction of $E(B-V)_s=0.05$ was added for the stars and of $E(B-V)_g=0.1$ for the gas. The reddening law of Cardelli, Clayton, & Mathis (1989) was adopted. For the spirals, internal reddening was taken to be 0.3, after Kennicutt (1983).

Reddenings from Schlegel et al. (1998) were considered early on, but we were uneasy that the Schlegel et al. values are systematically higher than those of Burstein and Heiles. For 49 Im and BCD galaxies, the Schlegel et al. $E(B-V)$ values are on average a factor of two times those of Burstein and Heiles. For most galaxies the difference is nevertheless insignificant, especially compared to the error we must make by adopting the same internal reddening for all galaxies and all H II regions within each galaxy. However, the higher values of Schlegel et al. do not make sense in some cases. For example, for the heavily reddened galaxy NGC 1569 optical spectroscopy of its H II regions yields an average total $E(B-V)$ of 0.70 ± 0.05 (see compilation in Hunter & Hoffman 1999). The Burstein and Heiles value for foreground reddening is 0.51 and the Schlegel et al. value, obtained from NED, is 0.70. Thus, the Schlegel et al. value would mean that the H II regions in NGC 1569 have no internal reddening while

the Burstein and Heiles value allows a reasonable 0.2 mag of internal reddening. Willick (1999), as quoted by NED, argues that both methods of determining foreground reddening are likely to have systematic errors. It is not clear to us at this point that one method is significantly superior to the other, and we have preferred to use the values of Burstein and Heiles for the reasons given.

3. The H α images

The H α images were obtained in 22 observing runs from 1988 to 1998. The telescopes, instruments, and exposure times are given in Table 2. Some of these images were discussed by Hunter, Hawley, & Gallagher (1993) in their search for extra-HII region ionized gas structures. Images are available from Hunter upon request.

The galaxies were imaged through narrow-band H α filters, usually with a FWHM \sim 30 Å. We had a series of 5 filters forming a red-shift set with some wavelength overlap between filters. The continuum-only off-band filter was centered at 6440 Å with a FWHM of 95 Å. Usually multiple images through the H α filter and sometimes also through the off-band filter were obtained and combined to remove cosmic rays. The off-band image was shifted, scaled, and subtracted from the H α image to remove the stellar continuum. The H α emission was calibrated using the known H α flux from the H II regions NGC 2363 (Kennicutt, Balick, & Heckman 1980) and NGC 604 (Appendix A) and from spectrophotometric standard stars. Calibrations determined from nebulae and standard stars observed on the same nights agreed to within 4%. The H α flux has been corrected for the shift of the bandpass with temperature and the contribution from [NII]. The latter contribution was usually of order 1%. Sky was subtracted from the image most often using a two-dimensional fit to the background.

Detection limits in H α photometry and comparison to measurements in common with others are discussed by Youngblood & Hunter (1999). They determined detection limits by artificially adding H II regions and determining the limit for recovering them. In Table 2 we also include the rms deviations in the background of the H α images given in terms of the corresponding H α surface brightness of a single pixel. Note, however, that these limits are for a single pixel; azimuthally-averaged surface photometry from ellipse photometry can be lower than these limits if a detectable H II region is located in an annulus with a large area.

We mention here a few studies with integrated H α measurements published after Youngblood & Hunter (1999). There are 12 galaxies in common with the sample of van Zee (2000). Differences in the integrated H α fluxes for these galaxies are on average 2.8σ , with three galaxies having a $0.2\text{--}0.3\sigma$ difference and two having a $7\text{--}9\sigma$ difference. From an alterna-

tive perspective, the differences are 21% of the flux on average except for two galaxies that differ by a factor of 2–3. Kniazen et al. (2000) have estimated the integrated H α flux of HS0822+3542 from slit spectroscopy. Our flux agrees with theirs to 6%. We have 34 galaxies in common with the H α survey of James et al. (2004). The average difference in the H α flux is 2.5σ with one galaxy having a difference of 6σ .

For doing azimuthally-averaged H α surface photometry, we have geometrically matched the H α image to the V-band image. The V-band images, to be presented in a separate paper, were used to determine the position angle, ellipticity, and center of the galaxy. The same ellipses used for photometry of the V-band images were used for the H α images. Thus, the H α surface photometry can be directly compared to that from the V image. The position angle PA, minor-to-major axis ratio b/a , step size, and galaxy center that were used for the ellipse photometry are given in Table 2. In a few cases V-band images were not available and we used instead H α off-band images or Digitized Sky Survey (DSS) extracts.

4. Results

4.1. Integrated star formation rates

We have used H α as a tracer of the most recent star formation in Im galaxies and $L_{H\alpha}$ as a measure of the star formation rate. Massive stars are short-lived and ionize the gas left over from the star formation process. The H α luminosity is a measure of the flux of ionizing photons bathing the left over gas and hence a measure of the number of massive stars that are present in the region. With the assumption of a stellar initial mass function we infer the presence of lower mass stars and then deduce the star formation rate. The stellar initial mass function has been found to be approximately constant among systems where it could be directly measured, so this is a reasonable assumption. Extinction due to dust is low, so we feel confident that H α is revealing the bulk of the star formation in these galaxies (Hopkins et al. 2001). One potential issue occurs for galaxies that are undergoing a burst of star formation. Weilbacher & Fritze-v. Alvensleben (2001) have shown that the H α luminosity does not translate into \dot{M} as simply in galaxies where the star formation rate is changing on short timescales as in galaxies where it is relatively constant. Here we have treated all galaxies in the same manner, but note that the \dot{M} deduced for galaxies with an unusually high star formation rate compared to that in the past may not be as well determined. Brinchmann et al. (2004) find that the relationship between star formation rate and $L_{H\alpha}$ is also a function of the stellar mass of the galaxy (driven primarily by the metallicity of the galaxy), the ratio of $L_{H\alpha}$ to star formation rate increasing to less massive galaxies. However, their models show that the simple method of converting $L_{H\alpha}$ to \dot{M} using

a single constant that we adopt here agrees with other methods for the low-mass galaxies of our survey (their Figure 8).

The reddening-corrected $L_{H\alpha}$ and star formation rates \dot{M} are listed in Table 3, and the number distribution of \dot{M} is shown in Figure 5. We converted $L_{H\alpha}$ to \dot{M} using the formula derived in Appendix B. This assumes that stars $0.1 M_{\odot}$ to $100 M_{\odot}$ form in the proportions first observed by Salpeter (1955). We also assume an efficiency factor η of $2/3$ for the absorption of ionizing photons by the nebulae (Gallagher, Hunter, & Tutukov 1984).

To compare star formation rates in galaxies we must normalize the star formation rate to the “size” of the galaxy. An obvious quantity for normalization would be the mass of the galaxy. However, determining the mass is fraught with uncertainties: There are varying amounts of dark matter, large uncertainties in determining the total stellar mass which increases with time, and a gas mass that is depleted with time. Therefore, operationally mass does not make a good normalizer. We have instead chosen to use the physical area of the galaxy. In the past we used R_{25} from which to calculate the area of the galaxy πR_{25}^2 . We did this because R_{25} was readily available from RC3 for a large number of galaxies. However, R_{25} is a surface-brightness defined size, and therefore, it will depend to some extent on the location and level of the star formation itself. Furthermore, there are some galaxies that fall everywhere below a B-band surface brightness of 25 mag of one arcsec² and yet are forming stars.

To address these problems, we have chosen here to use the scale-length R_D measured from V-band images to define the area of the galaxy. Of course, the scale-length assumes a reasonably well-behaved exponential disk, and most Im disks are (Hodge 1971, Hunter & Gallagher 1985b, van Zee 2000). Determining the scale-length has its own uncertainties, but we believe that R_D is a more meaningful measure of the size of a galaxy than R_{25} . There are some galaxies that are not characterized by a single fit to the surface brightness profile. These are 8 of the BCDs: Haro 20, Haro 23, Mrk 32, Mrk 408, Mrk 600, Mrk 757, UGCA 290, and VIIZw403. All but one of these shows a steeper profile in the center than in the outer parts. Since we would expect intense central star formation to bias the surface brightness profile, we have used the fit to the outer galaxy in these cases (see also Cairós et al. 2001, Noeske et al. 2003).

To ease the transition and for comparison to spirals for which we only have R_{25} , we include the star formation rate normalized to R_{25} \dot{M}_{25} , as well as the star formation rate normalized to R_D \dot{M}_D . These are given in Table 3. \dot{M}_{25} and \dot{M}_D are compared in Figure 6, and the number distributions of these two normalized star formation rates are shown in Figures 7 and 8. In order to represent galaxies with zero star formation rates on these log plots, we have plotted them at $\log \dot{M}_{25}$ and $\log \dot{M}_D$ of -6 to -6.5 . The R_{25} and R_D are given

in Table 4.

Although we use the area πR_D^2 as the area for normalizing \dot{M}_D , that does not imply that all of the star formation is found within R_D . In fact below we will see that most of the star formation is found within $3-7R_D$. We use πR_D^2 as the area simply as a way of normalizing by the relative physical size of the galaxy.

We see in Figure 6 that the lower star formation rate systems cluster around the line of $\dot{M}_{25} \sim \dot{M}_D$, while the higher star formation rate systems approximately follow a line in which $\dot{M}_D \sim 10 \times \dot{M}_{25}$, which corresponds to $R_{25} = \sqrt{10} R_D$. We can understand this as due to lower surface brightness systems having shorter R_{25} compared to R_D ; they reach 25 mag arcsec⁻² faster with radius than galaxies that start out brighter. Higher surface brightness galaxies have larger relative R_{25} , approximately $3R_D$ (see also Heller et al. 2000). This is a consequence of the higher star formation rate systems having higher central surface brightnesses, I_0 , because $R_{25}/R_D = \log(I_0/I_{25})$ for fixed surface brightness I_{25} at 25th mag arcsec⁻².

From Figures 7 and 8 one can see that star formation rates in Im galaxies forming stars span a factor of 300 in \dot{M}_{25} and 10^4 in \dot{M}_D . BCDs, as expected, do generally have high star formation rates although there is also a range (see also Hopkins, Schulte-Ladbeck, & Drozdovsky 2002). Sm galaxies have about the same distribution in rates as Im galaxies. In \dot{M}_{25} the irregular galaxies at the high end of the distribution have normalized rates that are comparable to those of spirals. Not all galaxies are forming stars, however: 10% of our Im (9 of 94) and 5% of our Sm galaxies (1 of 20) are not currently forming stars at a level that we can detect.

The typical \dot{M}_{25} star formation rate for the Im galaxies is $10^{-3} M_\odot \text{ yr}^{-1} \text{ kpc}^{-2}$. The typical spiral has an integrated star formation rate that is about 3 times higher. We have compared this to a sample of 11 Sc galaxies whose radial H α surface brightnesses are shown by Kennicutt (1989). We see that the Sc spirals reach this star formation rate per unit area between $0.35R_{25}$ and $0.81R_{25}$. The average is $0.5R_{25}$. Thus, the Im galaxies more closely resemble the outer parts of spirals in star formation rates.

The timescale τ to exhaust the current gas supply at the current star formation rate is given in Table 3; the gas mass is given in Table 4. The number distribution is shown in Figure 9. We include all of the gas associated with the galaxy in the current gas supply. Gas at large radii is problematical; we do not know what role that gas will play in the future nor can we say with confidence what role it is currently playing in star formation. In one Im galaxy, the bulk population in the outer parts is the same as everywhere else in the galaxy suggesting that star formation must be taking place out there at some level (Hunter, in

preparation). Recycling of gas from dying stars is not included in determining τ , but would add another factor of 1.5–4 to the timescale (Kennicutt, Tamblyn, & Congdon 1994).

Detailed studies of the stellar populations in dIm galaxies that have shown that most evolve with a star formation rate that varies in amplitude by a factor of only a few, as would be expected in small galaxies (Ferraro et al. 1989; Tosi et al. 1991; Greggio et al. 1993; Marconi et al. 1995; Gallart et al. 1996a,b; Aparicio et al. 1997a,b; Dohm-Palmer et al. 1998; Gallagher et al. 1998; Cole et al. 1999; Gallart et al. 1999; Kennicutt & Skillman 2001; Miller et al. 2001; Wyder 2001). This is even true of some BCD systems (Schulte-Ladbeck et al. 2000; Crone et al. 2002). Thus, one can see that most of the Im and Sm galaxies can sustain this rate for at least another Hubble time and some much longer (see also van Zee 2001).

However, this is not true of most BCDs and a few Im galaxies that have unusually high star formation rates. The galaxies in our sample with unusually high \dot{M} ($\dot{M}_D \geq -1$ in Table 3 and Figure 8) include IC 4662, NGC 1156, NGC 1569 among the Im systems and Haro 3, Haro 4, Haro29, HS0822+3542, Mrk 67, NGC 1705, and Zw2335 among the BCDs. Most of these systems are also the ones with low τ (Table 3 and Figure 9), indicating that this level of star formation is unsustainable.

This is what brought people early on to the belief that BCDs as a class are undergoing an unusually enhanced episode of star formation at the present time (Thuan 1991). Studies of the resolved stellar population of NGC 1569 find that the current star formation rate is unusual compared to what it has been in the past (Greggio et al. 1998). In the case of NGC 1569, interaction with a nearby HI gas cloud is believed to be responsible for the current elevated level of star formation (Stil & Israel 1998). Resolved stellar population studies of a few other Im galaxies also show evidence of higher amplitude variations either currently or in the past (Tolstoy 1996; Israel 1988; Tolstoy et al. 1998; Karachentsev, Aparicio, & Makarova 1999). But, what causes statistically large variations to occur in dwarfs that appear to be isolated is not known.

The current star formation rate does not correlate with many integrated properties of the galaxies (see also Hunter et al. 1982, Hunter & Gallagher 1985b, van Zee 2001). An expected correlation is between star formation activity and average surface brightness of the galaxy. This is shown in Figure 10. Galaxies with higher star formation rates are higher in surface brightness. However, there is no correlation between surface brightness and (U–B) or (B–V), which are longer term measures of the star formation state of a galaxy (see also McGaugh & Bothun 1994). In terms of other quantities, there is a slight trend with lower luminosity galaxies having lower star formation rates, shown in Figure 11, particularly when spiral galaxies are included to extend the range in M_V . However, at any given galactic

magnitude, the scatter in \dot{M} is very large. There is a stronger correlation between star formation rate and M_{HI}/L_B and between star formation and the fraction of the galactic mass (gas plus stars) that is gas. These are shown in Figures 12 and 13. The trends are in the sense that galaxies with higher ratios of gas relative to their luminosity or total baryonic mass have lower current star formation rates. This makes sense if star formation rates are approximately constant: galaxies forming stars at lower rates have locked less of their gas up in stars. Other studies have also shown that star formation rates are correlated with the gas surface density in late-type galaxies (Buat, Deharveng, & Donas 1989) and total gas mass (Pérez-González et al. 2003).

We were concerned about the effects that neighboring galaxies might have on the star formation processes in our survey galaxies (see, for example, Hashimoto et al. 1998, Noeske et al. 2001). In Figure 14 we plot the current star formation rate against the distance to the nearest catalogued galaxy, given in Table 1. Galaxies for which no obvious neighbor was found within our search parameters are plotted at a distance of 10000 kpc. One can see that galaxies with no neighbors span the range from very high \dot{M}_D to low \dot{M}_D , most of the observed range in our sample. Also, galaxies with a star formation rate of zero span the same range in distance to nearest neighbors. So, it would seem that a lack of neighbors has not been the cause of no star formation. However, three galaxies at the high end of the star formation rate range do fall outside the envelope defined by the other galaxies towards smaller distances as might be expected if gravitational interactions sometime in the past contributed to the current star formation activity.

Among the BCDs, we do not see evidence of systematically closer companions than for Im systems. This is consistent with the studies by Campos-Aguilar & Moles (1991) and Telles & Terlevich (1995) who also searched for bright companions. Recent studies have found significant evidence for an excess of faint companions to BCD galaxies, however. We return to this issue in Section 5.2. At the other extreme, Bothun et al. (1993) suggested that low surface brightness galaxies have a deficit of companions. A plot of the V-band surface brightness in one scale length μ_D against distance to the nearest galaxy shows only a somewhat broader range in distances for the lower surface brightness systems in this sample.

How do the two galaxies in voids (0467–074, 1397–049) compare with the other irregular galaxies? Their M_V place them at the bright end of the range for Im or BCD galaxies, more like Sm systems. Similarly, their R_D are larger than is typical for Im or BCD galaxies. However, except for 1397–049’s U–B, the colors, surface brightnesses, and star formation rates are typical of Im galaxies. These two galaxies do not have the higher surface brightness or star formation rates more typical of BCDs and, therefore, are not similar to the void dwarfs studied by Popescu, Hopp, & Rosa (1999). However, like Popescu et al. we find that

the galaxies in the voids are similar to systems in the field.

There have been several surveys published recently dealing with star-forming properties of large numbers of galaxies over the range of galaxy Hubble types, including Im and BCD systems. Their observational approaches are very different from ours, but it is worth commenting on where our survey fits in with theirs. The first is that of Gil de Paz et al. (2000) who use H α fluxes to determine star formation rates for a sample of galaxies found on objective-prism plates. Because of their method of detection, this survey is limited to galaxies that are currently forming stars. Their Figure 1(f) shows a histogram of H α luminosity. We see that the bright end of our survey begins just where their survey reaches its faint limit. Gil de Paz et al. normalize their star formation rates to the stellar mass of the galaxy, a quantity that changes as the galaxy evolves. If we compute the star formation rate for our galaxies using their Equation 4 and divide by the integrated galactic stellar mass, we find that our median $\log \dot{M} M_{stars}^{-1}$ (10^{-11} yr $^{-1}$) is 1.2 for the Im galaxies with a range from 0.2 to 2.0 and 1.4 for the BCDs with a range from 0.4 to 2.4. Their mean value of $\log \dot{M} M_{stars}^{-1}$ (10^{-11} yr $^{-1}$) for dwarf galaxies (based on 5 systems) is 1.9 ± 0.1 and for H II galaxies (based on 18 systems) is 2.1 ± 0.1 . Thus, the galaxies in our survey have lower average specific star formation rates. Gil de Paz et al. also find a correlation between integrated galactic stellar mass and the star formation per unit stellar mass (their Figure 7(b)). Our sample alone shows no correlation, but the relationship is quite broad and our range of parameter space more limited than theirs.

A second survey is that of Brinchmann et al. (2004) which uses Sloan Digital Sky Survey (SDSS) images and spectra. They also normalize to the integrated mass of the galaxy and find that the value of $\log \dot{M} M_{stars}^{-1}$ (yr $^{-1}$) increases on average as the mass of the galaxy increases, similar to Figure 7(b) of Gil de Paz et al. (2000). To compare to their Figure 22, we constructed histograms of $\log \dot{M} M_{stars}^{-1}$ (yr $^{-1}$) for our sample divided into two sets: those with integrated galactic stellar masses less than $10^9 M_{\odot}$ and those more massive than this. The median values in the two sub-samples are the same for the Im galaxies, only 0.2 dex different for the BCDs and only 0.1 dex different for the Sms. Brinchmann et al., on the other hand, would predict a shift to higher $\log \dot{M} M_{stars}^{-1}$ (yr $^{-1}$) of 0.4 dex, using their middle mass bins in these ranges. Thus, we do not see the correlation between $\dot{M} M_{stars}^{-1}$ and M_{stars} that they see. However, our data do show the correlation between \dot{M} and M_{stars} that they find (their Figure 17).

4.2. Star formation extents

The radius of the last annulus in which $H\alpha$ emission is detected in our images $R_{H\alpha}$ is given in Table 3. For most Im and Sm galaxies $R_{H\alpha}$ is the same, or nearly the same, as the radius of the furthest detectable discrete H II region R_{HII} . However, in some BCDs and starburst galaxies the furthest detectable $H\alpha$ emission is diffuse ionized gas from the outer parts of a very large H II region or extra-H II region ionized gas. In about 11 of our BCDs $R_{H\alpha}$ is somewhat greater than the location of the center of its furthest H II region because of extended ionized gas around the supergiant H II region. In the two starburst galaxies NGC 1569 and NGC 1705, extra-H II region ionized gas extends well beyond the main body of the optical galaxy and any star-forming regions. Therefore, in Table 3 we also include R_{HII} for each galaxy. This is the ellipse, from the ellipse photometry, that includes the center of the H II region which is most distant from the center. Also in Table 3 we give the ratio of R_{HII} to various measures of the size of the galaxy: R_{25} , R_H , and R_D . Histograms of R_{HII}/R_H and R_{HII}/R_D are shown in Figures 15 and 16.

We see that most of the detectable H II regions in our survey galaxies are found within the Holmberg radius R_H . However, in some, $H\alpha$ emission is found beyond this, even to 1.7 times R_H . Similarly, most of the star-formation is found within 3 disk scale-lengths, but in some, $H\alpha$ emission is found even to $6R_D$. This is just as Parodi & Binggeli (2003) found for bright lumps in B-band images of Im galaxies. In BCDs, the H II regions are significantly more concentrated toward the center than in Im and Sm galaxies, consistent with the starburst nature of the BCDs.

The location of H II regions, as a tracer of recent star formation, is consistent with most studies of resolved stellar populations in Im galaxies. Aparicio, Tikhonov, & Karachentsev (2000) found that there has been no recent star formation beyond R_H in DDO 187 and only old stars are found in the outer part of DDO 190 (Aparicio & Tikhonov 2000). WLM also has an extended halo of old stars (Minniti & Zijlstra 1997), as do DDO 216 (Gallagher et al. 1998) and NGC 3109 (Minniti, Zijlstra, & Alonso 1999). By contrast, Komiyama et al. (2003) have found an extended distribution of blue stars that follows the HI distribution in NGC 6822, well beyond the $H\alpha$. They estimate the age of these stars at 180 Myrs.

4.3. $H\alpha$ surface photometry

The $H\alpha$ surface photometry was done in the same way as the V-band or equivalent surface photometry, which will be discussed in a separate paper. The surface brightness plot of the first galaxy in our sample is shown in Figure 17. Plots for the rest of the galaxies

in the sample will be published in the paper presenting the broad-band images. The $H\alpha$ image is measuring the star formation activity over the past 10 Myr or so, while the V-band light is dominated by stars with lifetimes of order 1 Gyr if star-formation is on-going (a convolution of the numbers of stars formed and their brightness in the V-band, Gallagher, Hunter, & Tutukov 1984). Thus, the V-band starlight is a tracer of a somewhat older stellar population.

Hunter & Gallagher (1985b) and Hunter et al. (1998a) found that, for many Im galaxies in their sample, there was a correlation between the surface density of stars and the azimuthally-averaged star formation activity (see also Ryder & Dopita 1994; Brosch, Heller, & Almoznino 1998; Parodi & Binggeli 2003). This implies that star formation has been approximately constant with radius. They noted that this could be a causal connection if stellar energy input to the ISM acts as a feedback process to star formation (see also Dopita & Ryder 1994).

Our much larger sample here shows that the relationship between stars and star formation is more complex. We have examined the correspondence of surface photometry μ_V and $\Sigma_{H\alpha}$ by looking at the ratio of $L_{H\alpha}$ to L_V in the surface photometry annuli. The $H\alpha$ surface photometry is expected to be less smooth than the starlight since it represents a shorter-lived evolutionary stage. So, exact correspondence between μ_V and $\Sigma_{H\alpha}$ is not expected. The ratios $L_{H\alpha}/L_V$ as a function of radius are shown in Figure 18. We see that among the Im galaxies roughly half of the Im galaxies have a good correspondence between stellar density and star formation surface photometry. In the BCDs, on the other hand, the ratio $L_{H\alpha}/L_V$ most often drops steeply with radius. For Sm galaxies, the majority show a fairly constant ratio with radius.

We have used Figure 18 to assign the relationship between $L_{H\alpha}$ and L_V for each galaxy to one of three bins. The three bins are defined as 1) $H\alpha$ falls off approximately like V. That is, the ratio $L_{H\alpha}/L_V$ is roughly constant, with statistical variations and not large trends. 2) $H\alpha$ and V show some differences and some similarity, and 3) $H\alpha$ and V are dissimilar with large-scale trends. Some galaxies have too little star formation to be a part of this exercise. Of the Im galaxies, we find that approximately 44% (34 of 77) have $\Sigma_{H\alpha}$ that fall off with radius similar to μ_V , 40% (31 of 77) are quite different, and 16% (12 of 77) are in between. Of the BCD galaxies, 8% (2 of 25) are similar, 76% (19 of 25) are different, and 16% (4 of 25) are in between. Of the Sm galaxies, 55% (10 of 18) are similar, 28% (5 of 18) are different, and 17% (3 of 18) are in between. There is no correlation between presence of a stellar bar or the value of W_{20} , the FWHM of the integrated HI profile, of an Im galaxy and its bin type. There is also no correlation between bin type and distance to the nearest bright companion. However, there is a small preference for Im galaxies in bin 1 to be brighter overall in the

V-band, and this is shown in Figure 19.

5. Discussion

5.1. Sm galaxies

In keeping with their classification as late-type spirals, the Sm group falls at the high end of the range of absolute magnitude of our sample although there is considerable overlap. Our Sm sample ranges from -15.9 to -19.5 with a median of -17 . Because they tend to be more luminous, the Sm galaxies also are physically larger (see also Hodge 1971) and, as a group, tend to higher \dot{M} . In other properties, however, the Sm group covers the same range as the Im galaxies.

Most of the Sm galaxies have a roughly constant $L_{H\alpha}/L_V$ ratio with radius. This implies that the Sm galaxies are in a sense more stable. They are large enough and have enough star formation going on at all times that star formation as a function of radius is approximately constant (Hunter & Gallagher 1985b). This is also consistent with the trend for the brighter Im galaxies to also have roughly constant $L_{H\alpha}/L_V$ with radius. The statistical variations with location within smaller galaxies simply make this correlation harder to maintain. However, smaller galaxies may still maintain a correspondence integrated over a longer period of time, as “star formation bubbles around a galaxy” (Hunter & Gallagher 1986) propelled by changes in local characteristics.

5.2. BCD galaxies

In contrast to the Sm group, the BCD group covers the same range in M_V as the Im galaxies, but falls at the extremes in other properties. While the absolute star formation rate \dot{M} is only modestly high in BCDs compared to typical Ims, the normalized star formation rates \dot{M}_{25} and \dot{M}_D are significantly higher. In keeping with the higher star formation rates, the BCDs also have a smaller time scale to exhaust the gas τ and higher surface brightnesses.

Part of the contribution to higher \dot{M}_D is the smaller R_D of BCDs (see also Papaderos et al. 1996, Patterson & Thuan 1996, van Zee et al. 1998). This is illustrated in Figure 20 where one can see that the BCDs have smaller R_D relative to their absolute magnitude, implying that they have systematically steeper profiles. This is in spite of the fact that in 8 systems we have fit the V-band azimuthal profile only in the outer parts where the profile becomes less steep and that we have reached as far out as R_H in 13 of the 26 systems. Thus,

to the extent that the V-band images are affected by the intense star formation taking place in these galaxies, they appear to be affected over a fairly large portion of the optical galaxy or the galaxy beyond the affected region must be quite low in surface brightness (see also Noeske et al. 2003).

In addition, the star formation in BCDs is often concentrated to the central regions (see also Davies, Sugai, & Ward 1998). One can see this in Figures 15 and 16. However, R_{HII} does not take the intensity of the H II region into account, and in some galaxies small regions are located outside the dominant central star-forming region. The central concentration is even clearer in the plots of $\log L_{H\alpha}/L_V$ as a function of radius (Figure 18). There the ratios often fall steeply with radius, implying unusually high $L_{H\alpha}$ relative to L_V near the centers.

The central concentration of star formation may be accompanied by a similar concentration of neutral gas. While only 3 of our BCDs have published HI maps, other samples of BCDs have been mapped in HI. Taylor et al. (1995), van Zee et al. (1998), and Simpson & Gottesman (2000) have stated that the HI gas is centrally concentrated in their BCDs. Van Zee, Salzer, & Skillman (2001) further state that BCDs have systematically steeper rotation curves, although the rotation curves are not given. This is in contrast to galaxies at the other extreme; very low surface brightness galaxies have more slowly rising rotation curves (de Blok, McGaugh, & van der Hulst 1996; but see Swaters, Madore, & Trewhella 2000).

The radial variation of $L_{H\alpha}/L_V$ in a galaxy implies that the position of star formation has migrated to the center within the last Gyr, which is approximately the timescale for stars that dominate the light in the V-band for on-going star formation. A major shift in the location of star formation requires a significant amount of angular momentum loss from the gas. Such a loss is usually the result of bar torques or companion galaxy tidal torques. In the case of a merger, the torque also comes from gas pressure and shocks as the two interstellar media merge. For our BCD sample, and for the Im and Sm cases that also have $L_{H\alpha}/L_V$ gradients, there is no systematic evidence for strong bars or bright companions. Still, most of these low mass galaxies are clearly axisymmetric and irregular, and any slight shear in the presence of such irregularities can lead to bar-like torques and mass inflow.

Low mass galaxies also have dark matter halos with velocity dispersions comparable to the dispersion in the stars and gas, as may be inferred from their systematically thicker shapes (Hodge & Hitchcock 1966; van den Bergh 1988; Staveley-Smith, Davies, & Kinman 1992; Binggeli & Popescu 1995; Sung et al. 1998). In these cases, two-fluid or three-fluid instabilities involving the visible galaxy gravitationally coupled to a rotating dark matter halo could in principle lead to bar formation in the halo in much the same way as a stellar disk forms a bar in its center. The presence of such halo bars (e.g., Bekki & Freeman 2003) could be inferred from the rotation pattern of gas in the disk, which would show the characteristic

central twist in the iso-velocity lines of a velocity contour diagram (Bosma 1981). We note that the HI velocity distribution in the nearby BCD-like galaxy IC 10 (Wilcots & Miller 1998; see their Fig. 10) has twists and distortions in the center, and their tilted ring model for the rotation curve has sharp changes in the fitted inclinations and position angles of the inner disk when they force a circular rotation pattern (see their Fig. 5). Wilcots & Miller point out that a counter-rotating stream of HI in the outer part of IC 10 is a likely cause of the starburst, but the inner irregularities are interesting also as possible drivers of gas migration.

One tempting interpretation of the central concentration of gas in BCDs is that they have been affected by interactions with other galaxies sometime in the past. An interaction can strip angular momentum from the gas and stars and lead to overall disk contraction. The high gas density in the center then causes the starburst. For example, the ratio of R_{25} to R_D increases from ξ_1 to ξ_2 if $\xi_2 - \xi_1 = 2 \ln(S)$ where S is the shrinkage factor of an exponential disk that conserves mass. Our observations are consistent with $\xi_1 \sim 1.5$ for Im and $\xi_2 = 3$ for BCDs (cf. Fig. 6), in which case $S = 1.3$ requires only a modest disk shrinkage. Theoretical models by Noguchi (1988) were among the first to show how amorphous galaxies with mass inflow can result from the interaction of two galaxies of comparable mass passing on parabolic orbits. This might also be consistent with the otherwise smooth distribution of the HI in BCDs (Simpson & Gottesman 2000).

Recent observations are consistent with this picture. Taylor, Brinks & Skillman (1993) and Taylor et al. (1995) found previously unknown companions or HI clouds around half of the HII galaxies they surveyed compared to a companion fraction of 1/4 among comparable LSB dwarfs (Taylor et al. 1996). Taylor (1997) concluded from this that the incidence of companions for HII region galaxies is twice that for LSB dwarfs, implying that the companions triggered starbursts in some cases. The Fornax Cluster galaxy FCC 35 is another example of a BCD with a nearby intergalactic HI cloud (Putman et al. 1998), and NGC 1569 and IC 10 are examples of starbursts with large HI clouds in their outer parts (Stil & Israel 1998, Wilcots & Miller 1998). Méndez & Esteban (2000) observed a high fraction of irregular WR galaxies with uncatalogued low surface brightness companions and suggested these companions were responsible for the starbursts. Similar conclusions were reached by Pustilnik’s group: Pustilnik et al. (2001a) suggested that $> 80\%$ of the 86 BCDs in their survey had star formation triggered by faint visible companions or previous mergers. Pustilnik et al. (2001b) found that the BCD galaxy SBS 0335-052 is at a gas concentration in a giant HI cloud that also contains another BCD galaxy, and they suggested that the starbursts were triggered either by mutual interactions or by disturbances from a nearby giant galaxy. Pustilnik et al. (2003) also observed a faint, blue, low surface brightness dwarf within 11 kpc of the BCD galaxy HS 0822+3542, which was formerly thought to be isolated. Similarly,

Bravo-Alfaro et al. (2004) suggested that the BCD galaxy Haro 4 was interacting with the nearby spiral Haro 26. Sometimes the evidence for an interaction is indirect. For example, the warp and disturbed velocity field (Côté, Carignan & Freeman 2000) of the BCD galaxy NGC 625 suggested a recent interaction to Cannon et al. (2003). Östlin et al. (2001) also found irregular $H\alpha$ velocity fields and secondary dynamical components in the 6 BCDs they studied, and suggested these galaxies had mergers with gas-rich dwarfs or massive gas clouds.

Considering these recent discoveries, it is not surprising that BCD companions were hard to observe: most turn out to be very faint. For example, Telles & Maddox (2000) did not find a significant incidence of companions to HII galaxies in a plate-scanned survey of galaxies down to 20.5 mag in B-band, where the catalog was 90%-95% complete. The companions that are now implicated in BCD interactions are usually fainter than this limit, and fainter than our limit in Fig. 14. The faintness of triggering companions is probably reasonable, though. Most galaxies are dwarfs, so the most likely object to perturb any given galaxy is a dwarf. For large galaxies, these dwarf perturbations are indeed common but they do very little to enhance the star formation rate and gas concentration in the large galaxy. But for small galaxies, even a dwarf or HI cloud interaction can be significant, leading to angular momentum redistribution, mass inflow, and rapid star formation in a dense core. Thus the most likely significant disturbers of small galaxies are other small galaxies or small gas clouds.

Adding to the ambiguity of BCD origins is the likelihood that some interactions occurred long ago and the BCD has been bursting on and off regularly ever since. In a study of color-magnitude diagrams of BCDs, Schulte-Ladbeck, et al.(2001) found that there were no significant star formation gaps lasting longer than a few times 100 Myr over the last Gyr of evolution. Since the gas consumption time is ~ 1 Gyr, the interactions in some cases could have started this long ago (Lynds et al. 1998; Crone et al. 2002; Östlin et al. 2003). The primary remnant of these former interactions would simply be the low specific angular momentum of the present day disk; this would continue to drive starburst episodes as long as there is gas (e.g., van Zee, Salzer, & Skillman 2001). The low specific angular momentum of BCDs could also have resulted from the last big merger (Vitvitska et al. 2002), or from an old interaction that deformed the dark matter halo into a prolate spheroid, which then drove a disk response like a bar in a barred galaxy (Bekki & Freeman 2003).

Another possibility is an evolutionary scheme between dIm and BCDs. This has been proposed by Simpson & Gottesman (2000) in an optical and HI comparison of low surface brightness dIm and BCDs. The HI in numerous dIm takes on a ring-like morphology. The formation of these giant, sometimes galaxy-sized, rings would be easiest to explain as due to a starburst in the galaxy center that blew a very large hole in the gas. The energy

requirements are reasonable for this explanation. Thus, an evolution of BCD to dIm as the gas reservoir expands and dissipates has some appeal. However, there is a problem with the lack of evidence for the presence of an aging starburst population in the center of the HI ring in at least one such system (see Simpson, Hunter, & Knezek 2004). Also, differences in the scale-length suggest that there must be some redistribution of the stellar component as well, and this leads us once again back to gravitational interactions.

5.3. Probability Distribution Functions

The high star formation rates and dense core structures of BCD galaxies (see Figures 15, 16, and 18) do not necessarily imply that the star formation processes differ much from those in Im and Sm types – only that the star formation regions crowd closer together in the BCD centers, producing smaller R_D/R_{25} and higher luminosity densities. To compare the star formation processes in a global sense, we examined the probability density functions (pdf) of H α emission for each galaxy. In a turbulent medium with isothermal density and pressure variations, as in an HII region, the gas density should have a pdf that is approximately log-normal (Ostriker, Gammie & Stone 1999; Klessen 2000; Ostriker et al. 2001; Li et al. 2003) and the column density should have a pdf that is log-normal too, although somewhat diluted by the average of unrelated density elements on the lines of sight (Padoan et al. 2000; Ostriker et al. 2001; Vázquez-Semadeni & García 2001). The width of the pdf increases with the Mach number of the turbulence (Padoan et al. 2000). For star formation triggered globally in turbulent shocks (Elmegreen 1993; see review in Mac Low & Klessen 2004), the H α emission throughout a whole galaxy might be expected to follow this turbulent pdf too. We find this to be the case for all of our galaxies.

The pdfs for the H α images of our galaxies are shown in Figure 21. We constructed them from a histogram of the H α surface brightness of individual pixels in the H α image within the region used in the ellipse photometry (Table 2). Pixels without H α emission were rejected, but no cutoff was made for positive values of noise at the low count end. The surface brightness of each pixel was normalized to the azimuthally-averaged H α surface brightness at that radius (for example, Figure 17) in order to remove the exponential disk.

Figure 21 is plotted on log-log axes so that a log-normal is an inverted parabola. All of the pdfs in fact have this shape, and they all have about the same FWHM too, although their absolute brightnesses vary from galaxy to galaxy. In some cases there is a lower cutoff in the surface brightness that limits the pdf to the upper half, but even then most pdfs resemble a log-normal in the plotted parts. Some have a slight excess at the highest surface brightness, giving the pdfs a flair on the lower right.

There is apparently no systematic difference in the $H\alpha$ surface brightness pdfs for the various types of galaxies. The BCD pdfs look about the same as the Im and Sm pdfs. This implies that the Mach numbers of the turbulence in the ionized gas components are about the same, even though the areal densities of star formation are much higher in the BCDs. We conclude that the individual star formation regions are not intrinsically different in the various galaxy types, only that the regions are crowded more closely together in the BCDs. This crowding is not without consequences – it can lead to higher pressures and perhaps more massive clusters in proportion to the total star formation rate by the size of sample effect. But the expansion and turbulent speeds in BCD HII regions are not significantly higher than in other galaxies, and therefore the balance between pressurized triggering and spontaneous instabilities as causes of star formation is probably not much different either.

We are deeply grateful to Ralph Nye who did a great job making and keeping the Hall 1.1 m and Perkins 1.8 m telescopes and their instruments operating. We appreciate the TI CCD provided to Lowell Observatory by the National Science Foundation and another on loan from the U. S. Naval Observatory in Flagstaff. The $H\alpha$ imaging would not have been possible without filters purchased through funds provided by a Small Research Grant from the American Astronomical Society, National Science Foundation grant AST-9022046, and grant 960355 from JPL. Funding for this work was provided by the Lowell Research Fund and by the National Science Foundation through grants AST-0204922 to DAH and AST-0205097 to BGE.

Some of the observations presented here benefited from the Fabry-Perot focal reducer that was built by Ohio State University, and we appreciate the effort of M. Wagner to keep it working. We also wish to thank Emily Bowsher for geometrically matching the $H\alpha$ images to the V-band images for some of the galaxies as part of the 2003 Research Experiences for Undergraduates program of Northern Arizona University funded by the National Science Foundation through grant 9988007. This research has made use of the NASA/IPAC Extragalactic Database (NED) which is operated by the Jet Propulsion Laboratory, California Institute of Technology, under contract with the National Aeronautics and Space Administration.

A. Spectrophotometry of nebulae

Spectrophotometric observations with large apertures were obtained of several HII regions in nearby galaxies in 1981 October and December. We used the cooled dual-beam Intensified Reticon Scanner (IRS) mounted on the No. 1 0.9 m telescope at Kitt Peak Na-

tional Observatory. We used three gratings to cover from 3500 Å to 7450 Å with 4.5 Å spectral resolution. These observations were part of a program to observe stars for a stellar library, and the instrumentation, observations, and data reductions are discussed in more detail by Jacoby, Hunter, & Christian (1984). In Table 5 we present integrated spectrophotometry of the major emission-lines measured from spectra of H II regions observed at that time. The H α emission from NGC 604 was used to calibrate the H α images presented in this paper.

B. Determining the Star Formation Rate from $L_{H\alpha}$

Here we outline the derivation of the formula that we used to convert $L_{H\alpha}$ to the star formation rate in solar-masses per year. There are three quantitative assumptions that enter the derivation. First, we assume that when stars form from a gas cloud, the number of stars is a power law that depends on the mass of the star. That is, the number of stars formed of mass m is given by

$$\Phi(m) = Am^\gamma, \quad (\text{B1})$$

where the power law index γ is related to the “slope of the stellar initial mass function” Γ as $\Gamma = \gamma + 1$. Here we assume the Salpeter (1955) slope Γ of -1.35 .

Second, we assume an upper stellar mass limit of $100 M_\odot$. We know that stars as massive as $150 M_\odot$ are found in very rich star-forming regions (Massey & Hunter 1998), but they are relatively rare, and integrating the stellar IMF to $100 M_\odot$ is consistent with the vast majority of star-forming regions found in galaxies. We also assume that the lower stellar mass limit is $0.1 M_\odot$.

Third, we assume an efficiency factor η of $2/3$ for the absorption of ionizing photons by the nebula (Gallagher, Hunter, & Tutukov 1984). That is, $1/3$ of the ionizing photons emitted by massive stars in H II regions are absorbed by dust or escape the nebula, and $2/3$ of the emitted photons result in H II.

The number of ionizing photons N_L per second implied by the flux from a nebula is

$$N_L = \frac{L_{H\beta}}{h\nu_{H\beta}} \left(\frac{\alpha_B}{\alpha_{H\beta}} \right), \quad (\text{B2})$$

where $h\nu_{H\beta}$ is the energy of the H β photon and α_B and $\alpha_{H\beta}$ are the recombination coefficients for Case B recombination. α_B is given in Table 2.1 and $\alpha_{H\beta}$ in Table 4.4 of Osterbrock (1974). Table 4.4 also gives the ratio of the line intensity of H α to H β . Taking values for a nebular temperature of 10^4 K and density of 10^2 cm^{-3} , we have

$$N_L = 7.37 \times 10^{11} L_{H\alpha} \text{ photons s}^{-1}. \quad (\text{B3})$$

Therefore, from the integrated $L_{H\alpha}$ of the galaxy, we know the total number of ionizing photons required to ionize all of the H II regions, and, if we account for losses, we know the total number of ionizing photons N_L^G , in photons per second, being produced by massive stars in the galaxy:

$$N_L^G = \frac{7.37 \times 10^{11}}{\eta} L_{H\alpha} \text{ photons s}^{-1}. \quad (\text{B4})$$

The ionized gas is produced by stars with masses $18 M_\odot$ to $100 M_\odot$. The number of stars between $18 M_\odot$ and $100 M_\odot$ is, therefore,

$$n_{18}^{100} = \frac{N_L^G}{\langle N_L^* \rangle} = \frac{7.37 \times 10^{11} L_{H\alpha} / \eta}{\langle N_L^* \rangle}, \quad (\text{B5})$$

where $\langle N_L^* \rangle$ is the average number of ionizing photons produced per star. The number of stars between $18 M_\odot$ and $100 M_\odot$ is also given by the IMF:

$$n_{18}^{100} = \int_{18}^{100} A m^\gamma dm \quad (\text{B6})$$

and the total mass in stars M_* is given by

$$M_* = \int_{0.1}^{100} A m^\gamma m dm = \frac{n_{18}^{100}}{100^\Gamma - 18^\Gamma} \left(\frac{\Gamma}{\Gamma + 1} \right) (100^{\Gamma+1} - 0.1^{\Gamma+1}). \quad (\text{B7})$$

Thus,

$$M_* = 432 n_{18}^{100} M_\odot. \quad (\text{B8})$$

To put this altogether, we need the weighted average $\langle N_L^* \rangle$ output per star, where we weight by the IMF and by the Hydrogen-burning lifetime of the star. N_L^* is higher the more massive the star is, but the number of stars go down and the lifetime is shorter as the mass goes up. We have used the data compiled by Panagia (1973) to determine N_L^* as a function of the mass of the star. Below a mass of $18 M_\odot$ N_L^* drops precipitously, so we consider only stars with masses greater than or equal to $18 M_\odot$ as contributing to the ionization of the H II regions. A fit to the data of Panagia yields

$$\log N_L^* = \begin{cases} 44.129 + 3.276 \log m & 18 - 41 M_\odot \\ 47.170 + 1.417 \log m & \geq 41 M_\odot \end{cases}$$

We use the data of Schaerer et al. (1993) for the Hydrogen-burning lifetimes of massive stars at a $Z = 0.008$, a metallicity representative of many Im galaxies. A parameterization of the lifetime $t_{ms}(m)$ as function of the mass of the star is given by

$$\log t_{ms}(m) = \begin{cases} 8.475 - 1.160 \log m & 15 - 33 M_\odot \\ 7.472 - 0.501 \log m & \geq 33 M_\odot \end{cases}$$

where $t_{ms}(m)$ is in years. The IMF- and $t_{ms}(m)$ -weighted average $\langle N_L^* \rangle$ is given by

$$\langle N_L^* \rangle = \frac{\int_{18}^{100} N_L^*(m) t_{ms}(m) A m^\gamma dm}{\int_{18}^{100} A m^\gamma dm} = 2.52 \times 10^{63} \text{ photons}, \quad (\text{B9})$$

now integrated over the lifetimes of these stars. If we convert N_L^G from photons s^{-1} to photons yr^{-1} , we have the star formation rate \dot{M}

$$\dot{M} = 5.96 \times 10^{-42} L_{\text{H}\alpha} M_\odot \text{yr}^{-1}. \quad (\text{B10})$$

This star formation rate formula differs from others we have used in the past. It yields \dot{M} that are a factor of 1.2 lower than rates given by the formula of Hunter & Gallagher (1986) and 1.8 times lower than those of Gallagher et al. (1984). This formulation yields star formation rates that are 14% higher than those used by Kennicutt (1998), a factor of 10 lower than those determined by Gil de Paz et al. (2000), and 40% higher than numbers determined by Brinchmann et al. (2004) for the integrated galactic mass of a typical galaxy in our sample (their Figure 7).

Table 1. Galaxy Sample.

Galaxy	Other Names ^a	Type ^b	D (Mpc)	Ref ^c	E(B–V) _f ^d	Nearest Neighbor ^f		
						Δd (kpc)	ΔV_r (km/s)	Neighbor
Im Galaxies:								
A1004+10	PGC 29428, UGC 5456,	I0?	6.5	...	0.01	570	+13	UGC 5288 (Sdm:)
	IRASF10046+1036			...				
A2228+33	PGC 69019, UGC 12060, IRASF22282+3334	IBm	16.9	...	0.01	1545	–98	NGC 7320 (Sd)
CVnIdwA	UGCA 292	Im?	4.1	15	0.01	260	+2	UGC 7605 (Im)
D508-2	LSBC F508-V01	Im	29.9	...	0.00	2260	–103	KISSB 109 (-)
D575-5	LSBC F575-03	dI	6.2	...	0.03	730	–5	IC 798 (E0)
D634-3		dI	3.2	...	0.03	920	–17	DDO 70 (Im)
D646-8		Im	31.7	...	0.01	2110	–113	UGC 8114 (Sc)
DDO 9	PGC 4202, UGC 731, A0107+49	Im:	12.5	...	0.18	810	+1	NGC 278 (Sb)
DDO 22	PGC 9702, UGC 2014, A0229+38	Im:	10.5	...	0.05	400	+13	DDO 24 (Im)
DDO 24	PGC 9759, UGC 2034, A0230+40	Im	10.8	...	0.05	400	–13	DDO 22 (Im:)
DDO 25	PGC 9726, UGC 2023, A0230+33, IRASF02302+3316	Im:	11.0	...	0.09	400	–6	NGC 959 (Sdm:)
DDO 26	PGC 9808, UGC 2053, A0231+29	Im	17.3	...	0.09	730	–42	NGC 1012 (S0/a)
DDO 27	PGC 10117, UGC 2162, A0237+01	IB(s)m	18.4	...	0.01	2750	+26	NGC 1073 (Sc)
DDO 33	PGC 16030, UGC 3144, A0441+74	IBm	27.4	...	0.14	1580	+75	KUG0406+748 (S0)
DDO 34	PGC 16059, UGC 3174, A0446+00	IAB(s)m:	9.2	...	0.08	920	+47	NGC 1637 (Sc)
DDO 35	PGC 16644, UGC 3234, A0500+16	Im:	21.1	...	0.38
DDO 38	PGC 17445, UGC 3317, A0527+73	Im	21.2	...	0.12	1525	–97	KUG0539+735 (Sa)
DDO 39	PGC 18121, UGC 3371, A0549+75, Mailyan 011	Im:	14.7	...	0.12	825	–24	Mrk 5 (I?)
DDO 40	PGC 20116, UGC 3647, A0700+56, IRASF07007+5635	IBm	22.3	...	0.04	1080	+55	UGC 3574 (Scd)
DDO 43	PGC 21073, UGC 3860, A0724+40, KIG 0190	Im	5.5	...	0.05	270	+7	DDO 46 (Im)
DDO 46	PGC 21585, UGC 3966, A0738+40	Im	5.5	...	0.05	270	–7	DDO 43 (Im)
DDO 47	PGC 21600, UGC 3974, A0739+16	IB(s)m	5.2	16	0.02	1060	+42	UGC 3755 (Im)
DDO 50	PGC 23324, UGC 4305, A0813+70, Holmberg II, VII Zw223, KIG 0239, KUG 0814+708,	Im	3.4	14	0.02	110	+1	UGC 4483 (Im:)

Table 1—Continued

Galaxy	Other Names ^a	Type ^b	D (Mpc)	Ref ^c	E(B–V) _f ^d	Nearest Neighbor ^f		
						Δd (kpc)	ΔV_r (km/s)	Neighbor
DDO 52	IRASF08140+7052 PGC 23769, UGC 4426, A0825+42	Im:	6.0	...	0.03	880	+46	NGC 2537A (Sc)
DDO 53	PGC 24050, UGC 4459, A0829+66, VIIZw238, VV 499, IRASF08295+6621	Im	3.6	14	0.03	520	–16	NGC 2976 (Sc)
DDO 63	PGC 27605, Holmberg I, UGC 5139, KDG 057, A0936+71, Mailyan 044	IAB(s)m	3.8	14	0.01	620	–30	M81dwA (Im)
DDO 64	PGC 28317, UGC 5272, A0947+31, KUG 0947+317, IRASF09474+3143	Im	7.4	...	0.01	290	+15	UGC 5209 (Im)
DDO 68	PGC 28714, UGC 5340, A0953+29, VV 542	ImP:	7.0	...	0.01	235	–5	UGC 5427 (Sdm:)
DDO 69	PGC 28868, UGC 5364, A0956+30, Leo A, Leo III	IBm	0.8	5	0.00	800	–19	Milky Way (Sbc)
DDO 70	PGC 28913, UGC 5373, A0957+05, Sextans B, KIG 0388	IB(s)m	1.3	22	0.01	300	–16	Leo I (dSph)
DDO 75	PGC 29653, UGCA 205, A1008–04, Sextans A, IRASF10085–0427	IB(s)m	1.3	6	0.02	430	–23	DDO 70 (Im)
DDO 86	PGC 32048, UGC 5846, A1041+60, Mailyan 057	Im	16.9	...	0.00	860	–9	NGC 3359 (Sc)
DDO 87	PGC 32405, UGC 5918, KDG 072, A1046+65, VIIZw347	Im:	6.7	...	0.00	760	+10	UGC 5423 (Im)
DDO 99	PGC 37050, UGC 6817, A1148+39	Im	4.1	...	0.00	390	+2	NGC 4244 (Scd:)
DDO 101	PGC 37449, UGC 6900, A1153+31	Im:	9.0	...	0.01	370	–10	Mrk 757 (S0?)
DDO 105	PGC 37689, UGC 6955, A1155+38	IB(s)m:	14.3	...	0.00	395	+14	NGC 3930 (Sc)
DDO 115	PGC 39142, UGC 7254, IC 3059	Im:	3.2	...	0.00	430	–28	NGC 4222 (Sc)
DDO 120	PGC 39918, UGC 7408, A1218+46	IAm	8.0	...	0.00	490	+28	NGC 4460 (S0?)
DDO 125	PGC 40904, UGC 7577, A1225+43	Im	2.5	22	0.00	385	–4	DDO 168 (Im)
DDO 126	PGC 40791, UGC 7559, A1224+37	IBm	4.9	15	0.00	270	+11	HS1213+3636B (dS)
DDO 133	PGC 41636, UGC 7698, A1230+31	Im	6.1	20	0.00	410	–24	CVnIdwA (Im)
DDO 143	PGC 42901, UGC 7916, VV 127, IZw42, A1242+34	Im	9.8	...	0.00	710	+39	NGC 4656 (Gpair)
DDO 154	PGC 43869, UGC 8024,	IBsm	4.3	20	0.01	820	–43	DDO 133 (Im)

Table 1—Continued

Galaxy	Other Names ^a	Type ^b	D (Mpc)	Ref ^c	E(B–V) _f ^d	Nearest Neighbor ^f		
						Δd (kpc)	ΔV_r (km/s)	Neighbor
DDO 155	NGC 4789A PGC 44491, UGC 8091, GR8, A1256+14, VV 558, LSBC D646-07	Im	2.2	3,26	0.01	220	–8	IC 809 (E)
DDO 165	PGC 45372, UGC 8201, A1304+67, IIZw499, Mailyan 82	Im	4.8	10	0.01	590	–37	NGC 4236 (Sdm)
DDO 167	PGC 45939, UGC 8308, A1311+46	Im	4.2	15	0.00	430	+28	DDO 168 (Im)
DDO 168	PGC 46039, UGC 8320, A1312+46	IBm	3.5	...	0.00	410	+26	UGC 8215 (Im)
DDO 169	PGC 46127, UGC 8331, A1313+47	IAm	5.3	...	0.00	660	–42	UGC 8215 (Im)
DDO 171	PGC 46382, A1316–08	Im	18.7	...	0.02	1180	+23	NGC 4948 (Sdm)
DDO 183	PGC 49158, UGC 8760, A1348+38	Im	5.1	20	0.00	330	+8	DDO 181 (Im)
DDO 185	PGC 49448, UGC 8837, A1352+54, Holmberg IV	IB(s)msp	4.0	...	0.00	745	+6	UGC 9240 (Im)
DDO 187	PGC 50961, UGC 9128, A1413+23	Im	2.5	2	0.00	920	+39	UGC 8760 (Sdm)
DDO 210	PGC 65367, Aquarius Dwarf, A2044–13	IB(s)m	0.9	17	0.03	900	–23	Milky Way (Sbc)
DDO 215	PGC 69415, UGCA 433, A2236–05	Im:	14.7	...	0.03	920	+59	NGC 7351 (S0)
DDO 216	PGC 71538, UGC 12613, A2326+14, Peg DIG, Pegasus Dwarf	Im	0.9	1,8	0.02	450	+117	M31 (Sb)
DDO 220	PGC 72494, UGC 12791, A2346+25	Im:	14.9	...	0.03	690	–41	NGC 7741 (Scd)
F533-1		Im	22.7	...	0.11	640	–35	UGC 12029 (Im:)
F563-V1	LSBC D563-03	dI	58.0	...	0.03	1440	+89	NGC 2667 (-)
F563-V2	LSBC D563-02	Irr	71.0	...	0.04	840	+48	UGC 4657 (Sb)
F564-V3	LSBC D564-08	dI	6.2	...	0.02	480	+10	F565-V1 (dI)
F565-V1	LSBC D565-06	dI	6.3	...	0.04	480	–10	F564-V3 (dI)
F565-V2		dI	55.0	...	0.02	960	+49	NGC 2916 (Sb?)
F608-1	PGC 1124, UGC 159	Im:	17.7	...	0.02	1040	+31	UGC 31 (Im)
F615-1		dI	13.5	...	0.07	565	–34	UGC 2168 (Im:)
F651-2		dI/Im	28.1	...	0.01	800	+22	CGCG076–047 (-)
F721-V2	LSBC D721-10	dI	18.6	...	0.01	730	+9	UGC 8995 (Sdm)
F750-V1		Irr	16.7	...	0.04	1740	–66	UGC 17 (Sm:)
IC 10	PGC 1305, UGC 192, IRAS00177+5900	IBm?	1.0	11,21	0.75	250	–48	M31 (Sb)
IC 1613	PGC 3844, UGC 668, DDO 8, IRASF01024+0153	IB(s)m	0.7	7	0.00	400	–60	M33 (Sc)

Table 1—Continued

Galaxy	Other Names ^a	Type ^b	D (Mpc)	Ref ^c	E(B–V) _f ^d	Nearest Neighbor ^f		
						Δd (kpc)	ΔV_r (km/s)	Neighbor
IC 4662	PGC 60851, He2-269, IRASF17422–6437, HIPASS J1747-64, ESO 174212–6437.3	IBm	3.0	...	0.07
LGS 3	PGC 3792, Pisces dwarf	I?	0.6	23	0.04	280	+23	M31 (Sb)
M81dwA	PGC 23521, KDG 052	I?	3.6	7	0.02	370	–13	NGC 2366 (Im)
NGC 1156	PGC 11329, UGC 2455, KIG 0121, VV 531, IRASF02567+2502	IB(s)m	7.8	13	0.17	590	+36	LEDA169969 (-)
NGC 1569	PGC 15345, UGC 3056, Arp 210, VIIZw16, IRASF04260+6444	IBm	2.5	25	0.51	500	–23	Cam A (Irr)
NGC 2101	PGC 17793, IRASF05452–5206	IB(s)mP	15.2	...	0.00	680	–43	NGC 2104 (Scd)
NGC 2366	PGC 21102, UGC 3851, DDO 42, IRASF07234+6917	IB(s)m	3.2	14	0.04	520	+31	NGC 2403 (Scd)
NGC 3413	PGC 32543, UGC 5960, CG 0790, KUG 1048+330, IRASF10485+3301	S0sp	9.6	...	0.00	480	–16	DDO 84 (Im)
NGC 3738	PGC 35856, UGC 6565, Arp 234, KUG 1133+548, IRASF11330+5448	Im	4.9	15	0.00	490	–19	NGC 4068 (Im)
NGC 3952	PGC 37285, IRASF11511–0343	IBm:sp	22.4	...	0.01	235	–13	IC 2969 (Sbc)
NGC 4163	PGC 38881, NGC 4167, UGC 7199, CG 0891, KUG 1209+364	IAm	2.8	...	0.00	610	+31	DDO 125 (Im)
NGC 4214	PGC 39225, UGC 7278, KUG 1213+366, IRASF12131+3636	IAB(s)m	2.9	19	0.00	110	–7	DDO 113 (Im)
NGC 6822	PGC 63616, IC 4895, DDO 209, Barnard’s Galaxy, IRASF19420–1450	IB(s)m	0.5	9	0.22	500	+44	Milky Way (Sbc)
SagDIG	PGC 63287, Lowal’s Object, ESO 192708–1747.0	IB(s)m:	1.1	12,18	0.14	1100	+8	Milky Way (Sbc)
UGC 199	PGC 1336	Im:	29.8	...	0.04	2280	–137	UGC 132 (Sdm)
UGC 5209	PGC 27935	Im	7.8	...	0.00	250	+13	UGC 5196 (Im)
UGC 8011	PGC 43654, VIIZw216, LSBC D575-02	Im	11.6	...	0.04	1580	+87	F574-10 (Sd)
UGC 8055	PGC 44102	Im	8.5	...	0.00	620	+34	NGC 4173 (Sd)
UGC 8276	PGC 45840	Im:	13.3	...	0.00	480	–17	UGC 8285 (Sdm)
UGC 8508	PGC 47495, IZw60	IAM	2.6	...	0.00	670	+6	UGC 7242 (Scd:)
UGC 10140	PGC 56745, LSBC D584-02	Im:	41.9	...	0.02	1570	–102	UGCA 411 (Pec)
UGC 10281	PGC 57522, LSBC D656-02	Im:	18.3	...	0.03
WLM	PGC 143, UGCA 444, DDO 221, A2359–15,	IB(s)m	1.0	4,24	0.02	900	+58	M33 (Sc)

Table 1—Continued

Galaxy	Other Names ^a	Type ^b	D (Mpc)	Ref ^c	E(B–V) _f ^d	Nearest Neighbor ^f		
						Δd (kpc)	ΔV_r (km/s)	Neighbor
0467–074	Wolf-Lundmark-Melott 2dFGRS N293Z129, ISI96 1032–0121, APMUKS(BJ) B103250.07–012138.4	Irr	107.9	...	0.03	2020	–113	2dFGRSN294Z233 (-)
1397–049	ISI96 1051+0227, APMUKS(BJ) B105147.14+022734.5	Irr	118.7	...	0.02
BCD Galaxies:								
Haro 3	PGC 32103, UGC 5860, NGC 3353, Mrk 35, IRASF10422+5613	Sb?p	15.5	...	0.00	1880	–122	UGC 5848 (Sm)
Haro 4	PGC 33486, UGCA 225, Mrk 36, A1102+29, KUG 1102+294, CG 82, IRASF11022+2924	BCD	9.5	...	0.00	560	+35	NGC 3486 (Sc)
Haro 8	PGC 39628, UGC 7354, Mrk 49, A1216+04, Mrk 1318, VCC 324, IRASF12166+0407	Ep:	22.2	...	0.00	670	+10	NGC 4266 (Sa?)
Haro 14	PGC 2675, UGCA 010, NGC 244, VV 728, IRASF00432–1552	S0p?	15.1	...	0.01
Haro 20	PGC 12922, UGCA 073, A0325–17, IRASF03260–1735	E+?	27.6	...	0.03	670	+7	UGCA 71 (Sd)
Haro 23	PGC 29347, UGCA 201, A1003+29, CG 0050, IRASF10034+2911	S?	20.2	...	0.01	540	+15	UGC 5478 (Im)
Haro 29	PGC 40665, UGCA 281, Mrk 209, A1223+48, IZw36	S?	5.4	...	0.00	410	–16	NGC 4144 (Sed?)
Haro 36	PGC 43124, UGC 7950, A1244+51	Im	9.0	...	0.00	530	–34	DDO 150 (Sm:)
Haro 38	PGC 47938, UGC 8578, A1333+29, KUG 1333+294	S?	13.7	...	0.00	1680	+105	Mrk 67 (Im)
Haro 43	PGC 52193	S?	30.5	...	0.01
HS0822+3542		BCG	10.9	...	0.04
Mrk 5	PGC 19459, UGCA 130, A0635+75, KUG 0635+756, IRASF06353+754	I?	14.3	...	0.08	825	+24	DDO 39 (Im:)

Table 1—Continued

Galaxy	Other Names ^a	Type ^b	D (Mpc)	Ref ^c	E(B–V) _f ^d	Nearest Neighbor ^f		
						Δd (kpc)	ΔV_r (km/s)	Neighbor
Mrk 16	PGC 24949, UGCA 146, A0847+73, IRASF08479+7322	...	37.6	...	0.02	1050	–58	NGC 2634 (E1:)
Mrk 32	PGC 30715, UGCA 211, A1023+56	P	13.8	...	0.00	610	–12	UGC 5848 (Sm:)
Mrk 67	PGC 48501, UGCA 372, KUG 1339+307, A1339+30, IRASF13396+3046	BCD	15.5	...	0.00	1680	–105	Haro 38 (S?)
Mrk 178	PGC 35684, UGC 6541, A1130+49	Im	3.9	15	0.00	410	–20	NGC 3741 (Im)
Mrk 408	PGC 28169, A0945+33, CG 0289, KUG0945+331, IRASF09451+3306	...	23.3	...	0.00	300	+6	UGC 5282 (Sm:)
Mrk 600	PGC 10813, A0248+04, IRASZ02484+0414	SBb/BCD	15.7	...	0.05	370	+17	UGC 2275 (Sm)
Mrk 757	PGC 38277, KUG1202+311, CG0150	S0?	8.9	...	0.01	200	–12	NRGb181.11 (-)
NGC 1705	PGC 16282, IRASF04530-5326	SA0-P:	5.1	27	0.04	990	–34	PGC 72675 (Im)
NGC 6789	PGC 63000, UGC 11425	Im	3.6	...	0.08
SBS1415+437	PGC 51017, CG 0389	BCG	10.9	...	0.00	920	+54	NGC 5608 (Im)
UGCA 290	Arp211, VV042b	...	2.8	20	0.00	230	–5	PGC 41314 (Im)
IZw115	PGC 55381, UGC 9893, VV 720, A1531+46, KIG 686	P	12.3	...	0.01
VIIZw403	PGC 35286, UGC 6456, A1124+79, VV 574, IRASF11246+7916	Pec	4.4	22	0.02	900	–32	KDG073 (Im)
Zw2335	PGC 71938, UGCA 441, A2335+29, Barbon’s Galaxy, Mrk 328, KIG 1031, IRASF23352+2951	E?	24.1	...	0.05
Sm Galaxies:								
DDO 18	PGC 8332, UGC 1670, A0208+06	Sm	25.4	...	0.04	280	–18	UGC 1677 (Sd)
DDO 48	PGC 22369, UGC 4121, A0754+58	Sm:	17.8	...	0.03	1160	–53	NGC 2549 (S0)
DDO 54	PGC 25679, UGC 4797, A0905+06	Sm:	18.0	...	0.03	810	+46	NGC 2775 (Sab)
DDO 88	PGC 32226, UGC 5889, NGC 3377A	SAB(s)m	7.4	...	0.01	30	+1	LEDA 83341 (Im)
DDO 122	PGC 40367, UGC 7490, Mailyan 073, IRASF12223+7037	SAm	9.2	...	0.00	370	–7	UGC 7748 (Sdm:)
DDO 135	PGC 41746, UGC 7713,	SAB(s)m	3.4	...	0.02	250	+10	VCC 0413 (Im)

Table 1—Continued

Galaxy	Other Names ^a	Type ^b	D (Mpc)	Ref ^c	E(B–V) _f ^d	Nearest Neighbor ^f		
						Δd (kpc)	ΔV_r (km/s)	Neighbor
DDO 150	NGC 4523, VCC 1524, IRASF12313+1526 PGC 43255, UGC 7971,	Sm:	8.5	...	0.00	530	+34	Haro 36 (Im)
DDO 173	NGC 4707, IZw43 PGC 46563, UGC 8385, A1318+10	SABm	16.9	...	0.00	650	+23	UGC 8298 (Im)
DDO 180	PGC 48179, A1335–09, IRASF13355–0932	SB(s)m	18.8	...	0.03	1640	+7	DDO 171 (Im)
DDO 204	PGC 57678, UGC 10310, A1614+47, Arp 2, IRASF16148+4710	SB(s)m	13.5	...	0.00	690	+45	HS1614+4709 (BCG?)
DDO 214	PGC 69293, A2233–03, Arp 3	SA(s)m	28.3	...	0.04	2005	+64	UGC 12151 (Im:)
DDO 217	PGC 71596, UGC 12632, A2327+40	Sm:	9.6	...	0.13	210	–7	UGC 12588 (Sdm)
F561-1		Sm	72.0	...	0.04	790	–17	[ZBS97] A50 (?)
F567-2		Sm	86.0	...	0.03	1770	–39	UGC 5598 (S)
F583-1	LSBC D584-04	Sm/Irr	37.0	...	0.03	1070	–37	NGC 6035 (Sc)
NGC 2552	PGC 23340, UGC 4325, IRASF08156+5010	SA(s)m?a	8.5	...	0.04	450	–10	NGC 2500 (Sd)
NGC 3109	PGC 29128, UGCA 194, DDO 236	SB(s)msP	1.3	22	0.04	440	+19	ESO497–G003 (Sa:)
NGC 3510	PGC 33408, UGC 6126, Haro 26, CG 80, KUG 1101+291, IRASF11010+2909	SB(s)msP	10.4	...	0.00	100	–3	UGC 6102 (Im)
UGC 5716	PGC 31081, LSBC D500-02	Sm:	18.8	...	0.00	830	+14	UGC 5588 (S?)
UGC 11820	PGC 67421	Sm	19.9	...	0.08	1600	–11	UGC 11868 (Sm)

^aThis does not include all possible identifications. Identifications were obtained from NED.

^bMorphological Hubble types are from de Vaucouleurs et al. (1991). If no type is given there, we have used types given by NED.

^cReference for the distance to the galaxy. If no reference is given, the distance was determined from V_{GSR} given by de Vaucouleurs et al. (1991) and a Hubble constant of $65 \text{ km s}^{-1} \text{ Mpc}^{-1}$.

^dForeground reddening from Burstein & Heiles (1984).

^fNearest galaxy within 1 Mpc in the plane of the sky and $\pm 150 \text{ km s}^{-1}$. Distance to the galaxy Δd was taken as a combination of apparent distance on the sky and radial distance with a Hubble constant of $65 \text{ km s}^{-1} \text{ Mpc}^{-1}$. The search used NED.

References. — (1) Aparicio 1994; (2) Aparicio, Tikhonov, & Karachentsev 2000; (3) Dohm-Palmer et al. 1998; (4) Dolphin 2000; (5) Dolphin et al. 2002; (6) Dolphin et al. 2003; (7) Freedman et al. 2001; (8) Gallagher et al. 1998; (9) Gallart, Aparicio, & Vilchez 1996; (10) Hidalgo, Marín-Franch, & Aparicio 2003; (11) Hunter 2001; (12) Karachentsev, Aparicio, & Makarova 1999; (13) Karachentsev, Musella, & Grimaldi 1996; (14) Karachentsev et al. 2002; (15) Karachentsev et al. 2003a; (16) Karachentsev et al. 2003b; (17) Lee et al. 1999; (18) Lee & Kim 2000; (19) Maiz-Apellaniz, Cieza, & Mackenty 2002; (20) Makarova et al. 1998; (21) Massey & Armandroff 1995; (22) Méndez et al. 2002; (23) Miller et al. 2001; (24) Minniti & Zijlstra 1997; (25) O’Connell et al. 1994; (26) Tolstoy et al. 1995; and (27) Tosi et al. 2001.

Table 2. Observations and photometry parameters.

Galaxy	Mos ^b	Date	Instr ^c	Exposures ^d (s)	Seeing ^e (")	Scale (")	Ellipse photometry parameters ^a					log rms $\Sigma_{H\alpha}$ ^f (ergs/s/pc ²)
							PA (°)	b/a	Step (")	Center (2000) RA DEC		
Im Galaxies:												
A1004+10	...	9703	PT,4:1,NOTI	1×1800	3.4	0.43	-33.3	0.63	9.1	10:07:19.6	10:21:47	32.48
A2228+33	...	9410	PT,FP,NCCD	2×1800	2.3	0.49	38.5	0.92	11.3	22:30:34.0	33:49:14	32.16
CVnIdwA	...	0005	HT,2048	3×1800	3.1	1.13	79.5	0.78	11.3	12:38:40.2	32:45:40	32.19
D508-2	...	0004	HT,2048	3×1800	5.0	1.13	70.6	0.76	9.1	13:04:34.3	26:46:24	32.07
D575-5	...	9605	PT,4:1,NCCD	1×2700	2.0	0.41	55.2	0.51	9.1	12:55:41.0	19:12:35	32.32
D634-3	...	0001	HT,2048	3×2700	3.7	1.13	-9.4	0.76	5.7	9:08:53.8	14:35:03	32.04
D646-8	...	0004	HT,2048	3×1800	4.5	1.13	-32.4	0.62	5.7	12:52:03.9	12:54:26	32.00
DDO 9	...	9410	PT,FP,NCCD	2×1800	2.2	0.49	87.5	0.49	11.3	1:10:43.4	49:36:02	32.24
DDO 22	...	9410	PT,FP,NCCD	1×1800	1.8	0.49	-6.6	0.38	11.3	2:32:54.1	38:40:51	32.37
DDO 24	...	9410	PT,FP,NCCD	2×2700	2.0	0.49	0.1	0.93	11.3	2:33:43.2	40:31:51	32.21
DDO 25	...	9410	PT,FP,NCCD	1×1800	2.1	0.49	-56.3	0.88	11.3	2:33:18.5	33:29:26	32.38
...	...	9502	PT,FP,NCCD	2×2700
DDO 26	...	9410	PT,FP,NCCD	3×2700	2.1	0.49	34.1	0.39	8.4	2:34:29.2	29:45:04	32.11
DDO 27	...	9410	PT,FP,NCCD	3×3000	1.8	0.49	-51.5	0.61	9.1	2:40:22.7	1:13:54	32.08
DDO 33	...	9410	PT,FP,NCCD	1×1800	2.3	0.49	-68.6	0.61	11.3	4:47:59.7	74:55:42	32.40
DDO 34	...	9502	PT,FP,NCCD	2×3000	2.1	0.49	-82.7	0.42	9.1	4:48:34.2	00:14:30	32.54
DDO 35	...	9410	PT,FP,NCCD	2×1800	2.1	0.49	62.7	0.77	11.3	5:03:24.0	16:24:18	32.27
DDO 38	...	9410	PT,FP,NCCD	1×2700	1.9	0.49	-34.5	0.66	8.4	5:33:37.0	73:43:27	32.08
DDO 39	...	9502	PT,FP,NCCD	3×2700	2.0	0.49	-43.4	0.61	11.3	5:56:34.1	75:18:57	32.11
DDO 40	...	9410	PT,FP,NCCD	1×2400	1.7	0.49	-48.3	0.78	11.3	7:04:51.2	56:31:09	32.13
DDO 43	...	9502	PT,FP,NCCD	3×3000	1.7	0.49	6.1	0.70	11.3	7:28:17.8	40:46:13	32.06
DDO 46	...	9502	PT,FP,NCCD	3×3000	1.5	0.49	83.6	0.89	11.3	7:41:26.6	40:06:39	32.09
DDO 47	C	9502	PT,FP,NCCD	2×3000	1.6	0.49	-70.4	0.51	11.3	7:41:55.3	16:48:08	32.10
...	W	9502	PT,FP,NCCD	2×3000
...	E	9502	PT,FP,NCCD	1×3000
...	N	9502	PT,FP,NCCD	2×3000
DDO 50	C	9702	PT,4:1,NOTI	1×1800	1.6	0.43	18.1	0.72	11.3	8:19:08.7	70:43:25	32.39
...	...	9702	PT,4:1,NOTI	(1× 900)
...	N	9702	PT,4:1,NOTI	1×1800
...	S	9702	PT,4:1,NOTI	1×1800
...	W	9702	PT,4:1,NOTI	1×1800

Table 2—Continued

Galaxy	Mos ^b	Date	Instr ^c	Exposures ^d (s)	Seeing ^e (")	Scale (")	Ellipse photometry parameters ^a					log rms $\Sigma_{H\alpha}$ ^f (ergs/s/pc ²)
							PA (°)	<i>b/a</i>	Step (")	Center (2000) RA DEC		
...	E	9702	PT,4:1,NOTI	1×1800
DDO 52	...	9703	PT,4:1,NOTI	2×2700	3.2	0.43	4.5	0.67	11.3	8:28:28.5	41:51:21	32.25
DDO 53	...	9504	PT,FP,NCCD	1×2200	1.9	0.49	81.0	0.51	8.4	8:34:08.0	66:10:37	32.13
DDO 63	...	0005	HT,2048	3×1800	3.2	1.13	-0.2	1.00	11.3	9:40:30.4	71:11:02	32.16
DDO 64	...	9201	PT,FP,NCCD	1×3000	2.0	0.50	-63.9	0.32	11.3	9:50:22.4	31:29:16	32.54
DDO 68	...	9201	PT,FP,NCCD	1×3000	2.3	0.50	16.5	0.50	8.4	9:56:45.8	28:49:34	32.54
DDO 69	C	9201	PT,FP,NCCD	1×3000	1.8	0.49	-64.4	0.56	17.0	9:59:25.0	30:44:42	31.77
...	N	9201	PT,FP,NCCD	2×1500
...	E	9502	PT,FP,NCCD	2×3000
...	W	9502	PT,FP,NCCD	2×3000
DDO 70	...	9703	PT,4:1,NOTI	2×1800	2.0	0.43	87.6	0.59	17.0	10:00:00.9	5:19:51	32.37
DDO 75	C	9403	PT,FP,NCCD	3×1800	2.0	0.49	41.8	0.85	13.7	10:10:59.2	-04:41:56	32.30
...	NE	9503	PT,FP,NCCD	3×1800
...	N	9503	PT,FP,NCCD	1×1800
...	W	9504	PT,FP,NCCD	3×1800
DDO 86	...	9405	PT,FP,NCCD	2×2300	2.0	0.49	71.8	0.82	11.3	10:44:29.0	60:21:58	32.35
...	PT,FP,NCCD (2× 600)
DDO 87	...	9502	PT,FP,NCCD	3×3000	2.1	0.49	76.4	0.58	11.3	10:49:34.7	65:31:46	32.10
DDO 99	...	0005	HT,2048	3×1800	3.1	1.13	51.5	0.49	11.3	11:50:52.6	38:52:41	32.13
DDO 101	...	9405	PT,FP,NCCD	2×2400	1.8	0.49	-69.4	0.69	11.3	11:55:39.4	31:31:08	32.21
DDO 105	...	9502	PT,FP,NCCD	3×3000	1.6	0.49	63.6	0.43	11.3	11:58:29.0	38:04:29	31.98
DDO 115	...	9502	PT,FP,NCCD	1×3000	1.6	0.49	8.0	0.69	9.1	12:14:55.1	13:27:39	32.06
DDO 120	...	9405	PT,FP,NCCD	3×1800	1.9	0.49	86.5	0.68	11.3	12:21:15.8	45:48:46	32.57
DDO 125	...	9605	PT,4:1,NCCD	1×2400	1.8	0.41	-46.2	0.58	8.3	12:27:41.9	43:29:34	32.36
...	...	9703	PT,4:1,NOTI	(1×1800)
DDO 126	...	9702	PT,4:1,NOTI	3×1800	1.9	0.43	-41.4	0.47	11.3	12:27:06.5	37:08:23	32.37
...	...	9802	PT,4:1,NOTI	(1×1800)
DDO 133	C	9504	PT,FP,NCCD	2×2700	2.3	0.49	-6.4	0.69	11.3	12:32:55.4	31:32:14	31.87
...	NW	9504	PT,FP,NCCD	1×2700
DDO 143	...	0005	HT,2048	3×1800	4.1	1.13	-3.5	0.31	11.3	12:44:24.9	34:23:23	32.23
DDO 154	...	9604	PT,4:1,NCCD	1×1800	2.3	0.41	45.6	0.50	11.3	12:54:06.2	27:09:03	32.31
...	...	9605	PT,4:1,NCCD	1×2700
DDO 155	...	9605	PT,4:1,NCCD	2×1800	1.7	0.41	50.6	0.71	11.3	12:58:39.8	14:13:10	32.39

Table 2—Continued

Galaxy	Mos ^b	Date	Instr ^c	Exposures ^d (s)	Seeing ^e (")	Scale (")	Ellipse photometry parameters ^a					log rms $\Sigma_{H\alpha}$ ^f (ergs/s/pc ²)
							PA (°)	<i>b/a</i>	Step (")	Center (2000) RA DEC		
DDO 165	...	9502	PT,FP,NCCD	1×2300	1.8	0.49	88.6	0.54	11.3	13:06:25.3	67:42:25	32.16
DDO 167	...	9504	PT,FP,NCCD	1×3000	2.7	0.49	-23.6	0.65	11.3	13:13:22.9	46:19:11	32.07
DDO 168	...	9502	PT,FP,NCCD	2×2400	1.7	0.49	-24.9	0.63	11.3	13:14:27.2	45:55:46	32.11
DDO 169	...	9203	PT,FP,NCCD	1×3000	2.3	0.50	-45.2	0.31	11.3	13:15:29.9	47:29:59	32.41
DDO 171	...	9703	PT,4:1,NOTI	1×1800	3.2	0.43	-29.1	0.91	11.3	13:18:41.3	-8:26:43	32.54
DDO 183	...	9201	PT,FP,NCCD	1×3000	2.2	0.50	30.6	0.35	11.3	13:50:50.9	38:01:11	32.46
DDO 185	...	9605	PT,4:1,NCCD	2×2400	2.1	0.41	19.7	0.27	11.3	13:54:44.0	53:53:46	32.38
...	...	9703	PT,4:1,NOTI	(1×1800)
DDO 187	...	9502	PT,FP,NCCD	1×3000	1.5	0.49	36.6	0.80	11.3	14:15:56.7	23:03:19	32.03
DDO 210	...	0109	KPNO4m,Mos	3× 500	1.2	0.26	-84.8	0.48	18.9	20:46:52.0	-12:50:50	...
...	...	0109	HT,2048	3×1800	32.29
DDO 215	...	9410	PT,FP,NCCD	2×1800	1.4	0.49	66.3	0.38	9.1	22:39:09.1	-4:45:36	32.23
DDO 216	...	9610	PT,4:1,NOTI	3×2700	1.8	0.43	-57.9	0.45	31.5	23:28:35.0	14:44:30	32.24
DDO 220	...	9410	PT,FP,NCCD	2×1800	2.3	0.49	83.4	0.31	9.1	23:48:49.9	26:13:14	32.20
F533-1	...	9410	PT,FP,NCCD	3×2700	1.6	0.49	-49.0	0.89	9.1	22:28:07.1	23:22:32	32.06
F563-V1	...	9611	PT,4:1,NOTI	3×2700	1.8	0.43	-23.7	0.45	4.3	8:46:37.7	18:53:23	32.23
...	...	9702	PT,4:1,NOTI	(1×2700)
F563-V2	...	9611	PT,4:1,NOTI	3×2700	2.0	0.43	-31.1	0.77	7.3	8:53:03.4	18:26:14	32.50
...	...	9702	PT,4:1,NOTI	(1×2700)
F564-V3	...	9611	PT,4:1,NOTI	2×2700	1.8	0.43	7.3	0.83	7.3	9:02:53.9	20:04:29	32.34
F565-V1	...	9502	PT,FP,NCCD	1×3000	1.3	0.49	-79.3	0.55	7.3	9:19:30.3	21:36:11	32.15
F565-V2	...	9703	PT,4:1,NOTI	3×2700	1.9	0.43	0.0	0.48	4.3	9:37:30.1	21:45:37	32.13
F608-1	...	9410	PT,FP,NCCD	3×2700	1.7	0.49	33.5	0.69	7.3	0:17:15.9	17:31:17	32.05
F615-1	...	9410	PT,FP,NCCD	3×2700	2.0	0.49	39.7	0.50	7.3	2:43:25.8	16:43:56	32.11
F651-2	...	9605	PT,4:1,NOTI	2×2700	2.4	0.43	-40.4	0.62	7.3	14:46:24.2	14:12:40	32.48
F721-V2	...	9704	PT,4:1,NOTI	2×2700	1.8	0.43	-81.6	0.56	6.1	13:55:58.4	8:59:41	32.21
F750-V1	...	9410	PT,FP,NCCD	3×2700	1.8	0.49	22.0	0.53	6.1	23:54:19.4	10:56:49	32.07
IC 10	...	9211	PT,FP,NCCD	1×3000	2.2	0.49	-38.3	0.78	17.0	00:20:21.9	59:17:39	32.06
IC 1613	NE	9211	PT,FP,NCCD	1×3000	2.7	0.49	70.6	0.81	69.5	1:04:49.2	2:07:48	31.71
...	SE	9211	PT,FP,NCCD	1×3000
...	NW	9211	PT,FP,NCCD	1×3000
...	SW	9211	PT,FP,NCCD	1×3000
IC 4662	...	9909	CTIO1.5m	3×1200	1.2	0.43	-64.1	0.71	13.0	17:47:08.2	-64:38:35	32.56

Table 2—Continued

Galaxy	Mos ^b	Date	Instr ^c	Exposures ^d (s)	Seeing ^e (")	Scale (")	Ellipse photometry parameters ^a					log rms $\Sigma_{H\alpha}$ ^f (ergs/s/pc ²)
							PA (°)	<i>b/a</i>	Step (")	Center (2000) RA DEC		
LGS 3	...	9212	PT,FP,NCCD	1×3000	2.1	0.49	-3.4	0.51	17.0	1:03:55.2	21:52:39	32.01
M81dwA	...	0004	HT,2048	3×1800	3.7	1.13	85.8	0.73	6.8	8:23:57.2	71:01:51	32.17
NGC 1156	...	9502	PT,FP,NCCD	1×3000	1.8	0.49	41.7	0.86	11.3	2:59:41.9	25:14:21	32.38
NGC 1569	...	9211	PT,FP,NCCD	1×3000	2.3	0.49	-58.9	0.55	12.6	4:30:49.8	64:50:51	32.00
NGC 2101	...	9301	CTIO1.5m	1×1500	1.6	0.43	75.0	0.56	10.2	5:46:24.0	-52:05:22	31.60
NGC 2366	C	9403	PT,FP,NCCD	1×1800	2.3	0.49	32.6	0.42	29.4	7:28:48.8	69:12:22	32.19
...	N	9502	PT,FP,NCCD	2×3000
...	N2	9502	PT,FP,NCCD	2×3000
...	S	9502	PT,FP,NCCD	1×3000
...	W	9502	PT,FP,NCCD	2×3000
...	E	9503	PT,FP,NCCD	3×1800
NGC 3413	...	9201	PT,FP,NCCD	1×1800	2.0	0.50	-2.4	0.66	11.3	10:51:20.8	32:45:57	32.71
...	...	9802	PT,4:1,NOTI	(1× 900)
NGC 3738	...	9504	PT,FP,NCCD	1×1800	2.6	0.49	-0.4	1.00	11.3	11:35:49.0	54:31:23	32.18
NGC 3952	...	9703	PT,4:1,NOTI	2×1800	1.8	0.43	78.7	0.37	11.3	11:53:40.5	-3:59:50	32.53
NGC 4163	...	0004	HT,2048	4×1800	3.6	1.13	17.9	0.64	11.3	12:12:09.2	36:10:14	32.13
NGC 4214	C	9703	PT,4:1,NOTI	1×900	2.0	0.43	16.1	0.91	14.7	12:15:39.2	36:19:38	32.38
...	N	9703	PT,4:1,NOTI	2×1800
...	S	9703	PT,4:1,NOTI	2×1400
...	E	9703	PT,4:1,NOTI	2×1800
...	SE	9703	PT,4:1,NOTI	2×1800
...	W	9703	PT,4:1,NOTI	2×1800
...	...	9504	PT,FP,NCCD	(2×1800)
NGC 6822	...	0206	HT,2048	4×1800	3.2	1.13	8.0	0.80	42.8	19:44:56.4	-14:48:01	32.15
SagDIG	...	0005	HT,2048	3×1800	3.9	1.13	87.7	0.53	27.0	19:30:00.6	-17:40:56	32.22
UGC 199	...	9611	PT,4:1,NOTI	4×2700	1.7	0.43	-72.2	0.41	9.1	0:20:52.0	12:51:23	32.61
UGC 5209	...	9703	PT,4:1,NOTI	3×1800	2.3	0.43	-24.3	0.82	7.3	9:45:04.1	32:14:20	32.44
UGC 8011	...	9704	PT,4:1,NOTI	2×1800	3.2	0.43	35.6	0.46	11.3	12:52:22.4	21:37:51	32.41
UGC 8055	...	9703	PT,4:1,NOTI	3×1800	3.1	0.43	52.6	0.60	6.1	12:56:04.3	3:48:47	32.58
UGC 8276	...	9704	PT,4:1,NOTI	2×1800	2.6	0.43	-46.4	0.53	6.1	13:12:06.3	5:28:34	32.40
UGC 8508	...	9703	PT,4:1,NOTI	1×1800	3.2	0.43	-60.4	0.54	11.3	13:30:44.9	54:54:29	32.42
UGC 10140	...	9704	PT,4:1,NOTI	2×1800	2.0	0.43	58.6	0.65	6.1	16:01:49.7	18:43:20	32.43
UGC 10281	...	9703	PT,4:1,NOTI	2×1800	1.7	0.43	35.1	0.58	9.1	16:13:20.6	17:11:37	32.32

Table 2—Continued

Galaxy	Mos ^b	Date	Instr ^c	Exposures ^d (s)	Seeing ^e (")	Scale (")	Ellipse photometry parameters ^a					log rms $_{\Sigma H\alpha}$ ^f (ergs/s/pc ²)
							PA (°)	b/a	Step (")	Center (2000) RA DEC		
WLM	...	9211	PT,FP,NCCD	1×3000	2.5	0.49	-2.5	0.44	56.7	0:01:59.2	-15:27:41	32.06
...	...	9211	PT,FP,NCCD	1×3000
0467-074	...	9802	PT,4:1,NOTI	1×1800	2.4	0.43	49.6	0.85	4.3	10:35:23.1	-1:37:10	32.37
1397-049	...	9805	PT,2048	2×1800	2.2	0.61	66.1	0.74	3.0	10:54:21.6	2:11:35	31.00
...	...	9802	PT,4:1,NOTI	2×1800
BCD Galaxies:												
Haro 3	...	9704	PT,4:1,NOTI	1×1800	2.0	0.43	54.0	0.74	6.8	10:45:21.9	55:57:35	32.40
Haro 4	...	9704	PT,4:1,NOTI	1×1800	2.6	0.43	-27.1	0.54	6.1	11:04:58.5	29:08:15	32.64
Haro 8	...	9704	PT,4:1,NOTI	1×1800	2.6	0.43	53.0	0.80	6.1	12:19:09.8	3:51:16	32.45
Haro 14	...	9611	PT,4:1,NOTI	1×2700	1.7	0.43	13.4	0.84	6.1	0:45:46.8	-15:35:48	32.22
Haro 20	...	9611	PT,4:1,NOTI	2×1800	1.8	0.43	23.3	0.52	6.1	3:28:14.6	-17:25:12	32.32
...	...	9703	PT,4:1,NOTI	(1× 900)
Haro 23	...	9704	PT,4:1,NOTI	1×1800	2.3	0.43	-8.8	0.91	6.1	10:06:18.4	28:56:38	32.42
Haro 29	...	9704	PT,4:1,NOTI	3×1800	2.1	0.43	85.2	0.58	6.1	12:26:16.7	48:29:38	32.46
...	...	9704	PT,4:1,NOTI	(1× 900)
Haro 36	...	9704	PT,4:1,NOTI	2×1800	2.5	0.43	1.2	0.81	6.1	12:46:56.3	51:36:48	32.40
Haro 38	...	9703	PT,4:1,NOTI	1×1800	1.8	0.43	24.2	0.33	6.1	13:35:35.6	29:12:59	32.47
Haro 43	...	9605	PT,4:1,NCCD	2×1800	2.0	0.41	-38.4	0.42	4.9	14:36:08.8	28:26:59	32.34
HS0822+3542	...	0012	PT,2048	3×1800	2.0	0.61	-28.2	0.66	3.0	8:25:55.4	35:32:33	32.27
Mrk 5	...	9703	PT,4:1,NOTI	3×1800	2.8	0.43	10.1	0.76	6.8	6:42:15.6	75:37:38	32.33
Mrk 16	...	9704	PT,4:1,NOTI	1×1800	1.6	0.43	59.6	0.66	6.1	8:53:16.9	73:11:20	32.39
Mrk 32	...	9703	PT,4:1,NOTI	2×1800	3.5	0.43	6.2	0.58	6.1	10:27:02.1	56:16:12	32.31
Mrk 67	...	9704	PT,4:1,NOTI	1×1800	2.1	0.43	19.0	0.77	4.31	13:41:56.5	30:31:10	32.38
Mrk 178	...	9703	PT,4:1,NOTI	2×1800	1.8	0.43	-51.3	0.46	7.3	11:33:29.0	49:14:24	32.40
Mrk 408	...	9703	PT,4:1,NOTI	1×1800	1.5	0.43	-10.3	0.75	6.8	9:48:04.9	32:52:55	32.38
Mrk 600	...	9610	PT,4:1,NOTI	2×1800	2.1	0.43	-39.5	0.59	6.8	2:51:04.7	4:27:13	32.36
Mrk 757	...	9704	PT,4:1,NOTI	1×1800	2.5	0.43	-10.4	0.81	4.9	12:05:15.9	30:51:18	32.53
NGC 1705	...	9301	CTIO1.5m	1×1500	1.6	0.43	49.0	0.75	11.9	4:54:13.9	-53:21:33	32.68
NGC 6789	...	0112	HT,2048	2×1800	3.5	1.13	84.2	0.83	8.1	19:16:42.2	63:58:16	32.17
SBS1415+437	...	0204	HT,2048	5×1800	3.1	1.13	35.4	0.37	7.9	14:17:02.0	43:30:13	31.47
UGCA 290	...	0204	HT,2048	3×1800	2.7	1.13	47.4	0.51	5.7	12:37:22.3	38:44:40	32.17
IZw115	...	9605	PT,4:1,NCCD	2×1800	2.2	0.41	41.0	0.45	6.1	15:32:57.2	46:27:10	32.57

Table 2—Continued

Galaxy	Mos ^b	Date	Instr ^c	Exposures ^d (s)	Seeing ^e (")	Scale (")	Ellipse photometry parameters ^a					log rms _{ΣH_α} ^f (ergs/s/pc ²)
							PA (°)	<i>b/a</i>	Step (")	Center (2000) RA DEC		
VIIZw403	...	9502	PT,FP,NCCD	2×1300	1.6	0.49	-10.8	0.49	9.1	11:27:58.2	78:59:39	32.29
Zw2335	...	9611	PT,4:1,NOTI	1×2700	2.2	0.43	42.0	0.87	6.1	23:37:39.6	30:07:47	32.33
Sm Galaxies:												
DDO 18	...	9410	PT,FP,NCCD	3×2700	1.6	0.49	-32.6	0.85	11.3	2:10:44.7	6:45:32	32.27
...	...	9502	PT,FP,NCCD	(1× 900)
DDO 48	...	9502	PT,FP,NCCD	3×3000	2.1	0.49	-4.5	0.25	11.3	7:58:54.4	58:02:34	31.99
DDO 54	...	9410	PT,FP,NCCD	1×2100	2.2	0.49	-0.4	1.00	11.3	9:08:10.6	5:55:43	32.26
DDO 88	...	9504	PT,FP,NCCD	1×1800	2.2	0.49	49.6	0.92	11.3	10:47:22.4	14:04:16	32.35
DDO 122	...	9405	PT,FP,NCCD	2×1800	2.3	0.49	-0.1	1.00	11.3	12:24:24.2	70:19:58	32.32
DDO 135	...	9405	PT,FP,NCCD	1×2400	1.9	0.49	23.6	0.83	11.3	12:33:48.2	15:10:19	32.08
DDO 150	...	9405	PT,FP,NCCD	2×1800	2.4	0.49	30.6	0.74	11.3	12:48:23.2	51:09:47	32.29
DDO 173	...	9703	PT,4:1,NOTI	1×1800	1.7	0.43	-80.3	0.49	11.3	13:20:38.8	9:47:12	32.39
DDO 180	...	9703	PT,4:1,NCCD	1×1800	2.2	0.50	79.9	0.96	11.3	13:38:10.3	-9:48:06	32.36
DDO 204	...	9405	PT,FP,NCCD	1×2400	2.1	0.49	34.9	0.87	11.3	16:16:19.1	47:02:50	32.40
DDO 214	...	9410	PT,FP,NCCD	2×2700	1.5	0.49	-20.5	0.74	11.3	22:36:35.6	-2:54:35	32.30
DDO 217	N	9610	PT,4:1,NOTI	2×2700	1.9	0.43	26.0	0.61	11.3	23:29:58.8	40:59:39	32.10
...	S	9610	PT,4:1,NOTI	2×2700
...	NE	9610	PT,4:1,NOTI	2×2700
...	W	9611	PT,4:1,NOTI	3×2700
F561-1	...	9611	PT,4:1,NOTI	3×2700	2.0	0.43	28.3	0.90	4.3	8:09:41.4	22:33:34	32.13
F567-2	...	9605	PT,4:1,NCCD	2×2400	2.0	0.41	32.63
F583-1	...	9605	PT,4:1,NCCD	3×2400	2.4	0.41	-13.1	0.40	9.1	15:57:27.5	20:39:58	32.20
NGC 2552	...	9002	PT,4:1,NOTI	1×3600	1.8	0.43	53.6	0.67	11.3	8:19:21.9	50:00:33	32.67
...	...	9702	PT,4:1,NOTI	(1× 900)
NGC 3109	W	9301	CTIO1.5m	1×2700	1.6	0.43	-87.0	0.21	21.7	10:03:08.2	-26:09:29	32.40
...	E	9301	CTIO1.5m	1×3600
NGC 3510	...	9703	PT,4:1,NOTI	1×1800	2.9	0.43	-14.4	0.23	11.3	11:03:43.5	28:53:08	32.98
UGC 5716	...	9704	PT,4:1,NOTI	1×1800	2.3	0.43	-19.4	0.53	9.1	10:31:43.6	25:18:21	32.40
UGC 11820	...	9610	PT,4:1,NOTI	3×2700	1.7	0.43	-81.9	0.52	10.5	21:49:28.8	14:13:47	32.21

^aPosition angle PA, minor-to-major axis ratio *b/a*, ellipse semi-major axis step size, and position of center used to do photometry in concentric ellipses. The PA given here has been corrected for the PA of the CCD camera on the sky, usually about 0.5°, but the PA appropriate to the image itself was used for the photometry.

^bGalaxies that were, or were potentially, larger than the field of view were mosaiced. This column designates the relative pointing in the mosaic. A “C” designates the center. No entry means that the galaxy was not mosaiced.

^cTelescope, instrument, and detector used for the H α observations. Telescopes: PT=1.8 m Perkins Telescope at Lowell Observatory; HT=1.1 m Hall Telescope at Lowell Observatory; KPNO4m=Kitt Peak National Observatory 4 m telescope; CTIO1.5m=Cerro Tololo Inter-American Observatory 1.5 m telescope. Instruments: 4:1=4:1 focal reducer; FP=Ohio State University Fabry Perot used as a simple 3:1 focal reducer; those without a designation were direct cameras. Detectors: NCCD=a TI 800 \times 800 CCD provided to Lowell Observatory by the National Science Foundation; NOTI=a TI 800 \times 800 CCD on loan to Lowell Observatory from the US Naval Observatory, Flagstaff Station; 2048=SITE 2048 \times 2048 CCD; Mos=KPNO Mosaic camera.

^dA () designates images taken under clear sky conditions to calibrate the other frames taken under non-photometric conditions.

^eFWHM of a stellar profile on the final combined H α image.

^fThe H α surface brightness corresponding to the rms of one pixel in the original H α image.

Table 3. H α photometry, star formation rates, H α extents

Galaxy	$\log L_{H\alpha}$ (ergs/s)	$\log \dot{M}$ (M_{\odot} /yr)	$\log \dot{M}_{25}^a$ (M_{\odot} /yr/kpc 2)	$\log \dot{M}_D^b$ (M_{\odot} /yr/kpc 2)	$\log \tau^c$ (yr)	$R_{H\alpha}^d$ (')	R_{HII}^e (')	R_{HII}/R_{25}	R_{HII}/R_H	R_{HII}/R_D
Im Galaxies:										
A1004+10	39.52 \pm 0.00	-1.71	-2.42	-1.28	9.30	0.68	0.53	0.78	0.55	2.91
A2228+33	40.16 \pm 0.01	-1.07	-2.73	-2.39	10.42	1.61	1.80	2.32	1.20	3.46
CVnIdwA	38.70 \pm 0.05	-2.52	...	-2.64	10.44	0.66	0.47	...	0.54	0.87
D508-2	39.02 \pm 0.32	-2.20	-3.27	-3.21	11.38	0.53	0.53	2.39	0.96	2.56
D575-5	0.00
D634-3	0.00
D646-8	0.00
DDO 9	39.78 \pm 0.01	-1.45	-3.12	-2.93	10.74	2.36	2.36	2.23	1.09	2.78
DDO 22	39.06 \pm 0.02	-2.17	-3.08	-2.73	10.71	0.66	0.66	1.26	0.70	1.87
DDO 24	39.92 \pm 0.01	-1.31	-2.85	-2.03	10.44	1.61	1.61	1.51	...	3.93
DDO 25	40.17 \pm 0.01	-1.06	-2.69	-1.87	9.90	1.42	1.42	1.22	0.82	3.16
DDO 26	39.26 \pm 0.01	-1.96	-3.49	-2.91	11.39	1.33	1.33	2.06	1.25	3.99
DDO 27	39.23 \pm 0.03	-2.00	...	-2.87	10.86	0.84	0.84	...	1.35	2.93
DDO 33	40.54 \pm 0.01	-0.69	-2.92	-2.68	10.49	1.04	1.04	1.13	0.88	1.48
DDO 34	39.39 \pm 0.03	-1.84	-2.49	-2.40	10.52	1.60	1.60	3.61	1.57	3.98
DDO 35	40.78 \pm 0.00	-0.45	-2.53	-1.48	10.02	0.85	0.85	0.85	...	2.84
DDO 38	40.05 \pm 0.01	-1.18	-2.72	-2.61	10.57	1.05	1.05	1.94	1.02	2.22
DDO 39	39.61 \pm 0.02	-1.62	-2.95	-3.25	10.98	2.36	2.36	3.89	1.27	2.74
DDO 40	40.45 \pm 0.00	-0.78	-2.67	-2.02	10.09	1.23	1.23	1.61	0.99	3.39
DDO 43	38.80 \pm 0.01	-2.43	-2.91	-2.19	10.53	1.04	0.94	1.53	1.06	3.53
DDO 46	38.79 \pm 0.01	-2.43	-3.08	-2.96	10.69	0.85	0.85	1.15	...	1.32
DDO 47	39.25 \pm 0.01	-1.98	-2.55	-2.75	10.71	3.69	3.69	5.15	1.65	4.08
DDO 50	39.98 \pm 0.00	-1.25	-2.68	-1.83	10.24	99.99
DDO 52	38.22 \pm 0.02	-3.01	-3.30	-3.27	11.11	1.23	1.23	2.73	1.14	2.82
DDO 53	38.95 \pm 0.00	-2.28	-2.49	-2.50	10.67	1.19	1.05	1.53	0.77	1.52
DDO 63	38.97 \pm 0.05	-2.25	-3.06	-3.44	10.56	1.99	1.61	1.25	0.74	0.81
DDO 64	39.29 \pm 0.01	-1.94	-2.93	-2.68	10.46	1.23	1.04	1.26	0.85	1.69
DDO 68	38.61 \pm 0.12	-2.62	-3.41	-2.66	11.27	1.61	1.61	2.33	1.47	5.51
DDO 69	37.28 \pm 0.00	-3.95	-3.42	-3.28	11.08	3.26	3.26	2.49	1.36	2.92
DDO 70	38.22 \pm 0.01	-3.00	-3.31	-2.86	10.72	3.26	3.26	1.54	0.88	2.60
DDO 75	39.03 \pm 0.00	-2.20	-2.61	-1.40	10.21	3.08	3.08	1.30	1.00	5.22
DDO 86	39.70 \pm 0.02	-1.53	-2.85	-2.74	10.72	1.23	1.04	1.99	1.05	2.25

Table 3—Continued

Galaxy	$\log L_{H\alpha}$ (ergs/s)	$\log \dot{M}$ (M_{\odot} /yr)	$\log \dot{M}_{25}^a$ (M_{\odot} /yr/kpc ²)	$\log \dot{M}_D^b$ (M_{\odot} /yr/kpc ²)	$\log \tau^c$ (yr)	$R_{H\alpha}^d$ (')	R_{HII}^e (')	R_{HII}/R_{25}	R_{HII}/R_H	R_{HII}/R_D
DDO 87	38.75± 0.02	-2.47	...	-3.16	10.84	1.42	1.23	...	1.07	1.93
DDO 99	38.95± 0.04	-2.28	-2.91	-2.71	10.60	1.42	1.42	1.45	0.69	1.84
DDO 101	38.98± 0.02	-2.25	-3.26	-2.99	9.65	0.66	0.66	0.96	0.63	1.31
DDO 105	39.90± 0.01	-1.32	-3.00	-2.85	10.65	2.55	2.55	2.73	1.24	3.25
DDO 115	38.23± 0.01	-3.00	-3.07	-2.51	10.24	0.68	0.68	1.04	0.69	1.98
DDO 120	0.00
DDO 125	38.51± 0.05	-2.72	...	-2.58	10.48	1.65	1.65	2.49
DDO 126	39.16± 0.01	-2.06	-2.70	-2.45	10.33	1.99	1.89	2.30	1.08	3.08
DDO 133	39.45± 0.00	-1.77	-2.82	-2.93	10.48	2.55	2.55	2.40	1.10	2.12
DDO 143	39.53± 0.04	-1.70	...	-2.82	10.52	1.61	1.61	...	1.19	2.24
DDO 154	38.80± 0.01	-2.43	-3.02	-2.60	11.05	1.61	1.42	1.60	0.92	2.60
DDO 155	38.57± 0.00	-2.66	-2.36	-1.50	9.79	1.04	0.66	1.06	0.70	2.87
DDO 165	38.78± 0.02	-2.44	-3.53	-3.52	10.76	2.36	2.36	1.67	1.11	1.70
DDO 167	38.35± 0.01	-2.88	-2.93	-2.41	10.27	0.66	0.47	0.96	0.63	1.75
DDO 168	39.03± 0.00	-2.20	-3.02	-2.33	10.68	1.79	1.61	1.13	0.70	2.49
DDO 169	38.21± 0.14	-3.02	-3.57	-3.29	11.15	0.28	0.28	0.41	0.21	0.57
DDO 171	39.95± 0.02	-1.27	-3.01	-2.35	10.09	0.66	0.66	0.87	0.54	1.85
DDO 183	38.38± 0.04	-2.85	-3.47	-3.21	10.87	0.85	0.85	1.09	0.67	1.48
DDO 185	39.01± 0.01	-2.21	-2.87	-2.58	10.33	1.99	1.80	1.75	0.90	2.43
DDO 187	37.70± 0.02	-3.53	-3.43	-2.64	11.01	0.47	0.47	0.69	0.45	1.70
DDO 210	0.00
DDO 215	39.12± 0.04	-2.10	-3.05	-2.72	10.83	1.60	1.60	4.09	1.79	5.94
DDO 216	36.86± 0.03	-4.36	-4.08	-4.15	10.38	1.31	1.31	0.85	0.33	0.78
DDO 220	39.39± 0.01	-1.83	-3.13	-2.91	10.67	0.68	0.68	1.19	0.77	1.52
F533-1	39.17± 0.05	-2.05	-2.77	-2.68	...	0.53	0.53	2.73	1.16	3.02
F563-V1	39.31± 0.05	-1.91	...	-3.55	10.97	0.18	0.18	0.82
F563-V2	40.48± 0.04	-0.75	-2.96	-2.03	10.36	0.43	0.43	1.21	0.84	3.57
F564-V3	0.00
F565-V1	0.00
F565-V2	38.65± 0.05	-2.57	...	-3.44	11.68	0.32	0.32	3.37
F608-1	38.79± 0.04	-2.43	-2.63	-3.07	...	0.55	0.55	3.99	1.13	2.40
F615-1	36.97± 0.33	-4.25	...	-4.76	...	0.55	0.55	...	1.20	2.12
F651-2	39.71± 0.04	-1.52	-2.81	-2.91	...	0.79	0.73	2.39	1.08	2.14
F721-V2	39.14± 0.02	-2.09	-2.15	-2.51	...	0.25	0.15	1.34	0.43	0.89

Table 3—Continued

Galaxy	$\log L_{H\alpha}$ (ergs/s)	$\log \dot{M}$ (M_{\odot} /yr)	$\log \dot{M}_{25}^a$ (M_{\odot} /yr/kpc ²)	$\log \dot{M}_D^b$ (M_{\odot} /yr/kpc ²)	$\log \tau^c$ (yr)	$R_{H\alpha}^d$ (')	R_{HII}^e (')	R_{HII}/R_{25}	R_{HII}/R_H	R_{HII}/R_D
F750-V1	38.54± 0.05	-2.69	-3.07	-2.95	...	0.35	0.35	1.97	0.93	2.28
IC 10	39.92± 0.00	-1.31	...	-1.31	9.78	99.99
IC 1613	38.62± 0.00	-2.61	-3.13	-2.64	10.27	99.99
IC 4662	40.21± 0.00	-1.01	...	-0.48	9.65	1.62	1.62	4.66
LGS 3	0.00
M81dwA	0.00
NGC 1156	40.68± 0.00	-0.54	-2.20	-0.87	9.70	1.79	1.79	1.07	0.84	4.96
NGC 1569	40.74± 0.00	-0.49	...	0.11	8.61	99.99
NGC 2101	40.46± 0.05	-0.76	...	-1.25	10.16	0.94	0.94	4.20
NGC 2366	40.20± 0.00	-1.02	-2.40	-1.73	9.98	5.64	5.64	1.91	1.19	4.10
NGC 3413	39.68± 0.01	-1.55	-2.69	-1.50	10.16	0.47	0.47	0.63	0.45	2.47
NGC 3738	39.77± 0.00	-1.45	-2.63	-1.72	9.77	1.04	0.66	0.43	0.28	1.23
NGC 3952	40.77± 0.00	-0.45	-2.45	-1.34	9.79	0.85	0.85	0.99	0.70	3.56
NGC 4163	38.19± 0.08	-3.04	-3.26	-2.43	10.35	1.04	1.04	1.16	0.71	3.03
NGC 4214	40.35± 0.00	-0.88	-2.30	-1.10	9.76	99.99
NGC 6822	39.26± 0.00	-1.97	...	-1.96	10.21	99.99
SagDIG	37.43± 0.15	-3.79	-3.71	-3.02	10.82	1.58	1.58	0.98	...	2.17
UGC 199	39.23± 0.15	-2.00	-2.86	-3.40	11.04	0.68	0.68	3.90	0.97	2.09
UGC 5209	38.04± 0.07	-3.18	-3.45	-2.99	10.74	0.30	0.30	0.90	...	1.52
UGC 8011	38.97± 0.03	-2.26	...	-3.14	10.81	0.66	0.66	...	0.61	1.43
UGC 8055	38.62± 0.04	-2.60	-2.71	-2.67	10.90	0.56	0.56	2.17	...	2.25
UGC 8276	38.28± 0.07	-2.95	-3.54	-3.42	11.29	0.56	0.56	1.93	1.06	2.21
UGC 8508	38.45± 0.01	-2.77	-2.88	-2.12	10.31	1.04	0.84	1.00	0.66	2.39
UGC 10140	39.61± 0.04	-1.61	-3.01	-2.78	10.63	0.25	0.25	1.10	...	1.43
UGC 10281	39.02± 0.04	-2.21	-2.73	-3.19	11.02	0.68	0.68	3.54	0.94	2.10
WLM	38.39± 0.00	-2.84	-3.33	-2.85	10.74	4.25	4.25	1.25	0.73	2.15
0467-074	40.44± 0.03	-0.78	-3.06	-2.48	10.30	0.32	0.32	1.31	...	2.52
1397-049	39.06± 0.05	-2.16	-4.01	-3.74	11.79	0.00	0.00	0.00	0.00	0.00
BCD Galaxies:										
Haro 3	40.91± 0.00	-0.31	...	-0.16	9.26	0.51	0.51	4.86
Haro 4	39.97± 0.00	-1.26	-1.50	-0.29	8.91	0.46	0.15	0.56	0.37	2.24
Haro 8	40.58± 0.00	-0.65	-2.21	-1.05	9.22	0.46	0.15	0.28	0.20	1.08
Haro 14	40.12± 0.00	-1.11	-2.40	-1.03	9.73	0.46	0.25	0.44	0.35	2.14

Table 3—Continued

Galaxy	$\log L_{H\alpha}$ (ergs/s)	$\log \dot{M}$ (M_{\odot} /yr)	$\log \dot{M}_{25}^a$ (M_{\odot} /yr/kpc ²)	$\log \dot{M}_D^b$ (M_{\odot} /yr/kpc ²)	$\log \tau^c$ (yr)	$R_{H\alpha}^d$ (')	R_{HII}^e (')	R_{HII}/R_{25}	R_{HII}/R_H	R_{HII}/R_D
Haro 20	40.18± 0.01	-1.04	-2.74	-1.91	9.92	0.25	0.05	0.10	...	0.26
Haro 23	40.22± 0.00	-1.01	-2.33	-1.69	9.13	0.25	0.15	0.34	0.19	0.71
Haro 29	39.77± 0.00	-1.46	-1.72	-0.82	9.39	0.56	0.35	0.72	0.41	2.04
Haro 36	39.41± 0.01	-1.82	-2.87	-1.96	10.11	0.76	0.66	0.91	...	2.60
Haro 38	39.64± 0.01	-1.59	-2.40	-1.78	9.82	0.56	0.25	0.69	0.40	1.42
Haro 43	40.15± 0.00	-1.08	-2.33	-1.33	10.09	0.28	0.20	0.75	0.48	2.35
HS0822+3542	39.09± 0.01	-2.14	-1.86	-0.73	9.53	0.13	0.05	0.39	...	1.43
Mrk 5	39.88± 0.00	-1.35	-2.17	-1.14	9.57	0.40	0.17	0.49	...	1.60
Mrk 16	40.49± 0.01	-0.74	-2.58	-1.55	9.93	0.35	0.15	0.35	...	1.14
Mrk 32	39.20± 0.01	-2.02	-2.65	-2.10	10.29	0.25	0.15	0.52	0.31	0.99
Mrk 67	39.86± 0.05	-1.36	...	-0.55	8.93	0.25	0.04	0.82
Mrk 178	39.10± 0.00	-2.12	-2.31	-1.53	9.25	1.03	0.91	1.49	0.90	3.64
Mrk 408	40.23± 0.00	-1.00	-2.26	-1.09	9.68	0.28	0.06	0.17	0.12	0.65
Mrk 600	40.15± 0.00	-1.08	-2.10	-1.02	9.82	0.51	0.51	1.27	...	4.43
Mrk 757	39.25± 0.01	-1.98	-2.45	-1.53	9.51	0.20	0.08	0.21	...	0.62
NGC 1705	40.15± 0.00	-1.07	...	-0.82	9.29	1.54	0.45	1.58
NGC 6789	38.55± 0.04	-2.68	-2.98	-1.91	...	0.47	0.34	0.48	...	1.54
SBS1415+437	39.05± 0.01	-2.18	-2.92	-2.31	...	0.60	0.33	0.79	...	1.60
UGCA 290	37.92± 0.06	-3.31	-2.83	-1.77	...	0.62	0.43	1.08	0.79	3.68
IZw115	38.52± 0.05	-2.71	-3.75	-2.87	11.10	0.35	0.15	0.29	0.20	0.79
VIIZw403	39.34± 0.00	-1.88	-2.19	-1.82	9.86	0.99	0.68	1.09	0.61	1.67
Zw2335	40.20± 0.00	-1.02	-2.10	-0.89	9.27	0.15	0.01	0.04	0.02	0.14
Sm Galaxies:										
DDO 18	39.76± 0.05	-1.47	-3.30	-3.05	10.78	0.85	0.85	1.35	0.89	1.82
DDO 48	39.64± 0.01	-1.59	-2.57	-2.95	10.82	1.61	1.61	4.77	1.43	3.10
DDO 54	39.54± 0.04	-1.69	-3.36	-2.63	10.58	0.85	0.85	1.15	0.76	2.68
DDO 88	38.90± 0.03	-2.33	-3.33	-2.60	10.42	1.04	1.04	1.25	0.82	2.91
DDO 122	39.87± 0.00	-1.36	-2.91	-2.11	10.06	1.42	1.23	0.98	0.74	2.45
DDO 135	39.18± 0.00	-2.05	-2.78	-1.88	8.41	1.79	1.79	1.36	0.95	3.83
DDO 150	39.67± 0.00	-1.55	-2.86	-2.09	10.13	1.42	1.42	1.38	0.99	3.34
DDO 173	40.07± 0.01	-1.16	-2.93	-2.18	10.35	1.04	1.04	1.19	0.84	2.80
DDO 180	40.68± 0.00	-0.54	-2.64	-1.66	9.86	1.04	1.04	0.90	0.64	2.80
DDO 204	40.46± 0.00	-0.76	-2.62	-1.74	9.97	1.79	1.79	1.47	1.20	4.05

Table 3—Continued

Galaxy	$\log L_{H\alpha}$ (ergs/s)	$\log \dot{M}$ (M_{\odot} /yr)	$\log \dot{M}_{25}^a$ (M_{\odot} /yr/kpc ²)	$\log \dot{M}_D^b$ (M_{\odot} /yr/kpc ²)	$\log \tau^c$ (yr)	$R_{H\alpha}^d$ (')	R_{HII}^e (')	R_{HII}/R_{25}	R_{HII}/R_H	R_{HII}/R_D
DDO 214	40.71± 0.01	-0.51	-3.04	-2.36	10.12	1.23	1.23	0.98	0.76	2.14
DDO 217	40.13± 0.00	-1.09	-3.07	-2.73	10.44	3.50	3.50	1.78	1.20	2.64
F561-1	40.29± 0.05	-0.93	...	-2.68	10.42	0.47	0.47	2.33
F567-2	0.00
F583-1	39.96± 0.02	-1.26	-2.72	-2.57	10.75	0.99	0.91	3.25	1.29	3.87
NGC 2552	40.06± 0.00	-1.16	-2.83	-1.98	10.05	1.42	1.42	0.92	0.71	2.43
NGC 3109	39.52± 0.00	-1.71	...	-2.39	10.49	99.99
NGC 3510	40.43± 0.00	-0.80	-2.36	-1.52	10.11	1.79	1.79	1.59	0.99	4.19
UGC 5716	39.51± 0.03	-1.72	-2.93	-2.65	10.75	0.68	0.68	1.65	0.77	2.28
UGC 11820	40.07± 0.01	-1.15	-2.59	-2.74	10.59	2.01	1.92	3.95	1.33	3.33

^aIntegrated star formation rate normalized to the area of the galaxy within R_{25} .

^bIntegrated star formation rate normalized to the area of the galaxy within R_D .

^cTime scale to exhaust the total current gas content of the galaxy at the current star formation rate.

^dSemi-major axis of largest ellipse that contains $H\alpha$ emission. An entry of 99.99 means that the $H\alpha$ emission exceeded the size of the region that we imaged.

^eSemi-major axis of largest ellipse that contains the center of a discrete HII region. An entry of 99.99 means that the HII potentially extended beyond the region that we imaged.

Table 4. Other parameters.

Galaxy	R_{25} (kpc)	R_D (kpc)	M_V	$\log M_{gas}^a$ (M_\odot)	Ref ^b
Im Galaxies:					
A1004+10	1.29	0.35	-15.93	7.59	12
A2228+33	3.83	2.57	-17.75	9.35	11
CVnIdwA	...	0.65	-12.65	7.92	25
D508-2	1.94	1.81	-15.74	9.18	17
D575-5	...	0.85	-12.85	7.52	17
D634-3	0.09	0.13	-10.16	5.98	17
D646-8	...	2.02	-14.69	7.79	17
DDO 9	3.87	3.11	-17.46	9.29	7
DDO 22	1.61	1.09	-15.44	8.54	7
DDO 24	3.35	1.29	-17.09	9.13	7
DDO 25	3.72	1.44	-17.27	8.84	7
DDO 26	3.27	1.68	-16.80	9.43	11
DDO 27	...	1.54	-15.28	8.86	7
DDO 33	7.36	5.62	-18.63	9.80	7
DDO 34	1.19	1.08	-15.36	8.68	7
DDO 35	6.18	1.84	-18.74	9.57	7
DDO 38	3.36	2.93	-17.11	9.39	7
DDO 39	2.61	3.71	-17.42	9.36	7
DDO 40	4.97	2.36	-17.88	9.31	7
DDO 43	0.99	0.43	-14.31	8.10	11
DDO 46	1.19	1.03	-14.45	8.26	7
DDO 47	1.09	1.37	-15.46	8.73	11
DDO 50	2.93	1.11	-16.61	8.99	3
DDO 52	0.79	0.76	-14.27	8.10	7
DDO 53	0.72	0.73	-13.84	8.39	16
DDO 63	1.43	2.22	-14.73	8.31	18
DDO 64	1.78	1.33	-15.42	8.52	11
DDO 68	1.41	0.60	-15.17	8.65	11
DDO 69	0.31	0.26	-11.67	7.13	1
DDO 70	0.80	0.48	-14.10	7.72	11
DDO 75	0.90	0.22	-13.91	8.01	11
DDO 86	2.58	2.28	-16.51	9.19	7
DDO 87	...	1.25	-14.67	8.37	11
DDO 99	1.17	0.92	-14.88	8.32	18
DDO 101	1.81	1.32	-15.75	7.40	20
DDO 105	3.90	3.28	-17.70	9.33	7
DDO 115	0.61	0.32	-13.28	7.24	2
DDO 120	2.23	1.01	-16.33	8.33	7
DDO 125	...	0.48	-14.70	7.76	7
DDO 126	1.18	0.88	-14.85	8.27	7
DDO 133	1.89	2.15	-15.96	8.71	7
DDO 143	...	2.05	-15.58	8.82	2
DDO 154	1.11	0.69	-14.51	8.62	4

Table 4—Continued

Galaxy	R_{25} (kpc)	R_D (kpc)	M_V	$\log M_{gas}^a$ (M_\odot)	Ref ^b
DDO 155	0.40	0.15	-12.53	7.13	11
DDO 165	1.98	1.95	-15.69	8.32	7
DDO 167	0.60	0.33	-12.98	7.39	7
DDO 168	1.45	0.66	-15.27	8.48	11
DDO 169	1.06	0.78	-14.58	8.13	7
DDO 171	4.16	1.95	-17.90	8.82	7
DDO 183	1.16	0.86	-14.54	8.02	11
DDO 185	1.20	0.86	-14.95	8.12	21
DDO 187	0.50	0.20	-12.95	7.48	11
DDO 210	0.12	0.17	-10.88	6.52	14
DDO 215	1.67	1.15	-15.63	8.73	7
DDO 216	0.40	0.44	-13.29	6.02	7
DDO 220	2.49	1.94	-16.28	8.84	7
F533-1	1.29	1.17	-15.34
F563-V1	...	3.71	-17.22	9.05	5
F563-V2	7.26	2.47	-18.63	9.61	5
F564-V3	0.59	0.38	-13.24	7.27	5
F565-V1	0.34	0.32	-12.45
F565-V2	...	1.52	-16.17	9.10	5
F608-1	0.71	1.18	-14.86
F615-1	...	1.02	-13.89
F651-2	2.50	2.80	-16.42
F721-V2	0.61	0.92	-14.34
F750-V1	0.88	0.76	-14.34
IC 10	...	0.57	-17.11	8.47	10
IC 1613	1.03	0.59	-14.60	7.66	10
IC 4662	...	0.30	-16.56	8.64	2
LGS 3	...	0.20	-9.41	5.18	23
M81dwA	...	0.37	-11.73	7.26	19
NGC 1156	3.81	0.82	-18.67	9.16	11
NGC 1569	...	0.28	-17.57	8.12	12
NGC 2101	...	0.99	-17.69	9.40	2
NGC 2366	2.76	1.28	-16.66	8.96	7
NGC 3413	2.10	0.54	-17.16	8.61	2
NGC 3738	2.18	0.77	-17.12	8.32	11
NGC 3952	5.61	1.56	-18.91	9.34	2
NGC 4163	0.73	0.28	-14.37	7.31	2
NGC 4214	2.90	0.72	-17.56	8.88	2
NGC 6822	...	0.56	-15.12	8.24	6
SagDIG	0.52	0.23	-12.45	7.03	14
UGC 199	1.52	2.85	-16.48	9.04	24
UGC 5209	0.77	0.46	-13.76	7.56	2
UGC 8011	...	1.57	-15.56	8.55	2
UGC 8055	0.64	0.61	-13.62	8.30	2
UGC 8276	1.12	0.98	-14.57	8.34	2

Table 4—Continued

Galaxy	R_{25} (kpc)	R_D (kpc)	M_V	$\log M_{gas}^a$ (M_\odot)	Ref ^b
UGC 8508	0.64	0.27	-13.59	7.54	7
UGC 10140	2.81	2.17	-16.80	9.02	24
UGC 10281	1.03	1.74	-15.64	8.81	24
WLM	0.99	0.58	-14.39	7.90	10
0467-074	7.72	4.00	-18.69	9.52	9
1397-049	4.75	3.47	-17.73	9.63	9
BCD Galaxies:					
Haro 3	...	0.48	-18.23	8.95	12
Haro 4	0.74	0.19	-14.80	7.65	8
Haro 8	3.42	0.90	-17.91	8.57	8
Haro 14	2.49	0.52	-17.77	8.62	8
Haro 20	3.99	1.53	-18.32	8.88	8
Haro 23	2.58	1.24	-17.72	8.12	8
Haro 29	0.76	0.27	-14.47	7.93	8
Haro 36	1.90	0.67	-15.84	8.29	8
Haro 38	1.45	0.70	-15.22	8.23	8
Haro 43	2.39	0.76	-17.18	9.01	8
HS0822	0.41	0.11	-13.15	7.39	13
Mrk 5	1.45	0.44	-16.02	8.22	22
Mrk 16	4.72	1.44	-18.74	9.19	22
Mrk 32	1.16	0.61	-15.43	8.27	22
Mrk 67	...	2.61	...	7.57	22
Mrk 178	0.70	0.28	-14.11	7.13	22
Mrk 408	2.43	0.63	-18.02	8.68	22
Mrk 600	1.83	0.53	-16.30	8.74	22
Mrk 757	0.97	0.34	-15.46	7.53	22
NGC 1705	...	0.42	-16.25	8.22	15
NGC 6789	0.80	0.23	-14.77
SBS1415	1.32	0.66	-15.01
UGCA 290	0.33	0.10	-11.73
IZw115	1.88	0.68	-16.01	8.39	8
VIIZw403	0.80	0.52	-14.27	7.98	22
Zw2335	1.95	0.49	-17.47	8.25	8
Sm Galaxies:					
DDO 18	4.66	3.47	-17.52	9.31	7
DDO 48	1.75	2.70	-16.67	9.23	7
DDO 54	3.89	1.67	-17.39	8.89	7
DDO 88	1.80	0.77	-15.87	8.09	7
DDO 122	3.37	1.34	-17.15	8.70	7
DDO 135	1.31	0.47	-15.06	6.36	7
DDO 150	2.54	1.05	-16.31	8.58	7
DDO 173	4.32	1.84	-17.56	9.19	7
DDO 180	6.33	2.04	-19.19	9.32	7

Table 4—Continued

Galaxy	R ₂₅ (kpc)	R _D (kpc)	M _V	log M _{gas} ^a (M _⊙)	Ref ^b
DDO 204	4.80	1.75	-17.58	9.21	11
DDO 214	10.33	4.75	-19.48	9.61	7
DDO 217	5.52	3.71	-17.94	9.35	7
F561-1	...	4.21	-18.66	9.49	5
F567-2	-17.40	9.67	5
F583-1	3.03	2.54	-17.17	9.49	5
NGC 2552	3.84	1.45	-17.34	8.89	11
NGC 3109	...	1.24	...	8.79	7
NGC 3510	3.44	1.30	-17.27	9.31	11
UGC 5716	2.28	1.65	-16.30	9.03	2
UGC 11820	2.96	3.51	-17.56	9.44	2

^aTotal galactic atomic gas mass. The HI mass has been multiplied by 1.34 to account for He.

^bReference from which the HI mass was taken. Masses were modified to reflect the distances used here as necessary.

References. — (1) Allsopp 1978; (2) Bottinelli et al. 1990; (3) Bureau & Carignan 2002; (4) Carignan & Beaulieu 1989; (5) de Blok, McGaugh, & van der Hulst 1996; (6) de Blok & Walter 2000; (7) Fisher & Tully 1981; (8) Gordon & Gottesman 1981; (9) Huchtmeier, Hopp, & Kuhn 1997; (10) Huchtmeier, Seiradakis, & Materne 1981; (11) Hunter & Gallagher 1985a; (12) Hunter, Gallagher, & Rautenkranz 1982; (13) Kniazen et al. 2000; (14) Lo, Sargent, & Young 1993; (15) Meurer, Staveley-Smith, & Killeen 1998; (16) Nordgren et al., private communication; (17) Pildis, Schombert, & Eder 1997; (18) RC3; (19) Sargent, Sancisi, & Lo 1983; (20) Stil & Israel 2002; (21) Swaters 1999; (22) Thuan & Martin 1981; (23) Young & Lo 1997; (24) van Zee, Haynes, & Giovanelli 1995; and (25) van Zee et al. 1997.

Table 5. Spectrophometry of HII regions.

HII Region	Aperture ^a	[OII] λ 3727 ^b	[OIII] λ 5007 ^b	H β ^b	H α ^b	[NII] λ 6584 ^b	[SII] λ 6717,6731 ^b
NGC 595	13.5	5.95	4.37	3.47	18.31	2.01	1.54
	22.0	16.22	11.22	8.69
NGC 604	13.5	16.36	23.33	10.44	53.69	6.05	6.21
	22.0	51.19	50.31	25.27
NGC 2363	13.5	8.60	85.04	12.06	42.30	0.75	1.33
NGC 5461	13.5	4.41	...	3.36	22.42	3.46	2.69
NGC 5462	13.5	4.25	0.37	1.04

^aAperture diameter in arcseconds.

^bIntegrated emission in units of 10^{-13} ergs cm^{-2} s^{-1} .

REFERENCES

- Allsopp, N. J. 1978, MNRAS, 184, 397
- Aparicio, A. 1994, ApJ, 437, L27
- Aparicio, A., Gallart, C., & Bertelli, G. 1997a, AJ, 114, 669
- Aparicio, A., Gallart, C., & Bertelli, G. 1997b, AJ, 114, 680
- Aparicio, A., & Tikhonov, N. 2000, AJ, 119, 2183
- Aparicio, A., Tikhonov, N., & Karachentsev, I. 2000, AJ, 119, 177
- Bekki, K., & Freeman, K.C. 2003, ApJ, 574, L21
- Binggeli, B., & Popescu, C. C. 1995, A&A, 298, 63
- Bosma, A. 1981, AJ, 86, 1825
- Bothun, G. D., Schombert, J. M., Impey, C. D., Sprayberry, D., & McGaugh, S. S. 1993, AJ, 106, 530
- Bottinelli, L., Gouguenheim, L., Fouque, P., & Paturel, G. 1990, A&AS, 82, 391
- Bravo-Alfaro, H., Brinks, E., Baker, A. J., Walter, F., & Kunth, D. 2004, AJ, 127, 264
- Brinchmann, J., Charlot, S., White, S. D. M., Tremonti, C., Kauffmann, G., Heckman, T., & Brinkmann, J. 2004, MNRAS, in press
- Brosch, N., Heller, A., & Almoznino, E. 1998, ApJ, 504, 720
- Buat, V., Deharveng, J. M., & Donas, J. 1989, A&A, 223, 42
- Bureau, M., & Carignan, C. 2002, AJ, 123, 1316
- Burstein, D., & Heiles, C. 1984, ApJS, 54, 33
- Cairós, L. M., Vílchez, J. M., Pérez, J. N. G., & Igelsias-Páramo, J., & Caon, N. 2001, ApJS, 133, 321
- Campos-Aguilar, A., & Moles, M. 1991, A&A, 241, 358
- Cannon, J.M., Dohm-Palmer, R.C., Skillman, E.D., Bomans, D.J., Côté, S., & Miller, B.W. 2003. AJ, 126, 2806

- Cardelli, J. A., Clayton, G. C., & Mathis, J. S. 1989, *ApJ*, 345, 245
- Carignan, C., & Beaulieu, S. 1989, *ApJ*, 347, 760
- Chamaraux, P. 1977, *A&A*, 60, 67
- Cole, A. A., et al. 1999, *AJ*, 118, 1657
- Côté, S., Carignan, C., & Freeman, K. C. 2000, *AJ*, 120, 3027
- Crone, M. M., Schulte-Ladbeck, R. E., Greggio, L., & Hopp, U. 2002, *ApJ*, 567, 258
- Davies, R. I., Sugai, H., & Ward, M. J. 1998, *MNRAS*, 295, 43
- de Blok, W. J. G., & Walter, F. 2000, *ApJ*, 537, L95
- de Blok, W. J. G., McGaugh, S. S., & van der Hulst, J. M. 1996, *MNRAS*, 283, 18
- de Vaucouleurs, G., de Vaucouleurs, A., Corwin, H., Buta, R., Paturel, G., & Fouqué, P. 1991, *Third Reference Catalogue of Bright Galaxies* (New York, Springer-Verlag), =RC3
- Dohm-Palmer, R. C., et al. 1998, *AJ*, 116, 1227
- Dolphin, A. E. 2000, *ApJ*, 531, 804
- Dolphin, A. E., et al. 2002, *AJ*, 123, 3154
- Dolphin, A. E., et al. 2003, *AJ*, 125, 1261
- Dopita, M. A., & Ryder, S. D. 1994, *ApJ*, 430, 163
- Elmegreen, B. G. 1993, *ApJ*, 419, L29
- Elmegreen, B. G., & Elmegreen, D. M. 1986, *ApJ*, 311, 554
- Elmegreen, B. G., & Hunter, D. A. 2000, *ApJ*, 540, 814
- Ferraro, F. R., Pecci, F. F., Tosi, M., & Buonanno, R. 1989, *MNRAS*, 241, 433
- Fisher, J. R., & Tully, R. B. 1975, *A&A*, 44, 151
- Fisher, J. R., & Tully, R. B. 1981, *ApJS*, 47, 139
- Freedman, W. L. et al. 2001, *ApJ*, 553, 47
- Gallagher, J. S., Hunter, D. A., & Tutukov, A. V. 1984, *ApJ*, 284, 544

- Gallagher, J. S., Tolstoy, E., Dohm-Palmer, R. C., Skillman, E. D., Cole, A. A., Hoessel, J. G., Saha, A., & Mateo, M. 1998, *AJ*, 115, 1869
- Gallart, C., Aparicio, A., Bertelli, G., & Chiosi, C. 1996a, *AJ*, 112, 1950
- Gallart, C., Aparicio, A., Bertelli, G., & Chiosi, C. 1996b, *AJ*, 112, 2596
- Gallart, C., Aparicio, A., & Vilchez, J. M. 1996, *AJ*, 112, 1928
- Gallart, C., Freedman, W., Mateo, M., Chiosi, C., Thompson, I., Aparicio, A., Bertelli, G., Hodge, P., Lee, M., Olszewski, E., Saha, A., Stetson, P., & Suntzeff, N. 1999, *ApJ*, 514, 665
- Gil de Paz, A., Aragón-Salamanca, A., Gallego, J., Alonso-Herrero, A., Zamorano, J., & Kauffmann, G. 2000, *MNRAS*, 316, 357
- Gordon, D., & Gottesman, S. T. 1981, *AJ*, 86, 161
- Greggio, L., Marconi, G., Tosi, M., & Focardi, P. 1993, *AJ*, 105, 894
- Greggio, L., Tosi, M., Clampin, M., de Marchi, G., Leitherer, C., Nota, A., & Sirianni, M. 1998, *ApJ*, 504, 725
- Hashimoto, Y., Oemler, A., Jr., Lin, H., & Tucker, D. L. 1998, *ApJ*, 499, 589
- Heller, A.B., Brosch, N., Almozniño, E., van Zee, L., & Salzer, J.J. 2000, *MNRAS*, 316, 569
- Hidalgo, S. L., Marín-Franch, A., & Aparicio, A. 2003, *AJ*, 124, 1247
- Hodge, P. W. 1971, *Ann Rev A&A*, 9, 35
- Hodge, P. W., & Hitchcock, J. L. 1966, *PASP*, 78, 79
- Hopkins, A. M., Connolly, A. J., Haarsma, D. B., & Cram, L. E. 2001, *AJ*, 122, 288
- Hopkins, A. M., Schulte-Ladbeck, R. E., & Drozdovsky, I. O. 2002, *AJ*, 124, 862
- Huchtmeier, W. K., Hopp, U., & Kuhn, B. 1997, *A&A*, 319, 67
- Huchtmeier, W. K., Seiradakis, J. H., & Materne, J. 1981, *A&A*, 102, 134
- Hunter, D. A. 2001, *ApJ*, 559, 225
- Hunter, D. A., Elmegreen, B. G., & Baker, A. L. 1998a, *ApJ*, 493, 595
- Hunter, D. A., Elmegreen, B. G., van Woerden, H. 2001, *ApJ*, 556, 773

- Hunter, D. A., & Gallagher, J. S. 1985a, AJ, 90, 1789
- Hunter, D. A., & Gallagher, J. S. 1985b, ApJS, 58, 533
- Hunter, D. A., & Gallagher, J. S. 1986, PASP, 98, 5
- Hunter, D. A., Gallagher, J. S., & Rautenkranz, D. 1982, ApJS, 49, 53
- Hunter, D. A., Hawley, W. N., & Gallagher, J. S., III 1993, AJ, 106, 1797
- Hunter, D. A., & Hoffman, L. 1999, AJ, 117, 2789
- Hunter, D. A., Wilcots, E., van Woerden, H., Gallagher, J. S., & Kohle, S. 1998b, ApJ, 495, L47
- Israel, F. P. 1988, A&A, 194, 24
- Jacoby, G. H., Hunter, D. A., & Christian, C. A. 1984, ApJS, 56, 257
- James, P. A., Shane, N. S., Beckman, J. E., Cardwell, A., Collins, C. A., Etherton, J., de Jong, R. S., Fathi, K., Knapen, J. H., Peletier, R. F., Percival, S. M., Pollacco, D. L., Seigar, M. S., Stedman, S., & Steele, I. A. 2004, A&A, 414, 23
- Karachentsev, I. D., Aparicio, A., & Makarova, L. 1999, A&A, 352, 363
- Karachentsev, I. D., Musella, I., & Grimaldi, A. 1996, A&A, 310, 722
- Karachentsev, I. D., et al. 2002, A&A, 383, 125
- Karachentsev, I. D., et al. 2003a, A&A, 398, 467
- Karachentsev, I. D., et al. 2003b, A&A, 398, 479
- Kennicutt, R. C., Jr. 1983, ApJ, 272,54
- Kennicutt, R. C., Jr. 1989, ApJ, 344, 685
- Kennicutt, R. C., Jr. 1998, ARA&A, 36, 189
- Kennicutt, R. C., Balick, B., & Heckman, T. 1980, PASP, 92, 134
- Kennicutt, R. C., Jr., & Skillman, E. D. 2001, AJ, 121, 1461
- Kennicutt, R. C., Tamblyn, P., & Congdon, C. W. 1994, ApJ, 435, 22
- Klessen R.S. 2000, ApJ, 535, 869

- Kniazen, A. Y., et al. 2000, *A&A*, 357, 101
- Komiyama, Y., et al. 2003, *ApJ*, 590, L17
- in *Star-Forming Dwarf Galaxies* edited by D. Kunth, T. X. Thuan, & J. T. Thanh Van, (France:Editions Frontieres), p. 183
- Lee, M. G., Aparicio, A., Tikonov, N., Byun, Y.-I., & Kim, E. 1999, *AJ*, 118, 853
- Lee, M. G., & Kim, S. C. 2000, *AJ*, 119, 777
- Li, Y., Klessen, R.S., Mac Low, M.-M. 2003, *ApJ*, 592, 975
- Lo, K. Y., Sargent, W. L. W., & Young, K. 1993, *AJ*, 106, 507
- Lynds, R., Tolstoy, E., O’Neil, E. J., & Hunter, D. A. 1998, *AJ*, 116, 146
- Mac Low, M.-M., & Klessen, R. S. 2004, *Rev Mod Phys*, 76, 125
- Maiz-Apellaniz, J., Cieza, L., & Mackenty, J. W. 2002, *AJ*, 123, 1307
- Makarova, L., Karachentsev, I., Takalo, L. O., Heinaemaeki, P., & Valtonen, M. 1998, *A&AS*, 128, 459
- Marconi, G., Tosi, M., Greggio, L., & Focardi, P. 1995, *AJ*, 109, 173
- McGaugh, S. S., & Bothun, G. D. 1994, *AJ*, 107, 530
- Massey, P., & Armandroff, T. E. 1995, *AJ*, 109, 2470
- Massey, P., & Hunter, D. A. 1998, *ApJ*, 493, 180
- Méndez, B., Davis, M., Moustakas, J., Newman, J., Madore, B. F., & Freedman, W. L. 2002, *AJ*, 124, 213
- Méndez, D. I., & Esteban, C. 2000, *A&A*, 359, 493
- Meurer, G. R., Staveley-Smith, L., & Killeen, N. E. B. 1998, *MNRAS*, 300, 705
- Miller, B. W., Dolphin, A. E., Lee, M. O., Kim, S. C., & Hodge, P. 2001, *ApJ*, 562, 713
- Minniti, D., & Zijlstra, A. A. 1997, *AJ*, 114, 147
- Minniti, D., Zijlstra, A. A., & Alonso, M. V. 1999, *AJ*, 117, 881
- Noeske, K. G., Papaderos, P., Cairós, L. M., & Fricke, K. J. 2003, *ã*, 410, 481

- Noeske, K. G., Iglesias-Páramo, J., Vílchez, J. M., Papaderos, P., & Fricke, K. J. 2001, *A&A*, 371, 806
- Noguchi, M. 1988, *A&A*, 201, 37
- O’Connell, R. W., Gallagher, J. S., III, Hunter, D. A. 1994, *ApJ*, 433, 65
- Osterbrock, D. E. 1974, *Astrophysics of Gaseous Nebulae*, (San Francisco:W.H. Freeman and Company)
- Östlin, G., Amram, P., Bergvall, N., Masegosa, J., Boulesteix, J., & Márquez, I. 2001, *A&A*, 374, 800
- Östlin, G., Zackrisson, E., Bergvall, N., Rönnback, J. 2003, *A&A*, 408, 887
- Ostriker, E.C., Gammie, C.F., & Stone, J.M. 1999, *ApJ*, 513, 259
- Ostriker, E.C., Stone, J.M., Gammie, C.F. 2001, *ApJ*, 546, 980
- Padoan, P., Juvela, M., Bally, J., Nordlund, A. 2000, *ApJ*, 529, 259
- Panagia, N. 1973, *AJ*, 78, 929
- Papaderos, P., Loose, H.-H., Fricke, K. J., & Thuan, T. X. 1996, *A&A*, 314 59
- Parodi, B. R., & Binggeli, B. 2003, *A&A*, 398, 501
- Patterson, R. J., & Thuan, T. X. 1996, *ApJS*, 107, 103
- Pérez-González, P. G., Gil de Paz, A., Zamorano, J., Gallego, J., Alonso-Herrero, A., & Aragón-Salamanca, A. 2003, *MNRAS*, 338, 525
- Pildis, R. A., Schombert, J. M., & Eder, J. A. 1997, *ApJ*, 481, 157
- Popescu, C. C., Hopp, U., & Rosa, M. R. 1999, *A&A*, 350, 414
- Pustilnik, S.A., Kniazev, A.Y., Lipovetsky, V.A., & Ugryumov, A.V. 2001a, *A&A*, 373, 24
- Pustilnik, S.A., Brinks, E., Thuan, T.X., Lipovetsky, V.A., Izotov, Y.I. 2001b, *AJ*, 121, 1413
- Pustilnik, S.A., Kniazev, A.Y., Pramskij, A.G., Ugryumov, A.V., & Masegosa, J. 2003, *A&A*, 409, 917
- Putman, M. E., Bureau, M., Mould, J. R., Staveley-Smith, L., & Freeman, K. C. 1998, *AJ*, 115, 2345

- Roye, E. W., & Hunter, D. A. 2000, *AJ*, 119, 1145
- Ryder, S. D., & Dopita, M. A. 1994, *ApJ*, 430, 142
- Salpeter, E. E. 1955, *ApJ*, 121, 161
- Sargent, W. L. W., Sancisi, R., & Lo, K. Y. 1983, *ApJ*, 265, 711
- Schaerer, D., Meynet, G., Maeder, A., & Schaller, G. 1993, *A&AS*, 98, 523
- Schlegel, D. J., Finkbeiner, D. P., & Davis, M. 1998, *ApJ*, 500, 525
- Schombert, J. M., & Bothun, G. D. 1988, *AJ*, 95, 1389
- Schombert, J. M., Bothun, G. D., Schneider, S. E., & McGaugh, S. S. 1992, *AJ*, 103, 1107
- Schulte-Ladbeck, R. E., Hopp, U., Greggio, L., & Crone, M. M. 2000, *AJ*, 120, 1713
- Schulte-Ladbeck, R.E., Hopp, U., Greggio, L., Crone, M.M., & Drozdovsky, I.O. 2001, *AJ*, 121, 3007
- Simpson, C. E., & Gottesman, S. T. 2000, *AJ*, 120, 2975
- Simpson, C. E., Hunter, D. A., & Knezek, P. 2004, *AJ*, submitted
- Staveley-Smith, L., Davies, R. D., & Kinman, T. D. 1992, *MNRAS*, 258, 334
- Stil, J. M., & Israel, F. P. 1998, *A&A*, 337, 64
- Stil, J. M., & Israel, F. P. 2002, *A&A*, 389, 29
- Sung, E.-C., Han, C., Ryden, B. S., Patterson, R. J., Chun, M.-S., Kim, H.-I., Lee, W.-B., & Kim, D.-J. 1998, *ApJ*, 505, 199
- Swaters, R. 1999, Ph.D. thesis, Rijksuniversiteit Groningen
- Swaters, R. A., Madore, B. F., & Trewhella, M. 2000, *ApJ*, 531, L107
- Taylor, C. L. 1997, *ApJ*, 480, 524
- Taylor, C. L., Brinks, E., Grashuis, R. M., & Skillman, E. D. 1995, *ApJS*, 99, 427
- Taylor, C. L., Brinks, E., & Skillman, E. D. 1993, *AJ*, 105, 128
- Telles, E., & Maddox, S. 2000, *MNRAS*, 311, 307
- Telles, E., & Terlevich, R. 1995, *MNRAS*, 275, 1

- Thuan, T. X., & Martin, G. E. 1981, *ApJ*, 247, 823
- Thuan, T.X. 1991, in *Massive Stars in Starbursts*, ed. C. Leitherer, N. R. Walborn, T. M. Heckman, & C. A. Norman (Cambridge: Cambridge Univ. Press), 183
- Tolstoy, E. 1996, *ApJ*, 462, 684
- Tolstoy, E., Gallagher, J. S., Cole, A. A., Hoessel, J. G., Saha, A., Dohm-Palmer, R. C., Skillman, E. D., Mateo, M., & Hurley-Keller, D. 1998, *AJ*, 116, 1244
- Tolstoy, E., Saha, A., Hoessel, J. G., & Danielson, G. E. 1995, *AJ*, 109, 579
- Tosi, M., Greggio, L., Marconi, G., & Focardi, P. 1991, *AJ*, 102, 951
- Tosi, M., Sabbi, E., Bellazzini, M., Aloisi, A., Greggio, L., Leitherer, C., & Montegriffo, P. 2001, *AJ*, 122, 1271
- van den Bergh, S. 1959, *Publ David Dunlap Obs*, Vol 2, No 5, p 147
- van den Bergh, S. 1966, *AJ*, 71, 922
- van den Bergh, S. 1988, *PASP*, 100, 344
- van den Hoek, L. B., de Blok, W. J. G., van der Hulst, J. M., & de Jong, T. 2000, *A&A*, 357, 397
- van Zee, L., Skillman, E. D., & Salzer, J. J. 1998, *AJ*, 116, 1186
- van Zee, L. 2000, *AJ*, 119, 2757
- van Zee, L. 2001, *AJ*, 121, 2003
- van Zee, L., Salzer, J. J., & Skillman, E. D. 2001, *AJ*, 122, 121
- van Zee, L., Haynes, M. P., & Giovanelli, R. 1995, *AJ*, 109, 990
- van Zee, L., Maddalena, R. J., Haynes, M. P., Hogg, D. E., & Roberts, M. S. 1997, *AJ*, 113, 1638
- Vázquez-Semadeni, E., & García, N. 2001, *ApJ*, 557, 727
- Vitvitska, M., Klypin, A. A., Kravtsov, A. V., Wechsler, R. H., Primack, J. R., & Bullock, J. S. 2002, *ApJ*, 581, 799
- Weilbacher, P. M., & Fritze-v. Alvensleben, U. *A&A*, 2001, 373, L9

- Wilcots, E.M. & Miller, B.W. 1998, AJ, 116, 2363
- Willick, J. A. 1999, ApJ, 522, 647
- Wyder, T. K. 2001, AJ, 122, 2490
- Young, L. M., & Lo, K. Y. 1997, ApJ, 490, 710
- Youngblood, A. J., & Hunter, D. A. 1999, ApJ, 519, 55

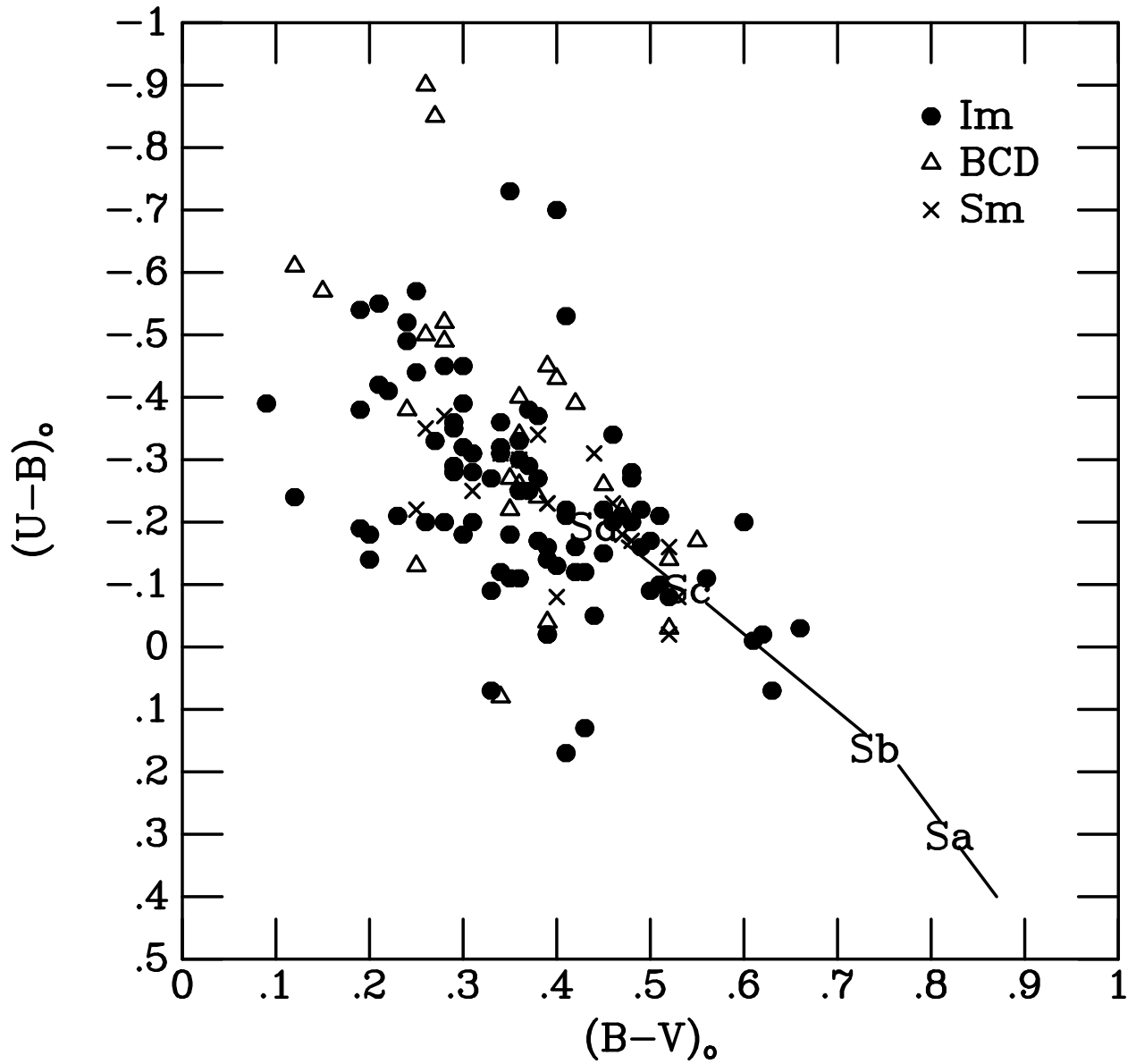


Fig. 1.— Integrated UBV colors of our survey galaxies. Average colors are shown for spiral galaxies (de Vaucouleurs & de Vaucouleurs 1972). The UBV colors are corrected for reddening using the foreground reddening of Burstein & Heiles (1984), an assumed internal reddening of $E(B-V)_s = 0.05$, and the reddening law of Cardelli et al. (1989).

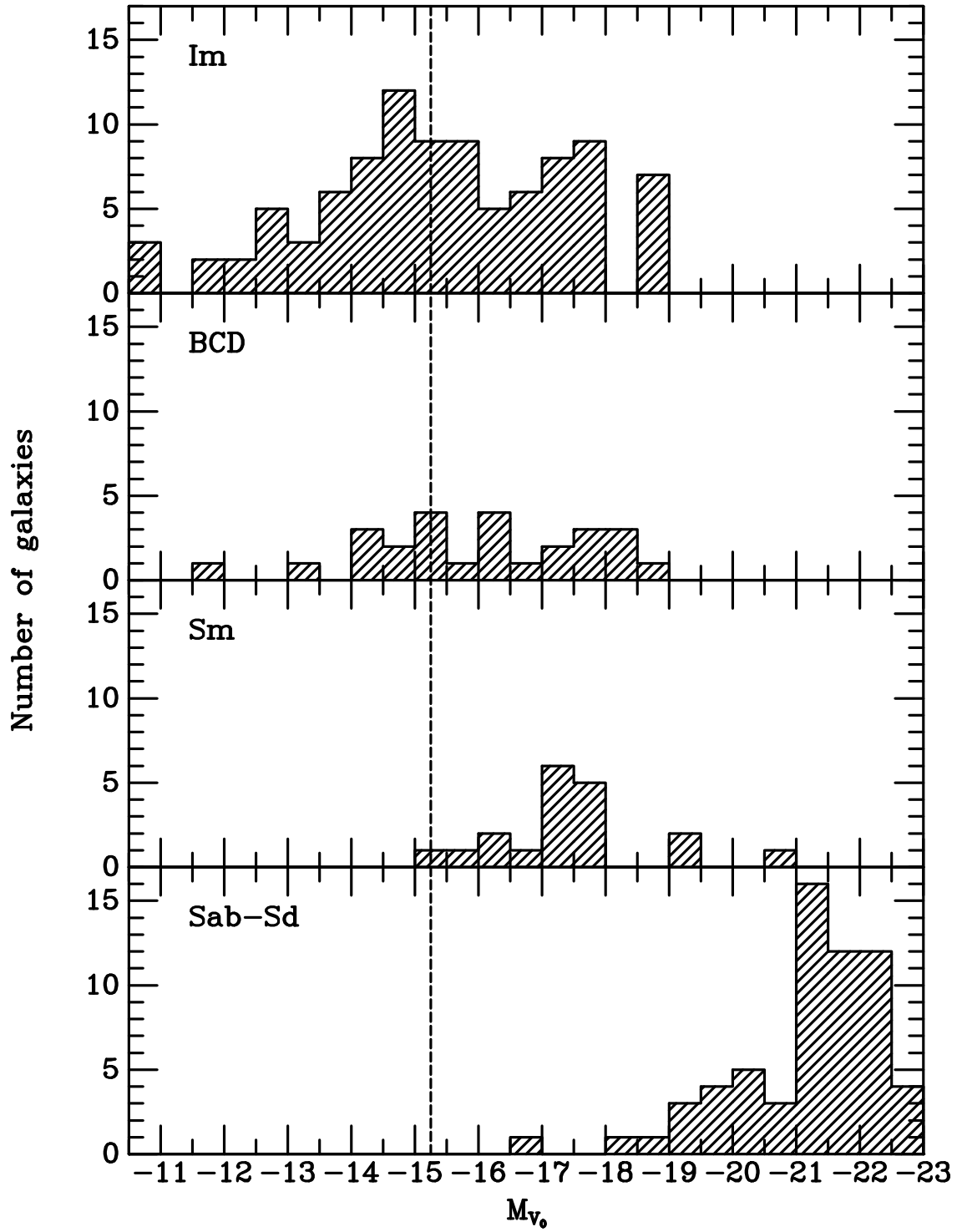


Fig. 2.— Number distribution of the survey galaxies in integrated M_V , corrected for reddening. The vertical dashed line marks the median value in M_{V_0} for the Im galaxies.

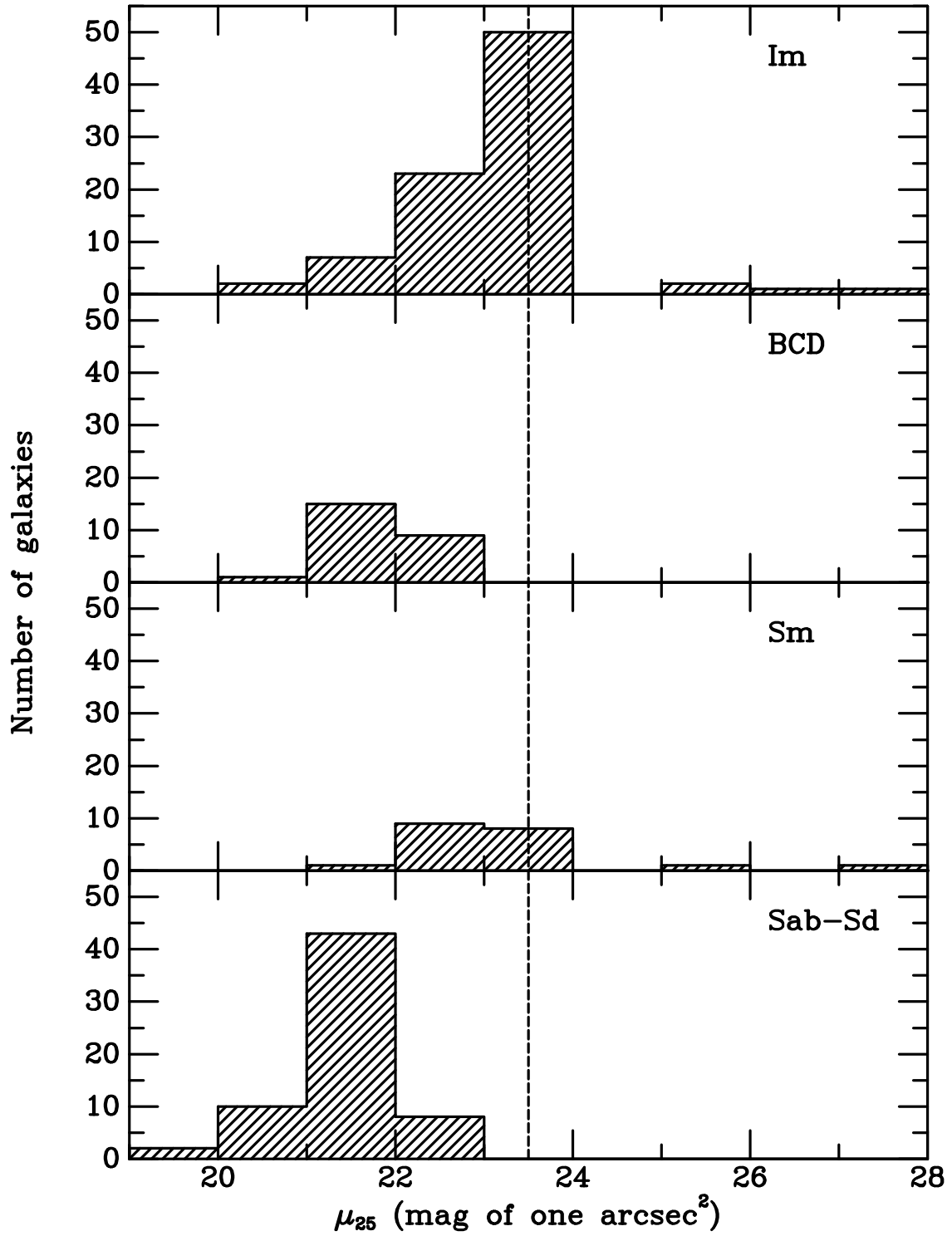


Fig. 3.— Number distribution of the survey galaxies in μ_{25} , the average surface brightness within a B-band isophote of 25 mag of one arcsec², corrected for reddening. The dashed vertical line marks the median value of μ_{25} for the Im group.

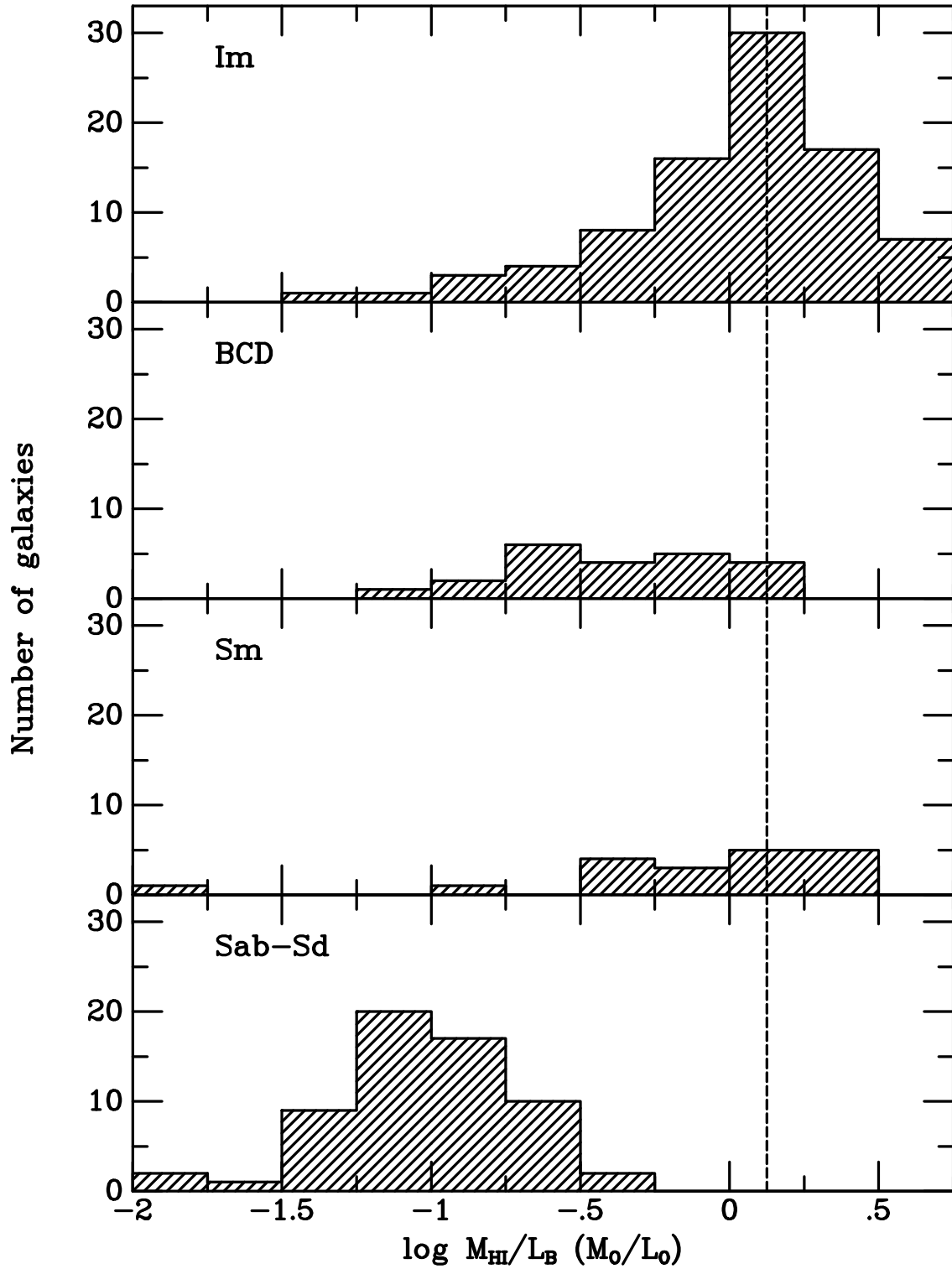


Fig. 4.— Number distribution of the survey galaxies in integrated M_{HI}/L_B . The vertical dashed line marks the median value of $\log M_{HI}/L_B$ for the Im galaxies to aid in comparison to the other galaxy types.

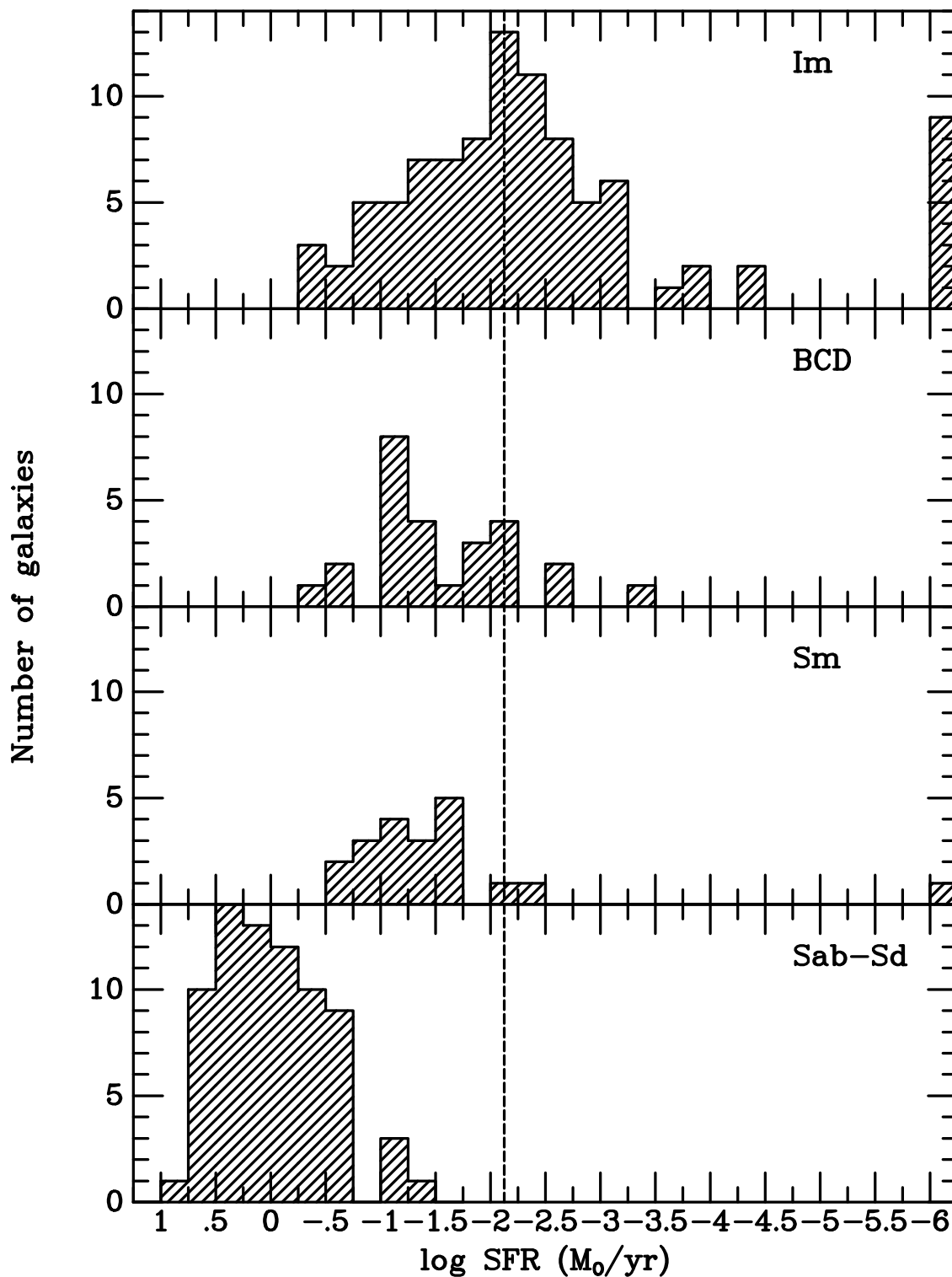


Fig. 5.— Number distribution of the survey galaxies and comparison spirals in integrated star formation rate. Galaxies at $\log \dot{M} \leq -6$ are those with zero star formation rates. The vertical dashed line marks the median value of $\log \dot{M}$ for the Im galaxies.

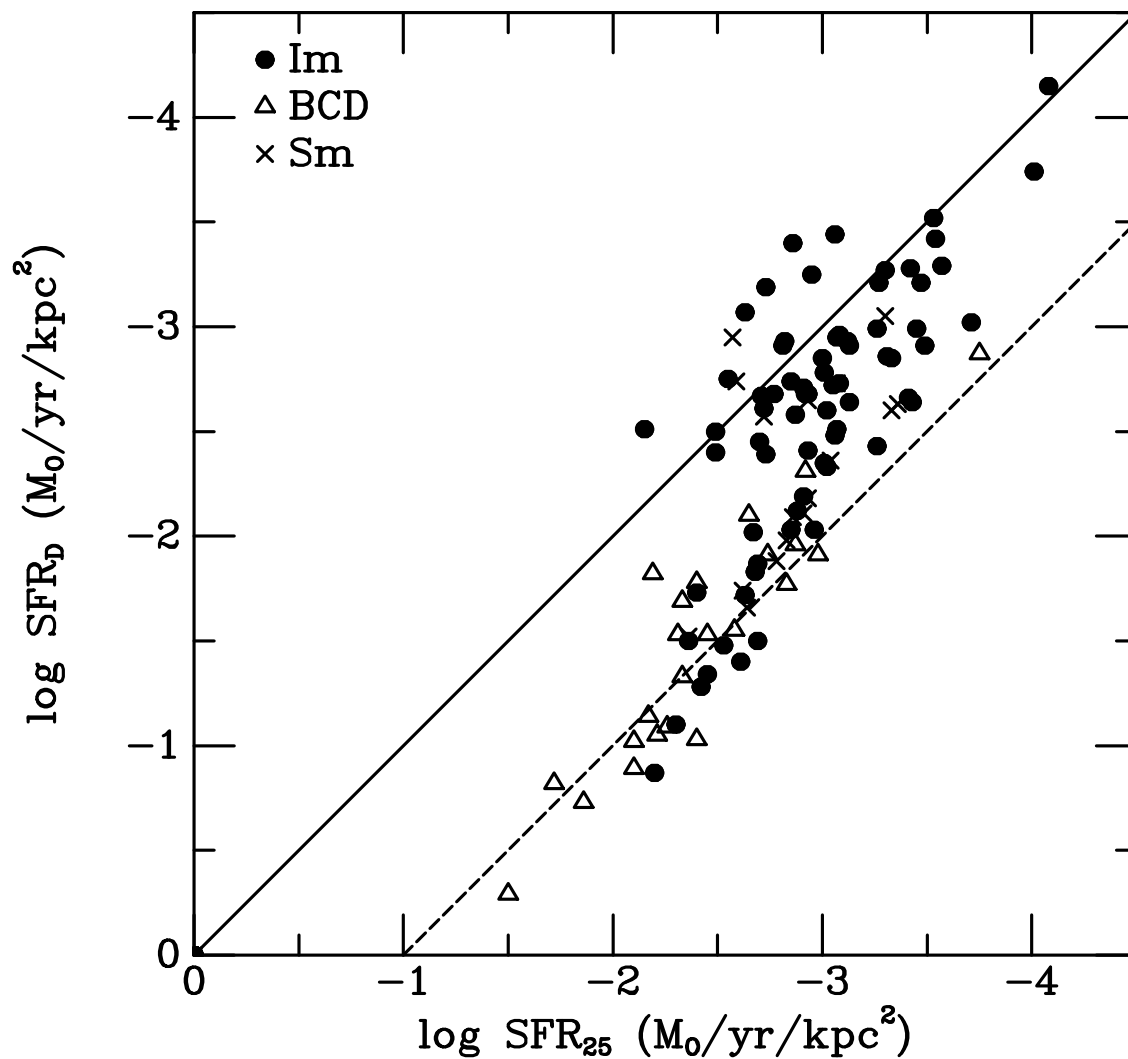


Fig. 6.— Comparison of integrated star formation rates \dot{M} normalized to the area of the galaxy determined from R_{25} and from R_D . The solid line deliniates equal quantities. The dashed line is for $\dot{M}_D = 10 \times \dot{M}_{25}$, which corresponds to $R_{25} = \sqrt{10}R_D$. The area of the galaxy is computed from πR^2 .

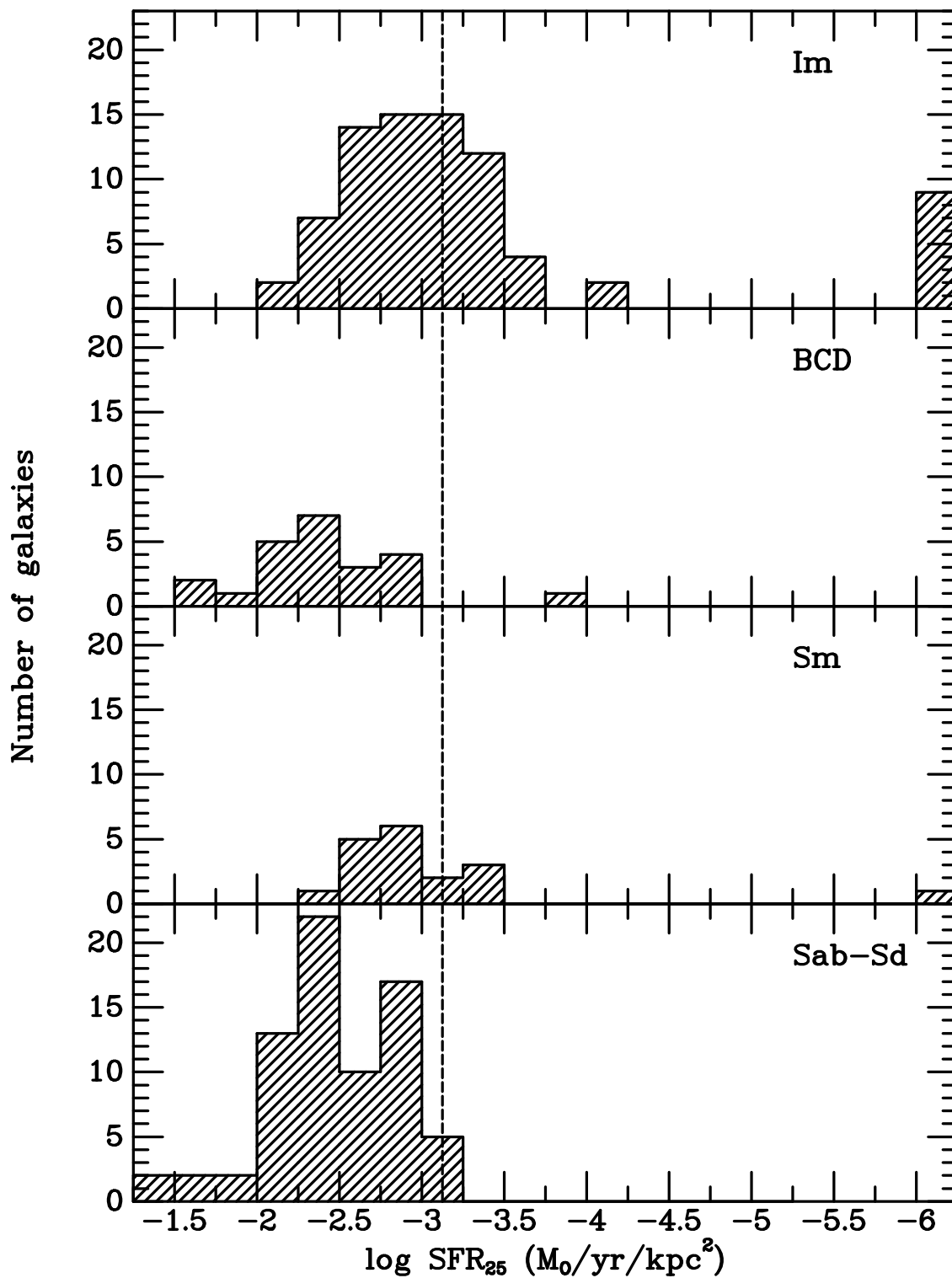


Fig. 7.— Number distribution of the survey galaxies and comparison spirals in integrated star formation rate normalized to the size of the galaxy within R_{25} . Galaxies at $\log \dot{M}_{25} \leq -6$ are those with zero star formation rates. The vertical dashed line marks the median star formation rate of an Im galaxy.

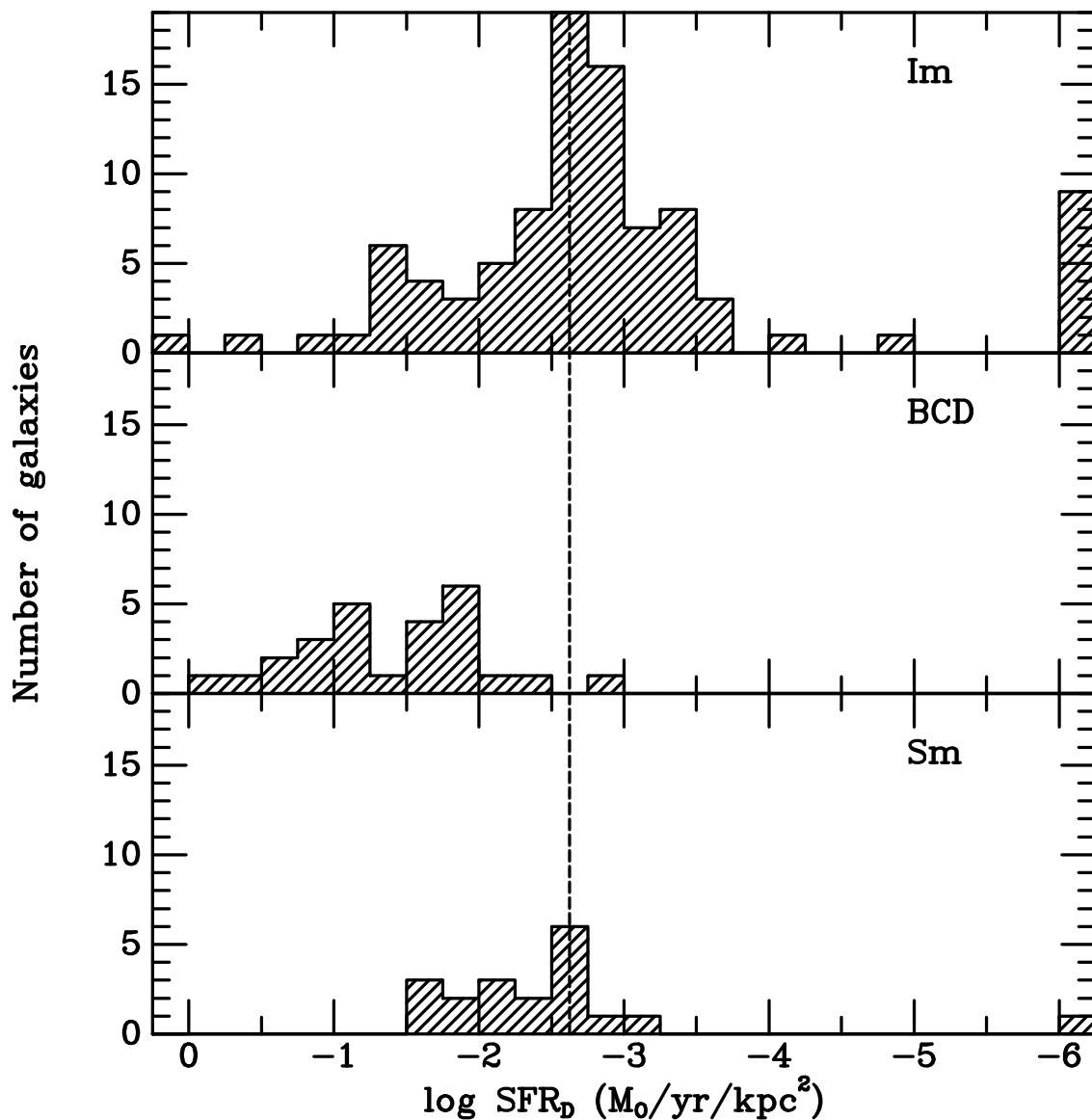


Fig. 8.— Number distribution of the survey galaxies and comparison spirals in integrated star formation rate normalized to the size of the galaxy within the scale-length R_D . Galaxies at $\log \dot{M}_{25} \leq -6$ are those with zero star formation rates. The vertical dashed line marks the median $\log \dot{M}_D$ for an Im galaxy.

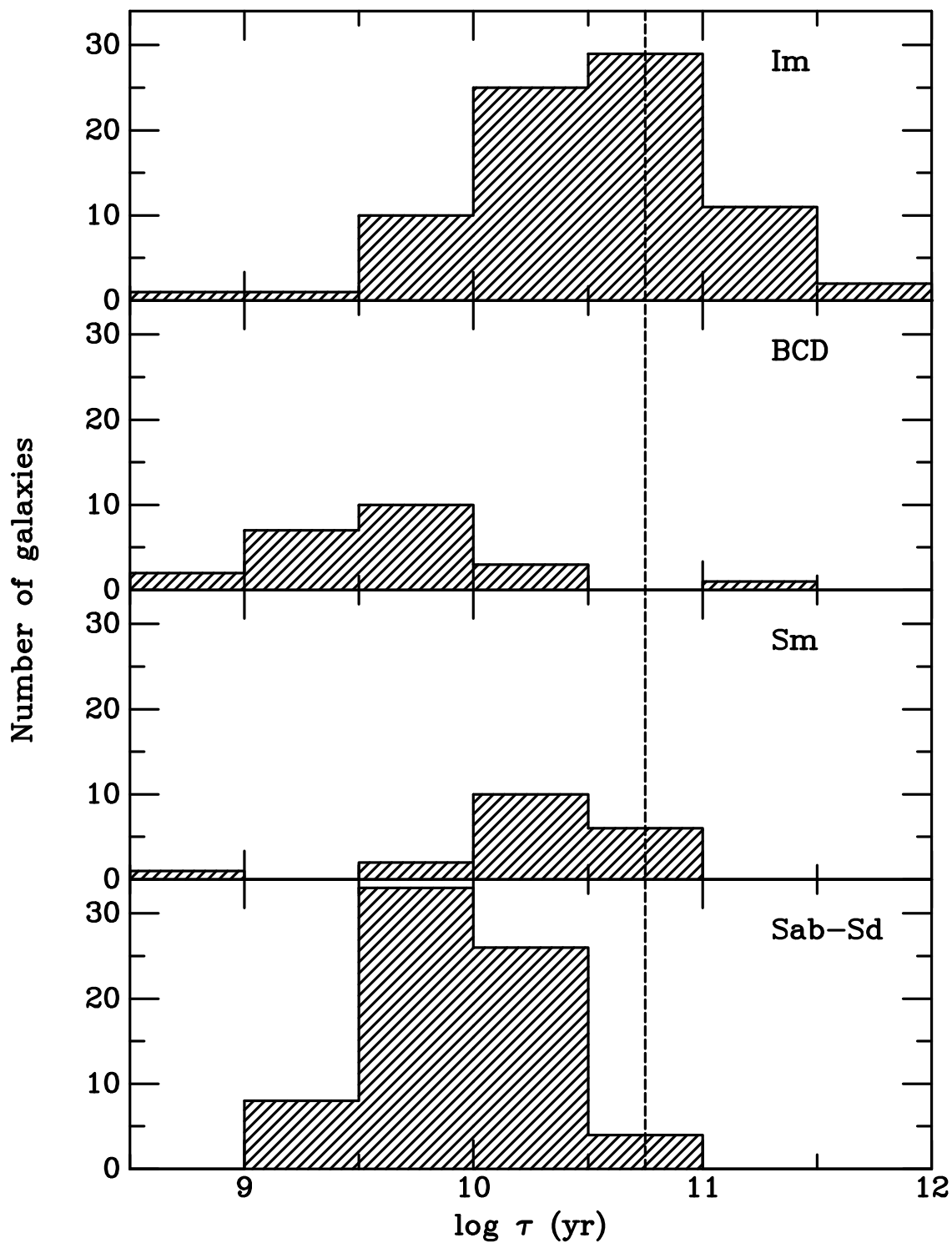


Fig. 9.— Number distribution of the survey galaxies and comparison spirals in timescale τ to exhaust the current gas supply at the current star formation rate. The gas supply is taken as the total gas associated with the galaxy, including HI and He. The vertical dashed line marks the median value of an Im galaxy.

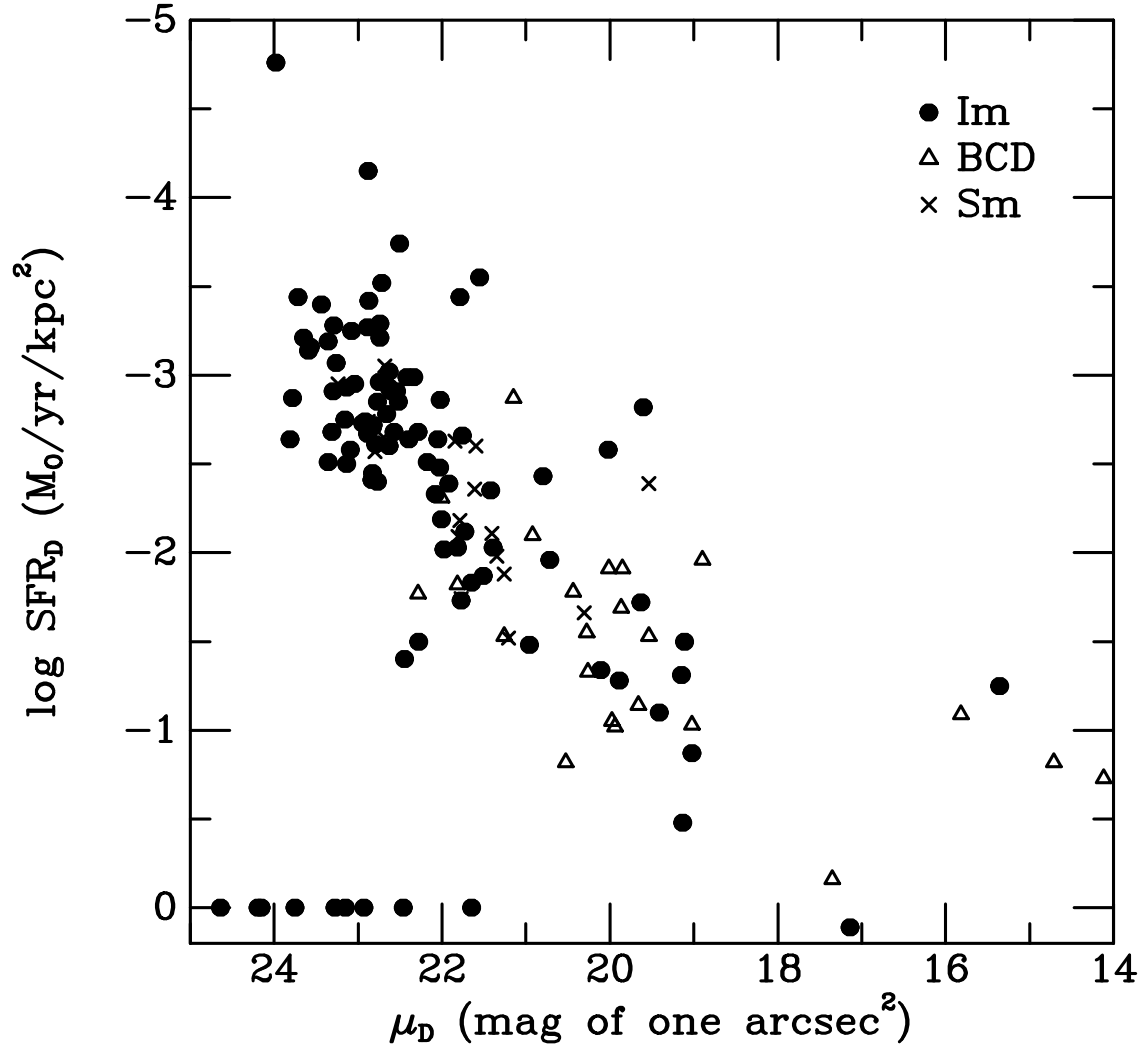


Fig. 10.— Normalized star-formation rate \dot{M}_D plotted against the average V-band surface brightness within one scale length μ_D . Galaxies with star formation rates of zero are plotted along the x axis at a log of 0. The Im, BCD, and Sm samples are shown with different symbols.

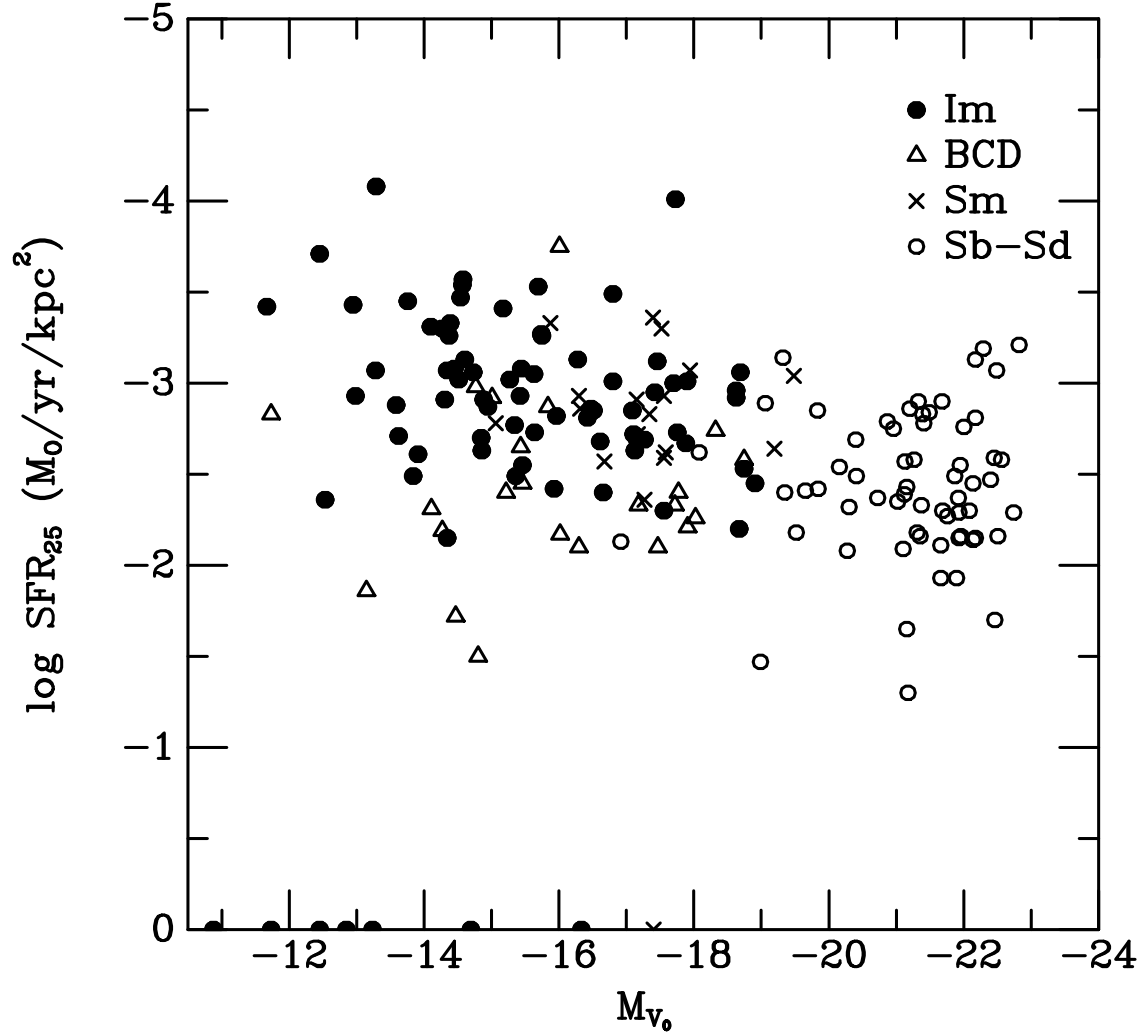


Fig. 11.— Normalized star-formation rate \dot{M}_{25} plotted against reddening-corrected galactic M_V . The Im, BCD, and Sm samples are shown with different symbols. The Sb-Sd galaxies are taken from the literature. Galaxies plotted at $\log \dot{M}_D = 0$ have a star formation rate of 0.

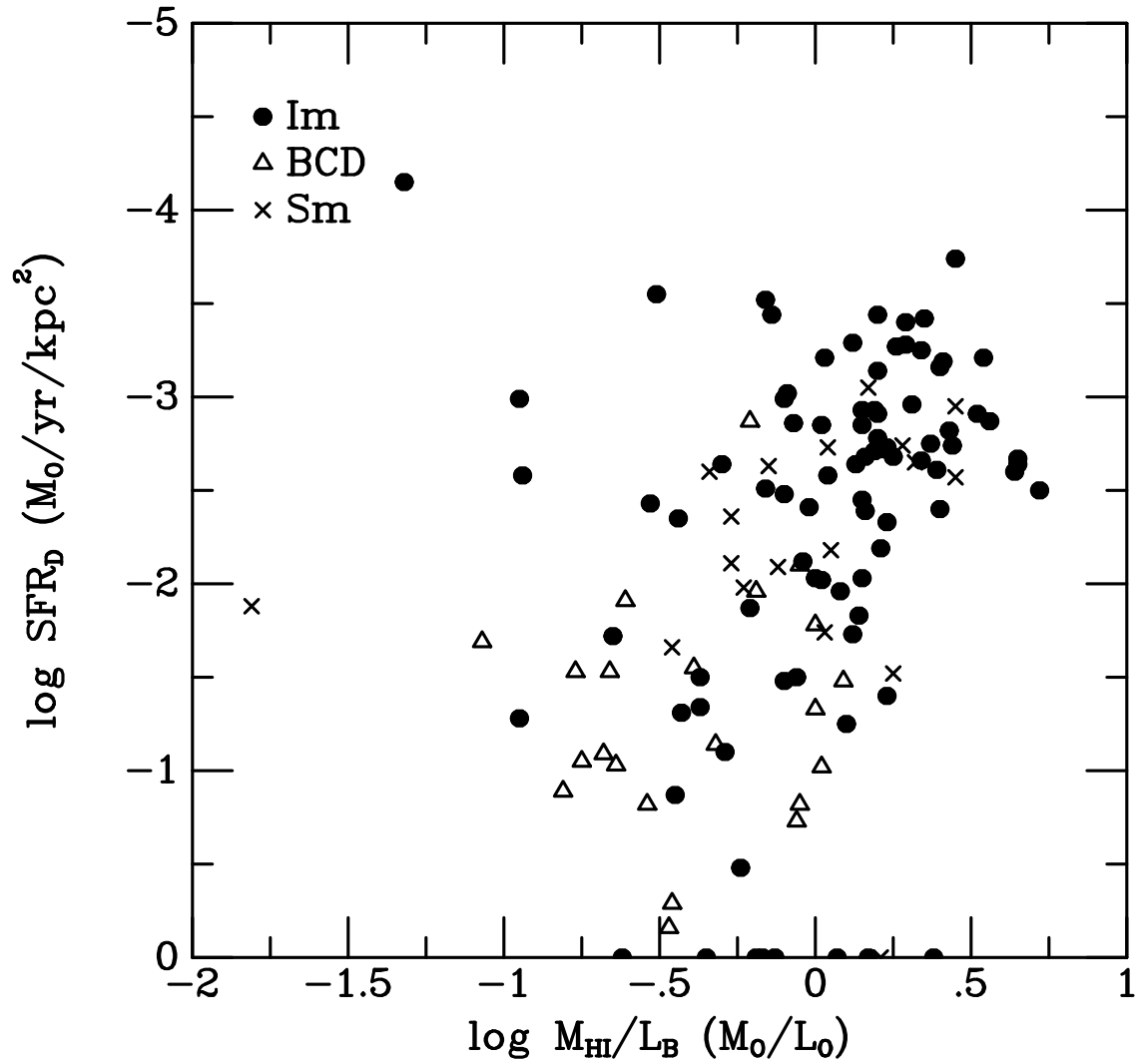


Fig. 12.— Normalized star-formation rate \dot{M}_D plotted against galactic M_{HI}/L_B . The Im, BCD, and Sm samples are shown with different symbols. Galaxies plotted at $\log \dot{M}_D = 0$ have a star formation rate of 0.

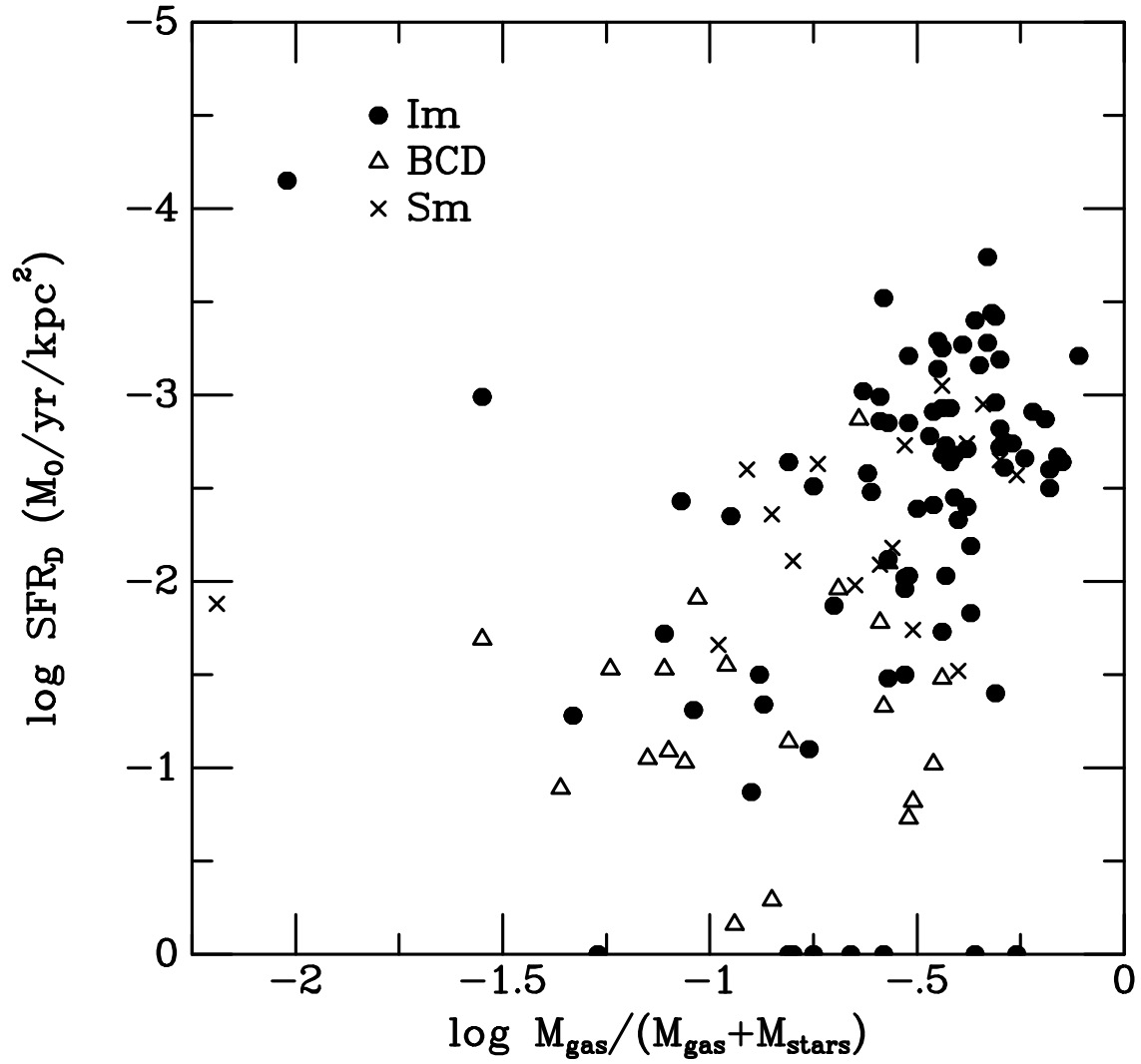


Fig. 13.— Normalized star-formation rate \dot{M}_D plotted against the gas fraction of the galaxy. The gas mass includes H I and He. The Im, BCD, and Sm samples are shown with different symbols. Galaxies without any current star formation are plotted at $\log \dot{M}_D = 0$.

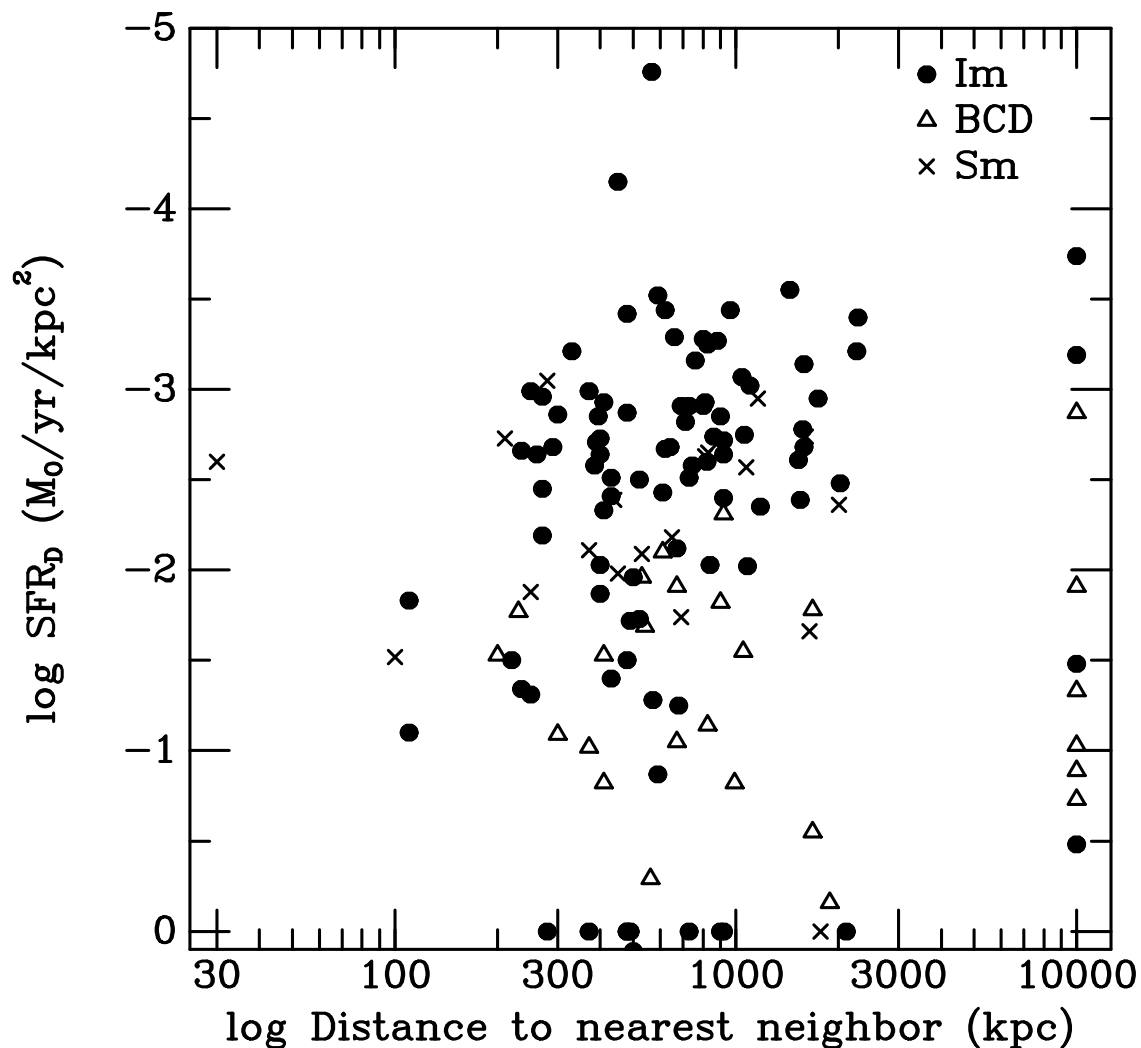


Fig. 14.— Normalized star-formation rate \dot{M}_D plotted against the log of the distance to the nearest neighboring galaxy. Those plotted at a distance of 10000 kpc are galaxies for which no neighbor was found within the search parameters: 1 Mpc and 150 km s^{-1} . The Im, BCD, and Sm samples are shown with different symbols. Galaxies plotted at $\log \dot{M}_D = 0$ have a star formation rate of 0.

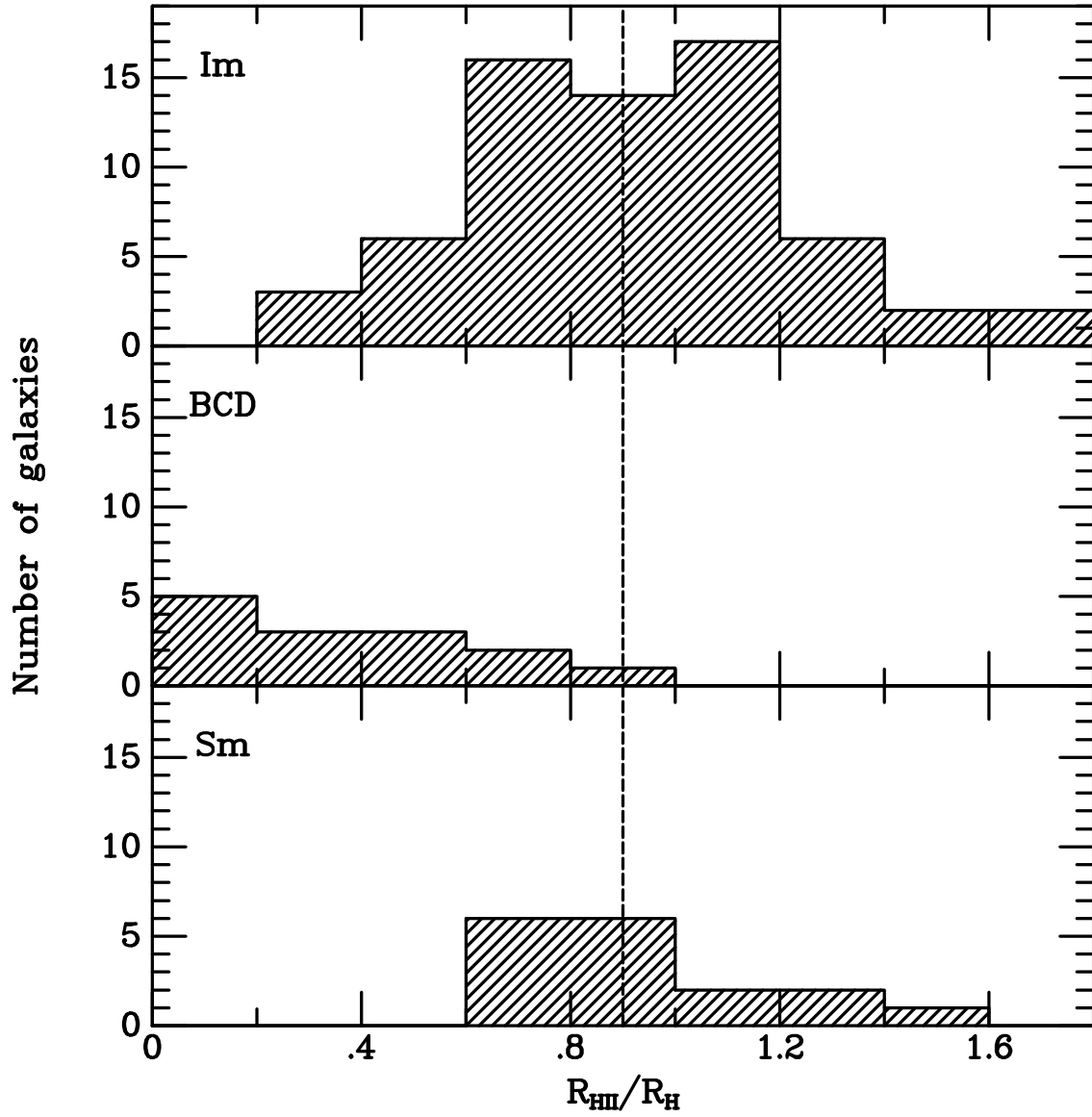


Fig. 15.— Number distribution of the extent of discrete H II regions relative to the Holmberg radius R_H . The vertical dashed line marks the median value of $R_{H\alpha}/R_H$ for the Im galaxies.

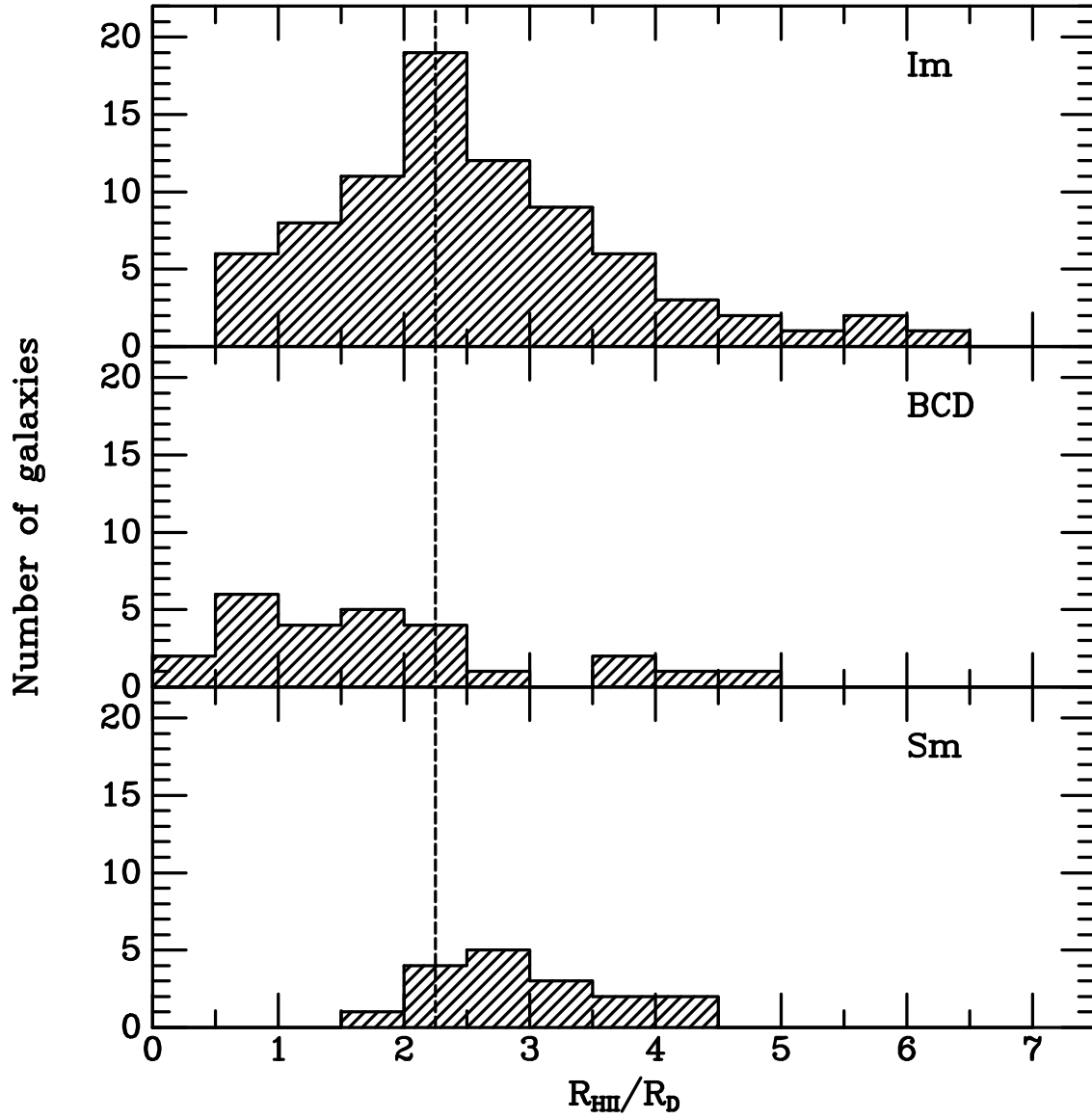


Fig. 16.— Number distribution of the extent of discrete H II regions relative to the scale length R_D . The vertical dashed line marks the median value of $R_{H\alpha}/R_D$ for the Im galaxies.

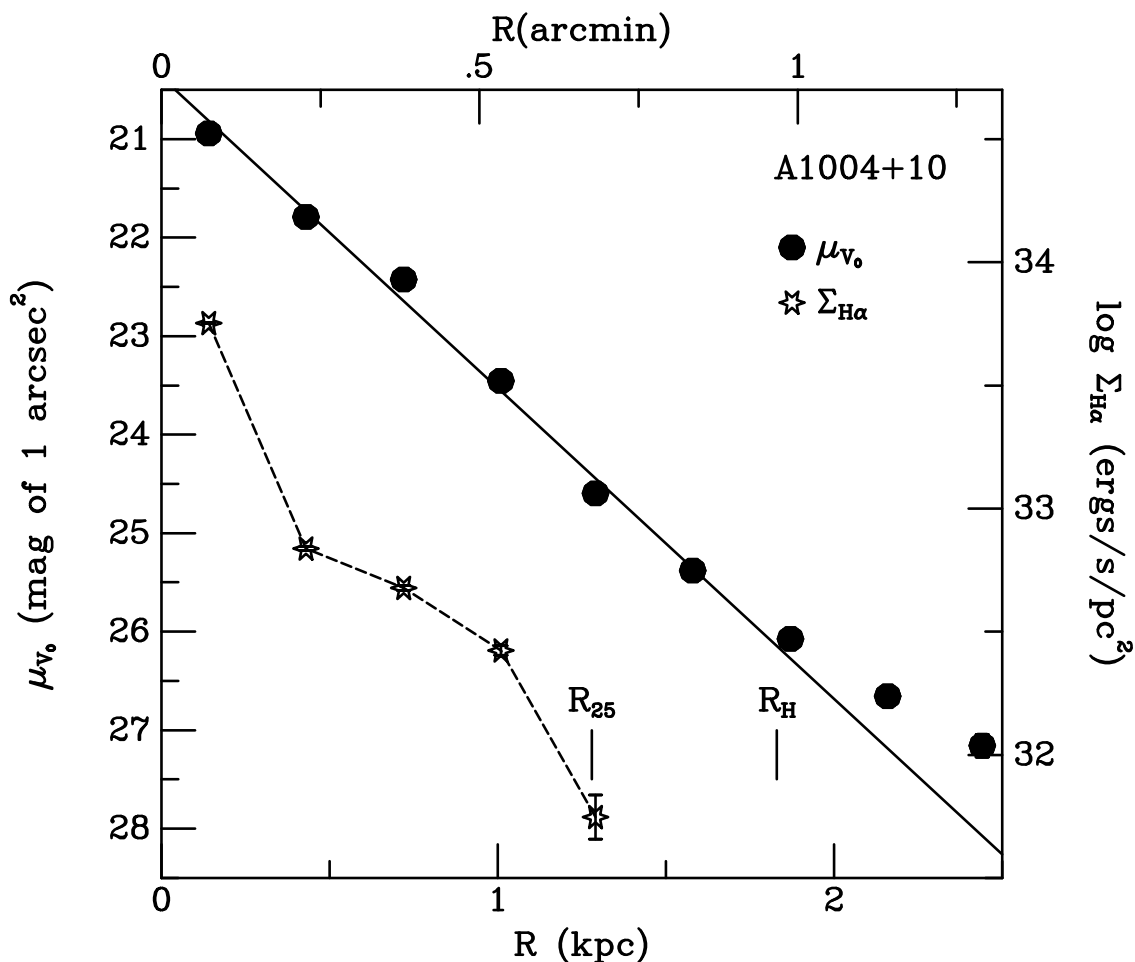


Fig. 17.— Azimuthally-averaged H α and V-band surface photometry. Both are corrected for reddening. The scales for $\Sigma_{H\alpha}$ and μ_{V_0} have been set so that they cover the same logarithmic interval. The solid line is a fit to the V-band surface photometry. The radii corresponding to R_{25} and R_H are marked with vertical lines near the bottom of the plot. This plot is the surface photometry for A1004+10, the first galaxy in our sample. For a few galaxies V-band images were not available; these are denoted “off” or “DSS” for use of the H α off-band image or Digitized Sky Survey. The galaxy A1004+10 is also an example of a good correspondence between μ_V and $\Sigma_{H\alpha}$.

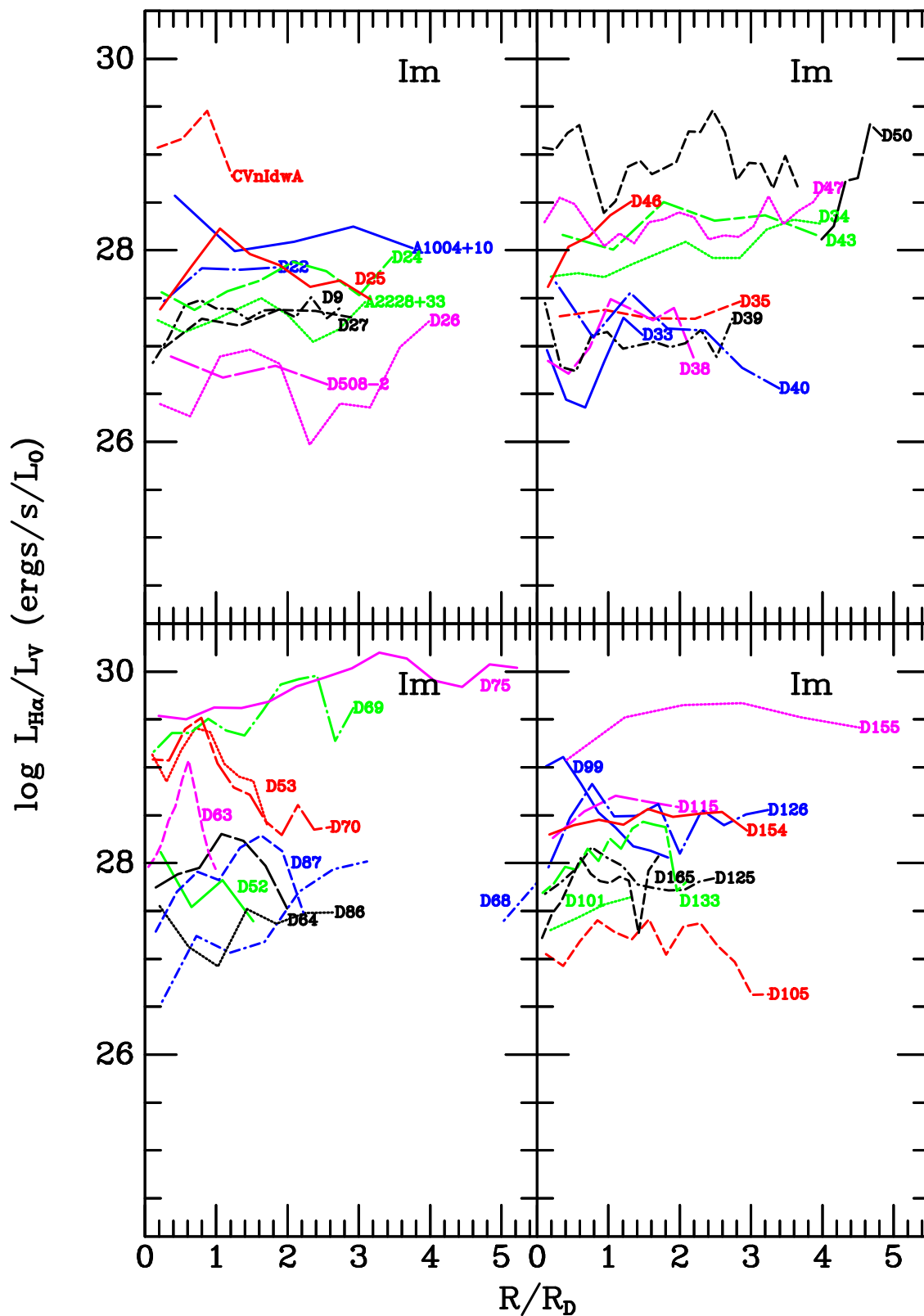
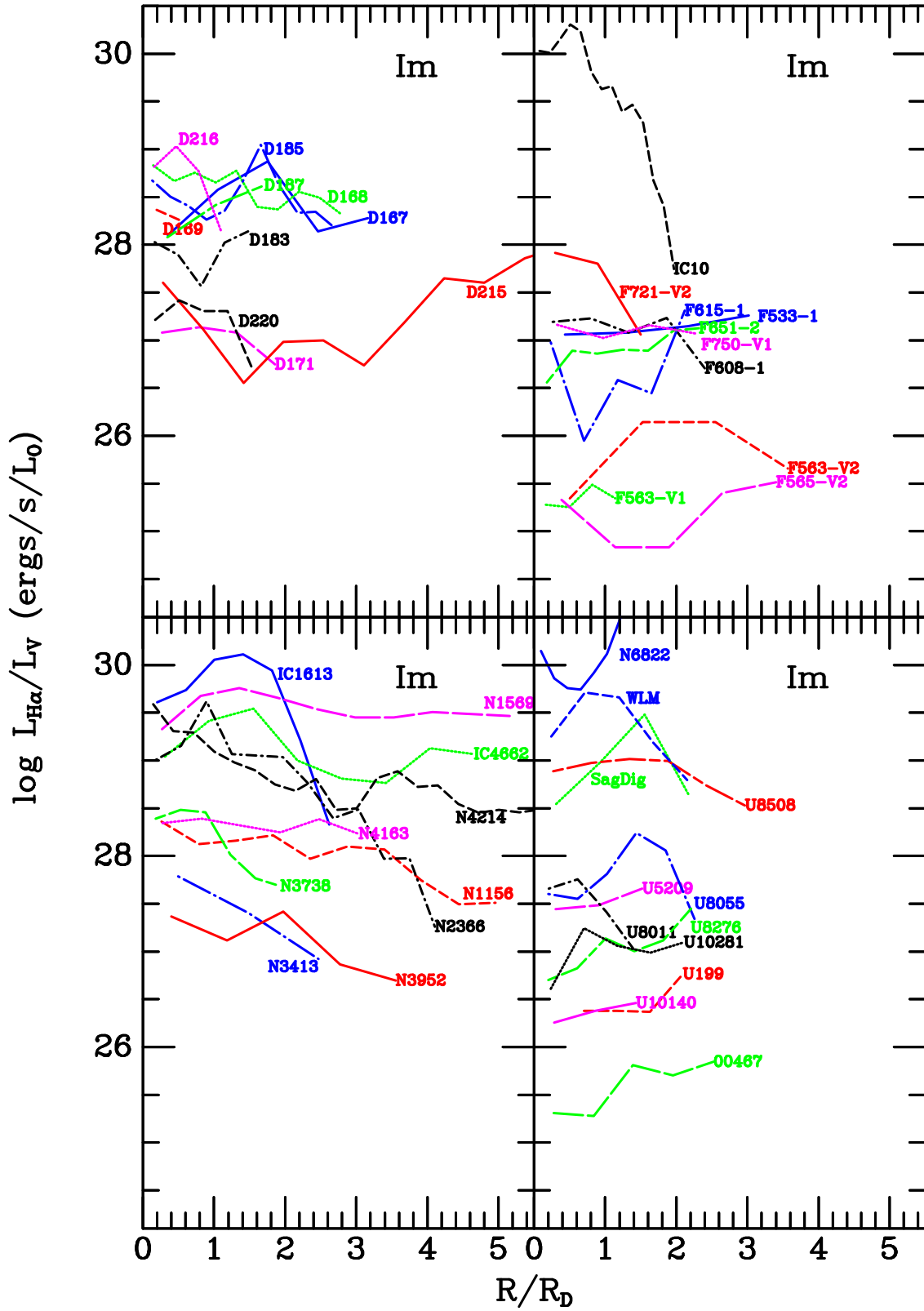
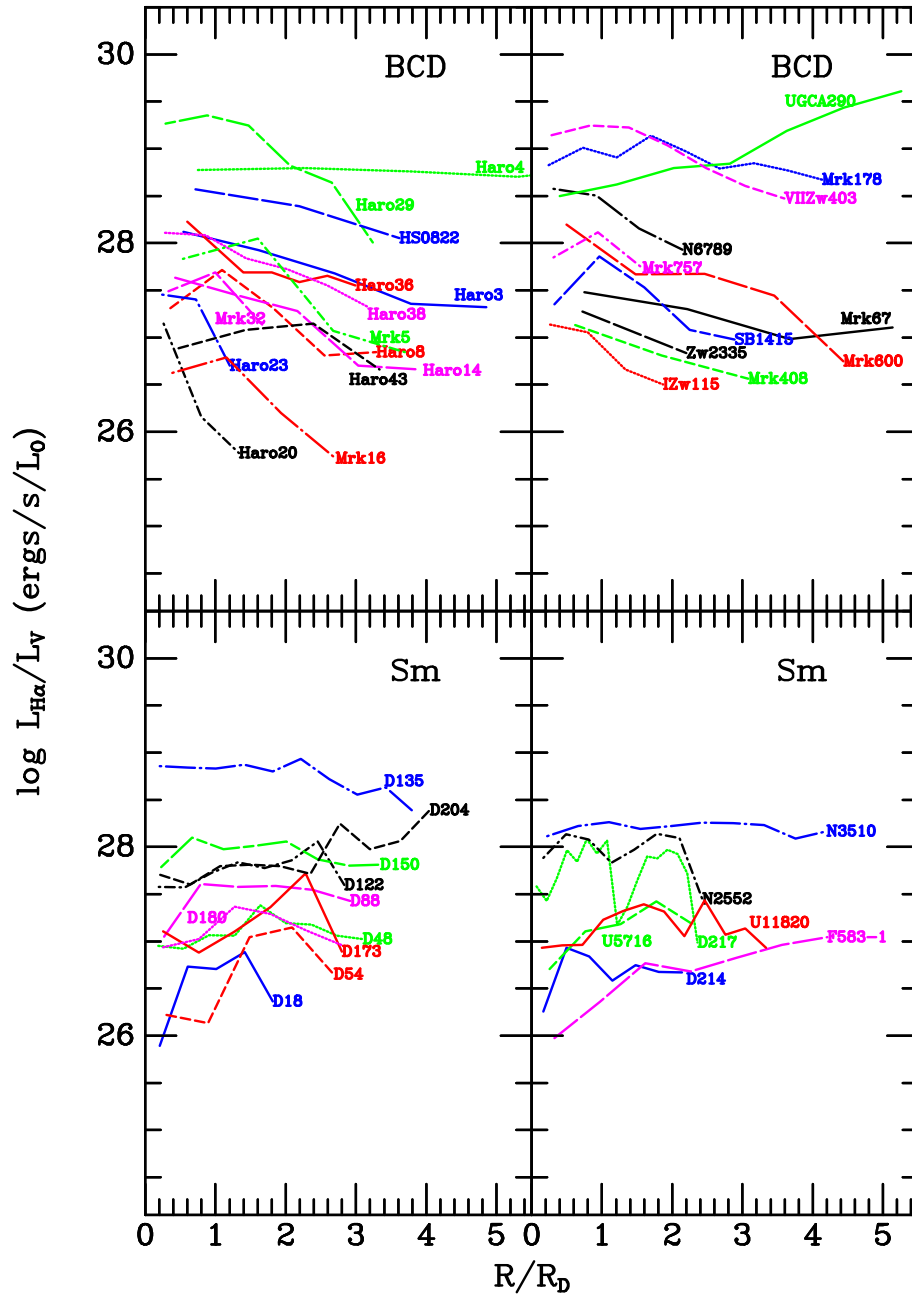


Fig. 18.— Azimuthally-averaged ratio of $L_{H\alpha}/L_V$ as a function of radius relative to the scale-length in the individual sample galaxies.





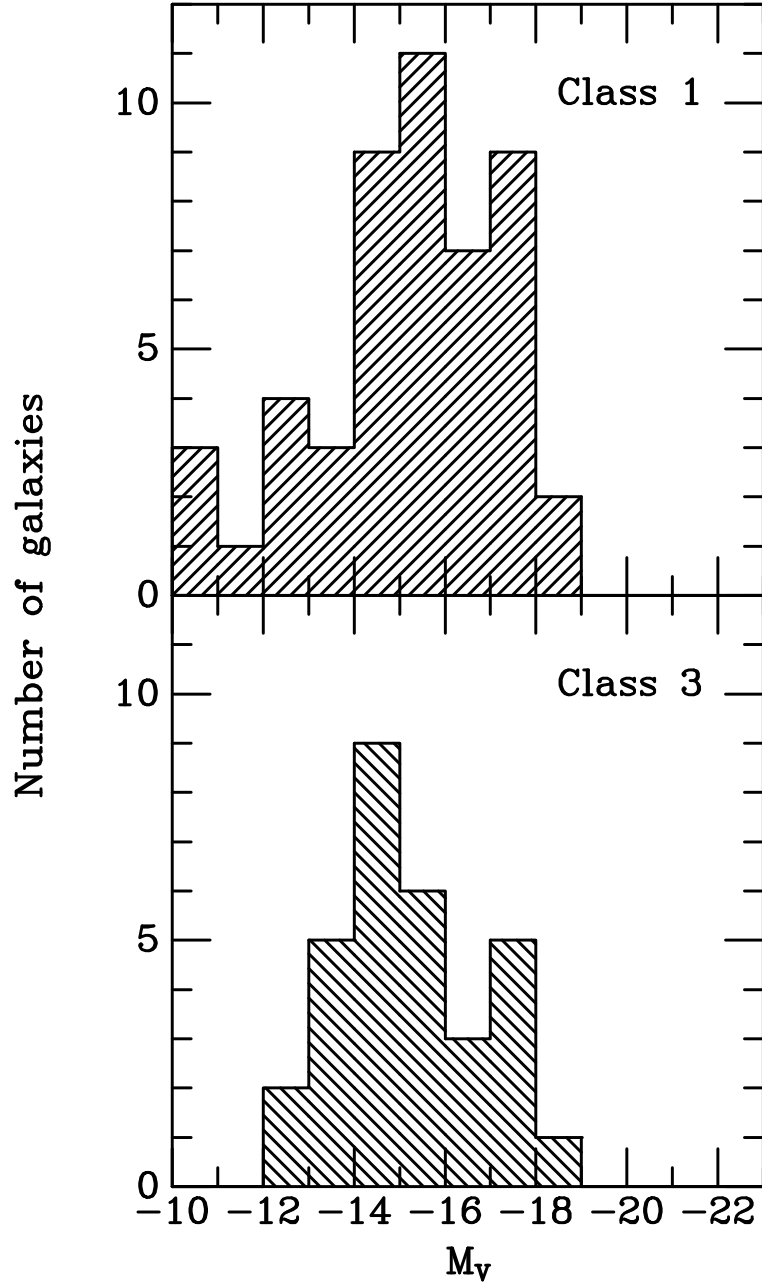


Fig. 19.— Number distribution of $L_{H\alpha}/L_V$ classes 1 and 3 as a function of M_V . Class 1 are galaxies in which the ratio $L_{H\alpha}/L_V$ is roughly constant with radius, and class 3 are those in which the ratio shows large-scale trends with radius.

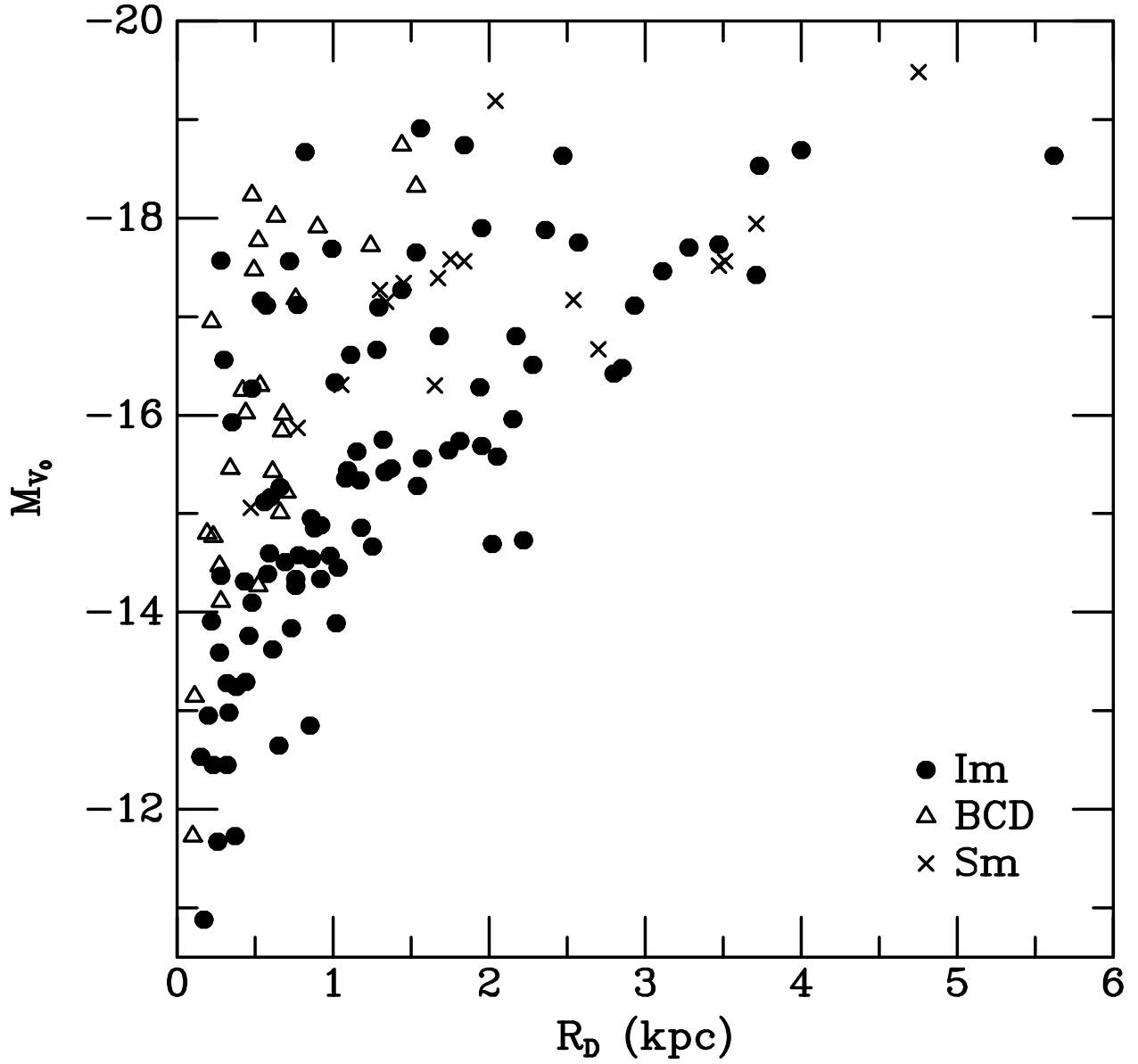


Fig. 20.— M_V , corrected for reddening, as a function of the scale-length R_D for the three types of galaxies.

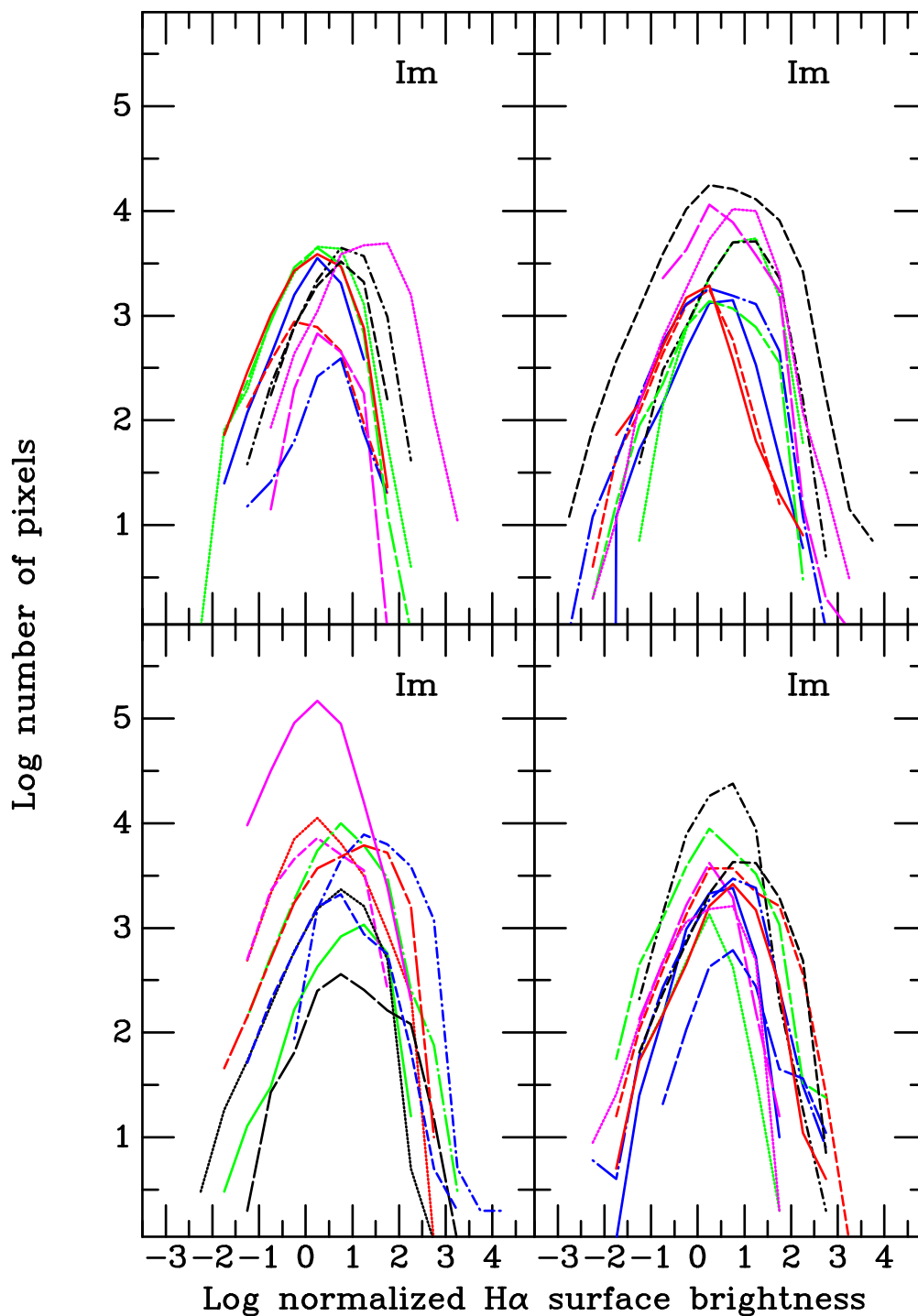


Fig. 21.— Probability distribution functions (pdfs) for the H α images of each galaxy. The logarithm of the number of pixels is plotted as a function of the logarithm of the normalized H α surface brightness of the pixel. The H α surface brightness of each pixel has been normalized to the azimuthally-averaged surface brightness profile at that radius.

